QADRI, SHAHNAZ MAJID, Ph.D. Nanocidals Therapy for Osteomyelitis. (2012)
Directed by Dr. Yousef Haik 129 pp.

Infection is a major medical problem that causes serious complications including patient death. The mortality rate of invasive infection has reduced significantly since the introduction of antibiotherapy. However, the resistance to antibiotic is becoming a serious medical problem that resulted in high medical cost. The overall aim of this study is to evaluate a potential inorganic route (*metalo-antibiotic*) to treat localized infections that require long-term antibiotic treatment combined with medical and surgical intervention. In this study osteomyelitis (bone infection) was selected as a model to evaluate the inorganic route to treat infection. Osteomyelitis is a progressive infection that could result in amputation and patient death. The metalo-antibiotics are faster to develop than antibiotics and have shown great efficacy against a wide range of bacterial infection.

A unique composition of particles with ability to extend their residual efficacy on bacteria for an extended time compared to conventional antibiotics was synthesized and evaluated in this study. The *in vitro* experiments demonstrated the metalo-antibiotics to treat cellular internal infections without damaging the home cell. The *in vivo* toxicity experiments demonstrated a tolerance of the particles for doses that are 20 times higher than the anticipated treatment dose. A murine mouse model for osteomyelitis was developed. The efficacy of the metalo-antibiotics on the induced osteomyelitis was evaluated. A significant decrease in infection in the bones treated with nanoparticles was

observed. By delivering optimal concentration of nanoparticles in mouse models there was no sign of pathology seen in mouse.

Overall, this study has two main impacts: a) creation of inorganic routes to fight against bacterial infection particularly those requiring long-term antibiotic or surgical treatment b) reduction of critical technical risk through generation of pre-clinical data of the employment of inorganic antibacterial complexes.

NANOCIDALS THERAPY FOR OSTEOMYELITIS

by

Shahnaz Majid Qadri

A Dissertation Submitted to
the Faculty of The Graduate School at
The University of North Carolina at Greensboro
in Partial Fulfillment
of the Requirements for the Degree
Doctor of Philosophy

Greensboro
2012

Approved by

_____
Committee Chair

This work is dedicated to my parents.

APPROVAL PAGE

This dissertation has been approved by the following committee of the Faculty of The Graduate School at The University of North Carolina at Greensboro.

Committee Chair Yousef Haik, Ph.D.

Committee Members

Dennis R LaJeunesse, Ph.D.

Gregory Ranner, Ph.D.

Adam R Hall, Ph.D.

10/18/2012
Date of Acceptance by Committee

10/18/2012
Date of Final Oral Examination

ACKNOWLEDGEMENTS

Generally speaking, working on PhD is a long journey, but I have hardly felt 5 years pass, time has flown and it has been a wonderful and overwhelming experience.

I am deeply grateful to my advisor Professor Yousef Haik. It has been honor to be your Ph.D. student, and I appreciate all your contributions of time and funding to make my Doctorate degree productive and stimulating. Your passion and enthusiasm for research was contagious to me! You have always listened my ideas irrespective of good or bad, and consulting you frequently led to key insights. I heartily admire your ability to balance research interests and personal pursuits. You made me feel as a friend which I again admire from the core of my heart. I will never forget your wonderful professionalism and the new career path that you helped me to take. You collaborated my work with a successful professor Basel K. Ramadi at United Arab Emirates University to accomplish the most challenging part of my dissertation.

I owe special thanks to Professor Basel K. Ramadi, for your insightful comments on my work and your approach to research in animal studies. I also deeply admire your highly motivated research team.

In addition, I am very grateful to my committee members; Dr. Gregory Ranner, Dr. Dennis LaJeunesse and Dr. Adam Hall for insightful comments in my work and in this dissertation and for many motivating discussions.

I am very grateful to Professor Eric Brown at University of Arab Emirates, you taught me surgical procedures and aside from work, I learned the great lessons of patience from you.

I would like to thank my wife Sarmadia Ashraf for her love and encouragement. And I thank you for your support that came when I have needed it the most. Thank you with all my heart.

Finally I would like to thank my family for their love and encouragement. You have raised me with love of science and supported me in all pursuits. Brother Aadil Majid, I am deeply grateful to you, for your continuous support morally and financially.

TABLE OF CONTENTS

Page

LIST OF TABLES

Page

LIST OF FIGURES

Page

CHAPTER I

INTRODUCTION

Osteomyelitis is the inflammation of bone tissue commonly caused by an infection. It is a progressive infection of bone marrow and cortex [1], which results in not only inflammation, but also destruction, and necrosis. The populations most commonly affected by this infection are immunocompromised patients, surgical patients, elderly individuals (especially those with diabetes), and infants. *Staphylococcus aureus* accounts for 50-75% of cases of osteomyelitis in adults and 90% of children. Treatment is very extensive with prolonged delivery of antibiotics, surgery and sometimes imputation [1]. Pathogenesis of *S. aureus*-induced osteomyelitis remains poorly understood. Osteomyelitis infection may occur through blood stream, usually common in infants and children, and affect long bones, while in adults beside long bone infection it very often involves vertebral bones. Osteomyelitis infection can occur from nearby infection due to traumatic injury, surgical procedures, or use of prosthetic devices. Patients with diabetes who develop foot ulcers are more susceptible to osteomyelitis as shown in figure 1.1 weak immune system as in patients with sickle cell disease, human immunodeficiency virus (HIV), or patients receiving immunosuppressive medications such as chemotherapy or steroids were attributed to develop osteomyelitis.

Figure 1.1. Osteomyelitis by diabetic foot infection, image obtained from talkondiabeties.org

The most commonly isolated gram-positive pathogen in osteomyelitis is *S. aureus* [2-4]. *S. aureus* is capable of colonizing in bone matrix and it is difficult to eradicate internalized bone infection mainly due to reduced blood supply and ischemia which protects the pathogen from antibiotics and immune system, which results the in long and expensive treatment [5-7]. Moreover, uncontrolled use of antibiotics leads to antibiotic resistance, more than 95% of *S. aureus* strains are resistant to penicillin and 40 – 50% has developed resistance to methicillin, making it even more difficult to treat chronic osteomyelitis [8, 9].

The aim of this study is to evaluate a potential inorganic route (*metalo-antibiotic*) to fight against bacterial infections and in particular internalized bone infection. The number of mortalities associated with bacterial infection is an alarming health concern. In 2002, the US Center for Disease Control and Prevention (CDC) estimated that at least

90,000 deaths a year in the US could be attributed to bacterial infection, more than half caused by bacteria resistant to at least one commonly used antibiotic [10]. In 2009 the CDC reported that the number of serious methicillin-resistant *S, aureus* (MRSA) infections was close to 100,000 a year with almost 19,000 related fatalities [10].

1.1. Internalization Of *S. aureus*

Osteomyelitis induced by *S. aureus* is not clearly understood. *S. aureus* attachment to osteoblast cells is the first step of internalization and mechanism involves the surface molecules of *S. aureus*. It has been shown that osteoblast cells form a fibronectin bridge between the surface-associated fibronectin binding proteins of bacteria and host integrins, this bridge leads to invasion of *S. aureus* [11].

Internalization requires cytoskeletal elements, including microtubules, and clathrin-coated pits, moreover, internalization does not require live *S. aureus* cells [12] (live and dead are equally internalized); however live osteoblasts are required for invasion [13].

Calcium channels play a role in the rearrangement of cytoskeleton [14] which could contribute to bacterial invasion [14]. *S aureus* invasion results in phosphorylation of the extracellular signal-regulated protein kinases (ERK1 and 2) that in turn may cause the activation of transcription factors ATF-2, ElK-1 and c-Jun [15, 16]. Phospholipases-A2 may also be activated by phosphorylated ERK-1 and ERK-2 which cause the production of leukotrienes [17]. This phenomenon causes the calcium channels to open on host cell membrane.

1.2. Role Of Osteoblasts In Immune Response

Primary role of osteoblasts are to regenerate bone matrix components and regulate the activity of osteoclast cells, which are bone resorbing cells [18]. *S. aureus* is capable of infecting bone, utilizing adhesion molecules that help in binding to bone tissue, resulting in secretion of pro-inflammatory cytokines including, IL12, IL-6 and MCP-1 [19-25]. This in turn leads to activation of several inflammatory mediators, including prostaglandin E2 and RANK-L, which act to modulate the activity of bone-resorptive osteoclasts [26-28]. IL12 is known to protect against intracellular pathogen [29]. T lymphocytes and natural killer cells are stimulated by IL12 to secrete interferon (IFN), activating macrophages and T-lymphocytes to initiate a Th1 response [30]. The bacterial infection can cause the up-regulating expression of chemokine CXCL10 (IP-10). IP-10 can recruit T lymphocytes to the site of bone infection [31].

Study by McCall *et al [Ref]* showed*, S. aureus* infection in osteoblasts also leads to the expression of NLRP3, that drives the innate immune response towards invading pathogens and cell damage, and maintains adaptive immune response [32, 33]. A novel intracellular pattern recognition receptor (NOD) expression, and Rip2 Kinase, a critical downstream effector molecule for NOD signaling has been observed in osteoblasts infected with *S. aureus* [34]. Bacteria invasion induced NOD expression may regulate pro-inflammatory pathways including Nf-κB (nuclear factor κB) and MAPKs (Mitogen-activated protein kinase) [35]. Extensive work has been done to understand the mechanism of *S. aureus* infection and immune response to infected osteoblasts, this

infection continues to progress to sever condition because intracellular infection remains protected from humoral immune response and several class of antibiotics [36-38].

1.3. Apoptosis Of Osteoblast Cells By *S. aureus* Invasion

Tucker et al [39] reported that bacterial infection in *in-vitro* causes apoptosis to osteoblast cells.. In apoptosis tumor necrosis factor-related apoptosis inducing ligand (TRAIL) is crucial step. *S. aureus* induced TRAIL in osteoblast cells was examined by Alexander *et al* [40], and determined that *S. aureus* attachment to osteoblasts is necessary for TRAIL induction. *S. aureus* induced expression of NLRP3 in osteoblasts provides a possible mechanism of apoptosis of host cells [32]. In general, loss of osteoblast cells results in bone destruction or decreased matrix deposition of bone [37].

1.4. Destruction Of Bone By Inflammation Or Osteoclasts

Normal bone health and remodeling, needs the balance between osteoblast and osteoclast lineages [40]. This explains apoptosis alone is not responsible for bone destruction. However, osteoclast recruitment and other immunocytes plays significant role in the re-sorption and bone destruction. The stimulation of monocytes and fibroblasts by surface associated proteins fraction to release osteolytic cytokines including MCP-1, colony-stimulating factors and interleukines [25]. The macrophages and some T lymphocytes are recruited to areas of inflammation with the help of MCP-1 hence macrophages and T lymphocytes may be responsible for inflammatory damage [41, 42]. *S. aureus* infected osteoblast cells produced IL-6, may directly or indirectly modulate the activity of osteoclasts and may cause the differentiation of osteoclasts and osteoclast mediated bone mineralization [43]. Other factors like CSF is also responsible for bone

resorption, it has been found that high levels of granulocyte-macrophages-CSF (GM-CSF) and G-CSF production by osteoblast infected with *S. aureus* may induce osteoclastogenesis and result in bone resorption [20].

In osteomyelitis patients it has been shown that 70% of all lesions mainly found in lower limbs, where femur and tibia accounts for 58%. The osteomyelitis infection sites are shown in figure 1.2. In chronic osteomyelitis when the bone loss is 50% or more is visible under X-ray, in a clinical study (figure 1.3) the chronic osteomyelitis was in tibia bone, however the figure also shows reconstruction of bone after treatment and eradication of *S. aureus* infection [44].

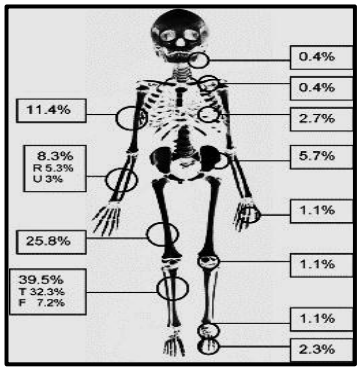

Figure 1.2. Sites of Osteomyelitis. (R: radius; U: ulna; T: tibia; F: fibula).

1.5. Treatment: Prophylaxis, Medical Or Surgical Treatment

1. Prophylaxis

Prophylaxis of an already established bone infection consists of intravenous administered antibiotics with second-generation caphalosporins being the most common choice [45]. During surgical operations laminar airflow is used to prevent from spreading airborne infections [46].

2. Medical

Antimicrobial drug sensitivity test is performed for isolated microorganisms. The antibiotic treatment is usually carried for 4 – 6 weeks, clinical and para-clinical parameters are monitored until complete recovery of patient [47].

3. Surgical

Surgical procedures are only options at certain chronic stages of osteomyelitis supplemented with antibiotics. The aim of surgery is to remove the necrotic and infected tissue surrounding infection and this is turn increase the revascularization of infected

place [48] (see figure 1.3). In some cases surgical treatments are employed with supplement of beads loaded with antibiotics for slow release [49].

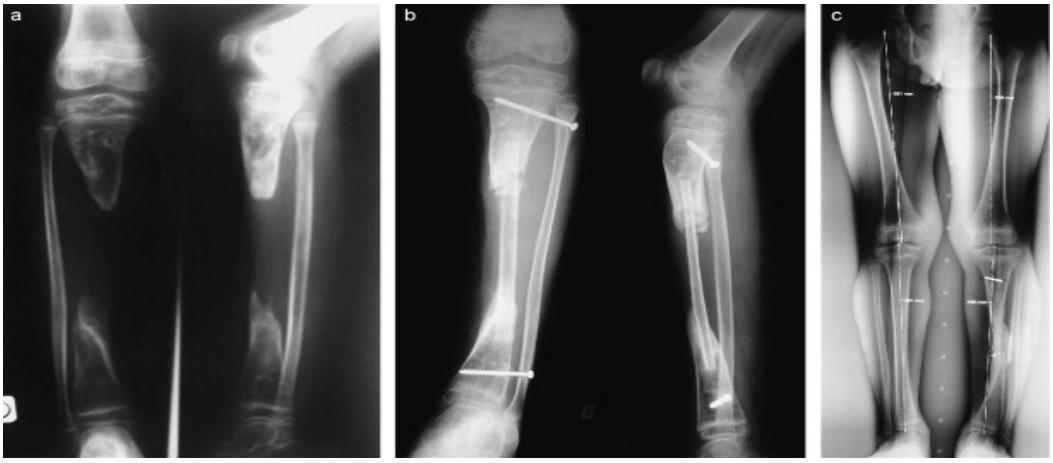

Figure 1.3. Chronic osteomyelitis. (a) severe chronic osteomyelitis sequela after removal of a subtotal tibial shaft sequestrum. Proximal and distal metaphysis appear undamaged, (b) reconstruction after eradication of bacterial infection, (c) at three years post grafting.

1.6. Nanoparticle Antimicrobial Therapy

Silver nanoparticles or silver based nano-alloys have received wide attention in the field of nanotechnology for their attractive properties in the field of biology, chemistry and physics, including sensing, microelectronics, catalysis, conductivity, and interestingly optical properties for use in bio-diagnostics. With the exceptionally high extinction co-efficient of silver nanoparticles that makes its ability in Raman spectroscopy, led to its use in biological applications such as detection of proteins DNA or amino acids [50-54]. One of the most interesting features of silver nanoparticles or silver-alloys is its potential for antimicrobials. The global threat of microorganisms developing resistance against organic antibiotics enlighten research in the antimicrobial

properties of sliver [55]. Silver antimicrobial properties have resulted in their worldwide use in consumer products such as fabrics, deodorants, filters, toothpastes, washing machines, toys and humidifiers. Silver has been used in treatment of wounds, burns, since early 1900 century [56, 57].

Besides silver, for many years, other metals like zinc and copper have shown antimicrobial activity. Copper is more potent antimicrobial agent than zinc but lesser than silver. Copper nanoparticles has been known to have antimicrobial activity for gram positive and gram negative bacteria [58]. Copper nanoparticles have showed more interest in electronic devices. Plasmonic properties of copper have been studied recently and explained how copper oxide interferes with plasmon peaks [59]. Silver – copper alloys have recently been studied as strong antimicrobial nanoparticles comparing to silver alone or copper alone nanoparticles [55], it was observed silver – copper nano alloy has MIC of 0.5 μg/ml comparing to silver 150 μg/ml.

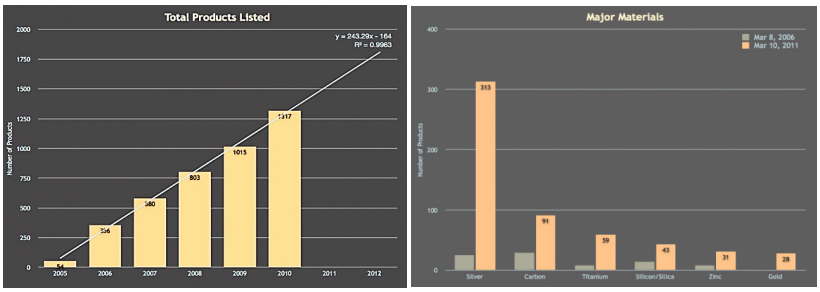

Figure 1.4. Growth of industry in silver based products

Overall nanotechnology based consumer products including silver based products are growing tremendously. In recent years nanotechnology industry has shown tremendous growth in consumer products and linearly growing as shown in figure 14. Data from http://www.nanotechproject.org has shown the linear growth in last 5 years and has grown nearly 521% and products containing silver increased from few to over 300 in five years.

1.7. Aim Of The Study

The number of mortality associated with bacterial infection is an alarming concern to the medical community. It is commonly recited that the scientific community is only one antibiotic ahead of bacteria resistance. Inorganic nanoparticle routes to fight against bacterial infection has been reported for external and tropical applications, however internal application of these antimicrobials have not been fully explored. Some of the major challenges associated with the application of metallic antimicrobial are associated with potential toxicity profile and method of administration to patients.

This study aim is to evaluate a potential inorganic route (metalo-antibiotic) to fight against bacterial infections. The target of this study is to evaluate the inorganic

bactericidal against ***localized infections***, that require long-term antibiotic treatment combined with medical and surgical interventions [60]. This study focuses on osteomyelitis, as it is commonly believed that it is challenging to treat cellular internalized infections by conventional antibiotics. Osteomyelitis is progressive infection, which results in not only inflammation but destruction, and necrosis [61]. The organism that is most prevalent in cases of osteomyelitis is *S. aureus* [62].

Novel classes of antimicrobial nano-alloys composed Ag-Cu-B, and Ag-Cu complexes [63-65] were developed. These nano-alloys have shown noticeable effectiveness against both gram-positive and gram negative bacteria [66, 67], against fungi [68, 69], and polymicrobes [66] when compared to single element (such as silver) bactericidal [69]. The residual effect coupled with their non-toxicity against human tissue makes them a suitable candidate to be considered for the fight against bacterial infection. The mechanism of interaction of these metallic biocidal, which includes protein membrane damage, production of superoxide radicals, and release of ions that interact with the cellular granules and form condensed molecules [69].

1.8. Study Scope

In this study each chapter hereafter we will discuss as follows

1. Synthesis of nanoparticles

   The Synthesis techniques and modifications of nanoparticles, their characterizati--ion for suitable use in antimicrobial therapy.

2. Antimicrobial activity of nanoparticles

This study involves the quantification of antimicrobial activity of ACL and ACB nanoparticles by standard method of counting bacterial colony forming units, spectrophotometric and bioluminescence techniques.

3. Toxicity Assay for ACL nanoparticles

   In this study assessment of toxicity in in-vitro for ACL nanoparticles using differe--nt markers of proliferation or oxidative stress.

4. Toxicity Assay for ACB nanoparticles

   Similar assays of toxicity like ACL were performed to assess the toxicity in in-vitro studies, in addition several other assays were performed for cell toxicity, membrane damage or lipid oxidation.

5. Toxicity in animal studies

   BALB/c animals were used in this study to assess the toxicity associated among vital organs. Blood profile was analyzed for hematological studies and immune response by B-cell proliferation.

6. Osteomyelitis in Animal model

   Murine mouse model was established with induced osteomyelitis to study the antimicrobial efficiency of nanocidals which were delivered either locally or i.v. Further investigations of oxidative stress and histology were performed in animal groups used in osteomyelitis treatment.

7. New generation Silver –Copper alloy – luminescent

   Synthesis of poly-crystalline Silver-copper glycine nanoparticles are our future directions to use as antimicrobial therapy. We believe they may be less toxic in

animals and they exhibit luminescence property which will help in tracking in-vitro or in-vivo during treatment.

CHAPTER II

SYNTHESIS OF NANOPARTICLES

Silver nanoparticles synthesis have been reported since more than a decade, since then different methods have been used for synthesis and surface modification of nanoparticles from aqueous phase to organic phases such as micro-emulsion method by Sun *et al.* (2001) [70], reverse micelles by Taleb et al.(2000) [71], sonochemical method by Liu and Lin (2004) [72], silver flakes of different shapes and sizes by Wang et al. (2005) [73], liquid – liquid by Cai *et al* (2004) [74], inorganic phase by He *et al*. (2001) [75], Sun and Luo (2005) used the thermal method [76] and Lin et al. used oleic acid (2003) [77]. Aqueous method with sodium hydroxide and sodium acrylate has been a common practice for better yield of silver nanoparticles [78]. The importance of sodium hydroxide in synthesis of silver nanoparticles was studied by Nishimura et al [79]. Silver nanoparticles and silver – copper alloy have been also reported by Tanner *et al* [55] with the aid of sodium hydroxide and sodium borohydride.

We have synthesized silver – copper – lithium nano alloys using aqueous phase technique with the aid of sodium hydroxide, and silver – copper – boron nano alloys using boric acid along with sodium hydroxide which results in sodium borohydride.

2.1. Methods And Materials For Silver – Copper - Lithium (ACL)

Materials and chemicals: Copper (II) sulfate 99.0% Sigma Aldrich *Cat# C1297*, silver nitrate 99.999% Sigma Aldrich *Cat#L9650,* lithium hydroxide Sigma *Cat #545856* sodium hydroxide 97.0% *Electron microscopy sciences Cat#21160*, deionized water, heater, sand bath, double neck conical flask, Teflon rod, and homogenizer.

Procedure.

0.1 Molar salt of copper sulfate, silver chloride and Lithium hydroxide were prepared in 100ml deionized water in a ratio of 70:20:10 (Silver:Copper:Lithium). Salt solution was heated at 90^0C temperature in a double neck flask with constant mixing by using Teflon rod fixed with homogenizer under the fume hood. Flask was purged with argon gas and continuous stream of argon used throughout the reaction, drop wise 100 ml of 8 M Sodium hydroxide was added from the side neck of flask and was allowed to heat at 90^0C for one hour with stirring at high speed 2000 rpm, . The suspension was allowed to reach room temperature and followed by centrifugation, supernatant was discarded and obtained pellet was washed three times by double distilled deionized water. Washed nanoparticles were re-suspended in 50 ml of double distilled deionized water and sonicated for one hour, then they were filtered through whatman filter paper and filtrate was freeze dried and stored in 20 ml glass vial with screw cap bottle. Prior to using the nanoparticles, particles were weighed from freeze dried stock and 1 mg/ml suspension was made and sonicated for 1 hour by using micro tip probe. In order to avoid agglomeration and further oxidation of copper it was immediately used post sonication.

2.2. Characterization Techniques

2.2.1. Electron microscopy

Hitachi cold FE_SEM S-4800 and Auriga Zeiss SEM were used for characterization of size and shape of nanoparticles. Hitachi FE-SEM S-4800 was also installed with Oxford EDS (Energy dispersive X-ray spectroscopy) for the elemental analysis; however limitation of EDS were for elements with atomic number 3 or less were not detected. Furthermore 100 mM of lactic acid treatment for 10 minutes was used to break the nanoparticles in smaller size, particles were collected by centrifugation and washing was repeated for 3 times to remove the lactic acid from samples. Double sided carbon tape SEM grade was used to load samples on SEM stub. A drop of nanoparticle suspension with and without sonication was placed on carbon tape attached to SEM stub and immediately water was evaporated under argon gas stream, after drying, sample on SEM stub was placed in desiccator for overnight in order to make the sample is absolutely free from moisture.

Silver-copper-lithium nanoparticles were long rectangular in shape as shown in Figure 2.1 (a). Nanoparticles were 100 to 200 nm long and 50 to 70 nm wide. However, with Lactic acid treatment, nanoparticles were spherical and average diameter of 40 nm as shown in figure 2.1 (c).

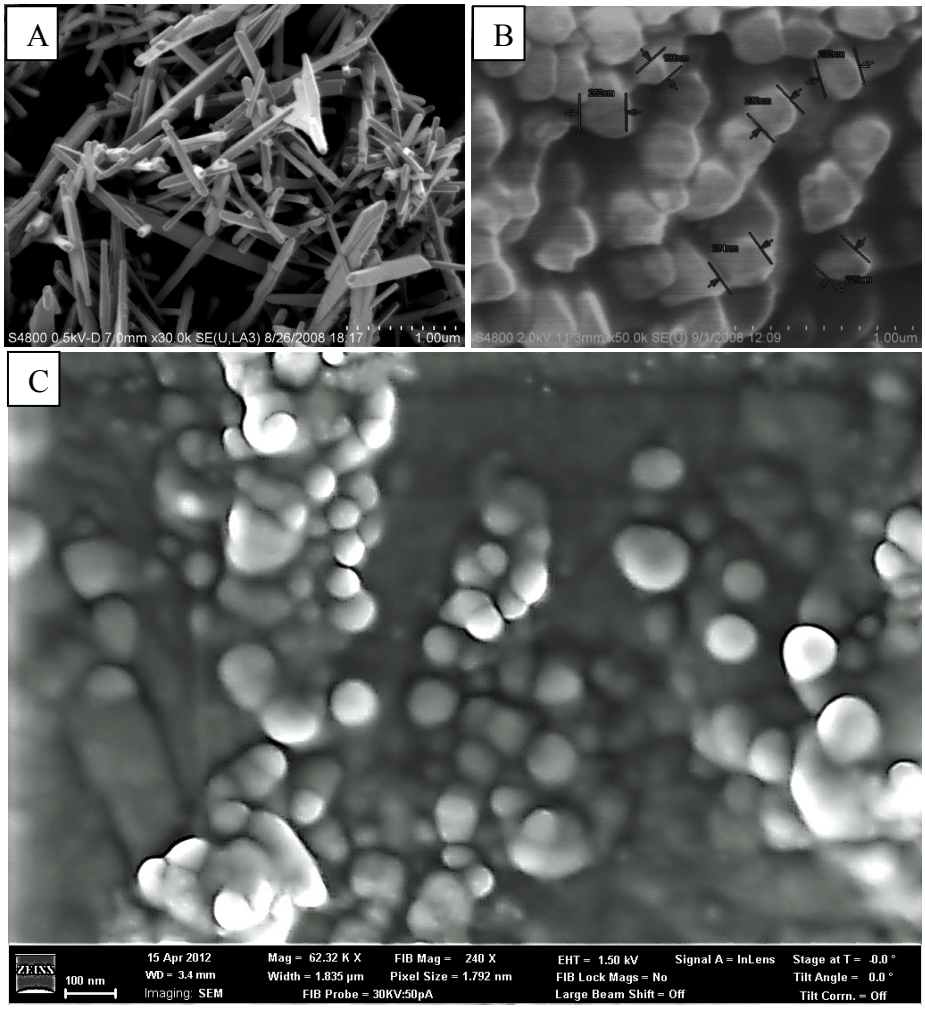

Figure 2.1. ACL nanoparticles without any treatment or sonication. (A) ACL particles Sonicated for one hour (B). Post sonication nanoparticles treated with lactic acid (C).

2.2.2. Elemental Analysis

EDS (Energy dispersive X-ray spectroscopy) provided the average distribution of elements within the nanoparticles and EDS results are summarized in Table 2.1 and EDS spectrum shown in figure 2.2 Silver and copper calculations came close to calculated ratio 70:20. EDS spectrum has shown the peaks for silver, copper and oxygen. Copper is

readily oxidized to CuO, so the presence of oxygen was fairly understood as shown in Table 2.1. However lithium cannot be detected because of it lower atomic number for Oxford EDS machine.

Table 2.1. EDS analysis of ACL nanoparticles.

Element	App Conc.	Intensity Corrn	Weight%	Weight% Sigma	Atomic%
O K	1..77	0.7803	9.57	1.7	34.66
Cu L	2.03	0..5293	16.21	1.89	14.77
Ag L	15.65	0..9214	71.72	2.38	38.51
C K	0.88	1.4931	2.5	0.89	12.06
Totals			100.00		

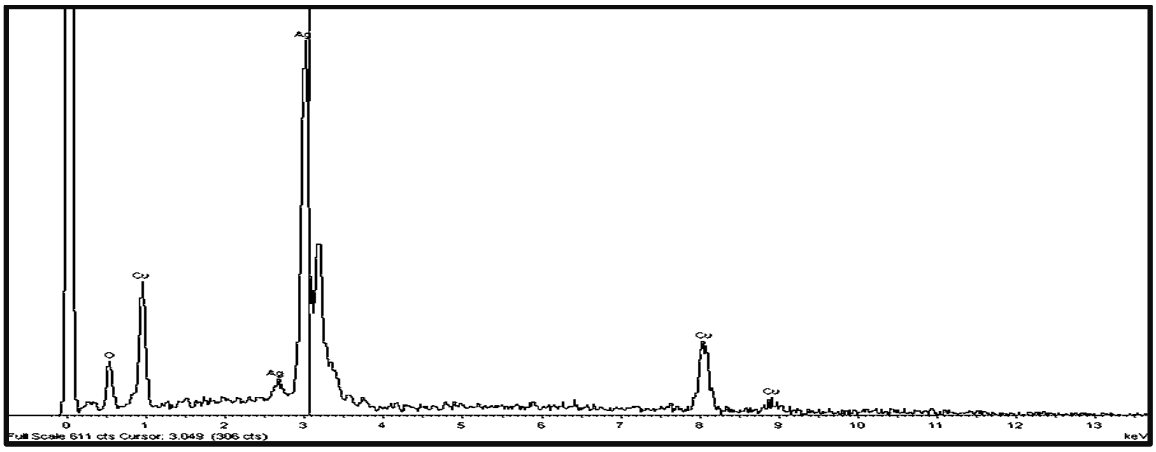

Figure 2.2. EDS spectrum of ACL nanoparticles.

2.2.3. ICP-OES 700

1 ml of 10mg/ml of nanoparticles was digested in 5% nitric acid with final concentration of 10 ppm in a volumetric flask which was covered by tin foil to protect from light and was kept for 2 hours at room temperature. Standard addition method was used to detect the concentration of silver and copper. Standard curve was generated by standard addition method in which samples were spiked with 1, 5 and 10 ppm from multi-element standard solution containing silver, copper and lithium elements in a final volume with 5% nitric acid. Calibration test was passed for silver, copper and lithium; the detection limit was 50 ppb for each element. We found silver concentration as 7.5 ppm and copper 1.8 ppm which was close to our calculated ratio of 70:20 (silver:copper). However lithium was not detected in the nanoparticles this could be due to the fact that lithium may be below the detection limit.

2.2.4. Zeta potential

Malvern Zetasizer – Nano Z, a laser doppler micro-electrophoresis, is used to measure zeta potential. An electric field is applied to a solution of molecules or a dispersion of particles, which then move with a velocity related to their zeta potential. This velocity is measured using a laser interferometric technique called M3-PALS (Phase analysis Light Scattering). This enables the calculation of electrophoretic mobility and from this the zeta potential for the accurate measurement of wide variety of sample types and dispersion media including high salt concentration and zeta potential distribution. The zeta potential for the particles is shown in figure 2.3. The zeta-potential of silver-copper-lithium nanoparticles was found to be -29 mV, which explains the moderate colloidal suspension; negative zeta-potential also depicted the oxidation of copper on surface of nanoparticles.

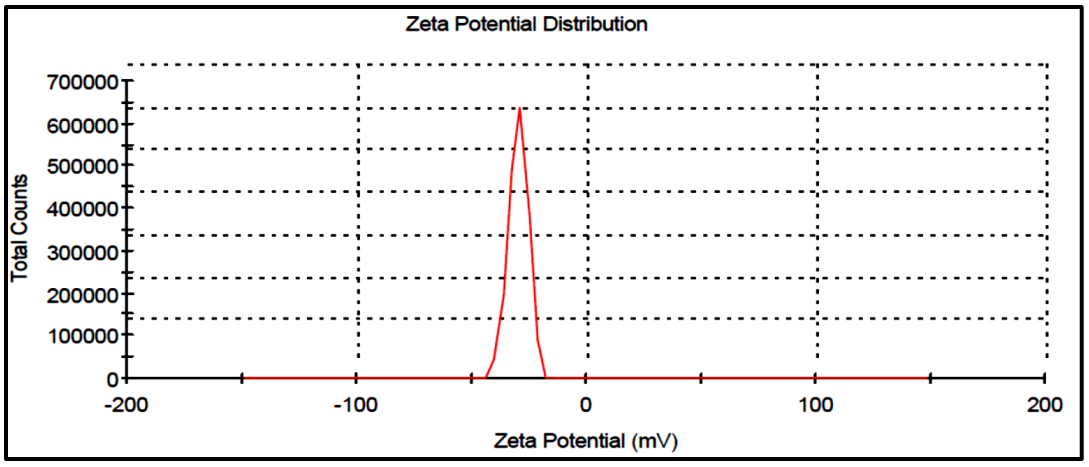

Figure 2.3. Zeta potential of silver copper lithium nanoparticles.

2.3. Methods And Materials For Silver-Copper-Boron Nanoparticles (ACB)

Copper (II) sulfate 99.0% *sigma Cat#C1297*, silver nitrate 99.0% *Sigma Cat#s6506*, sodium hydroxide 97.0% *Electron microscopy sciences Cat#21160*, Boric acid 99.5% *Sigm*a Cat# *B6768,* deionized water, heater, sand bath, double neck conical flask, Teflon rod, and homogenizer were available in lab.

Silver-copper-boron (ACB) was synthesized by preparing 0.1 M salt of silver nitrate, copper sulfate and boric acid in a ratio of 70:20:10 respectively. Solution was heated up to 90^{o} C in a triple neck flask under vigorous stirring by Teflon double blade with the aid of homogenizer with continuous flow of argon gas. 8 M NaOH was added drop wise until the formation of black precipitate and heated for 20 minutes, precipitate turned to greyish black. The precipitate formed was washed repeatedly more than three times in deionized water by centrifugation at 4000 rpm for 10 minutes. Final pellet was sonicated for one hour on ice bath to reduce the temperature rise during sonication. After sonication sample was filtered through Whatman filter paper and nanoparticles were

obtained from filtrate by centrifugation at 4000 rpm. Pellet obtained was freeze dried and were stored in a glass vial with airtight screw cap. Prior to using the nanoparticles, particles were weighed from freeze dried stock and suspended in deionized water followed by sonication and were used immediately. Every time nanoparticles are weighed fresh from freeze dried stock for each experiment. Old stock in suspension was discarded because of copper oxide growth leads to aggregation of nanoparticles.

2.3.1. Characterization techniques

SEM Hitachi S-4800 with EDS Oxford, Auriga Zeiss SEM, Zeta sizer ZS – Malvern, ICP-OES – 700 Agilent, was used for characterization of size and shape as mentioned earlier. In addition XRD – diffractometer (Agilent/Oxford Gemini) was used to confirm the crystal structure of silver –copper –boron nanoparticles.

2.3.2. XRD – Diffractometery

The XRD technique (Molybdenum source: Voltage 50 kV and with 30 mA current and λ_{Mo}= 0.709 °A) was used to study the phase formation and morphology in the Ag-Cu-B system. The major diffraction peaks of silver are clearly seen and indexed in the figure 2.4 and Table 2.2. A considerable amount of the CuO and the Cu_2O phases are also formed in the microstructure of the alloy. From the calculations of the peak intensities and the *d*-values of the atomic spacing, a relatively high degree of crystallinity is observed. However, no traces of boron and its phases have been observed in this pattern. It is well known that the behavior of boron depends upon the crystallinity of the sample, temperature, particle size, and purity. At higher temperatures, boron does burn to form boron (III) oxide, B_2O_3. However, due to the low reactivity of boron with silver at

relatively low temperature, the XRD pattern was not able to reveal the boron peaks or any related phases. It is also worth mentioning that the addition of small amount of boron nanoparticles below the detection limit of the diffractometer may explain the absence of the boron peaks. Moreover, for alloys with small copper concentrations, it is difficult to incorporate boron in the alloy due to low solubility of boron in a silver-rich phase. Therefore, in this study our aim is to look for the optimum dose of the Ag-Cu base alloy, which will be ideal for the incorporation of maximum amount of boron. It is suggested that the boron content in the Ag-Cu system increases within the copper rich (dark) phases.

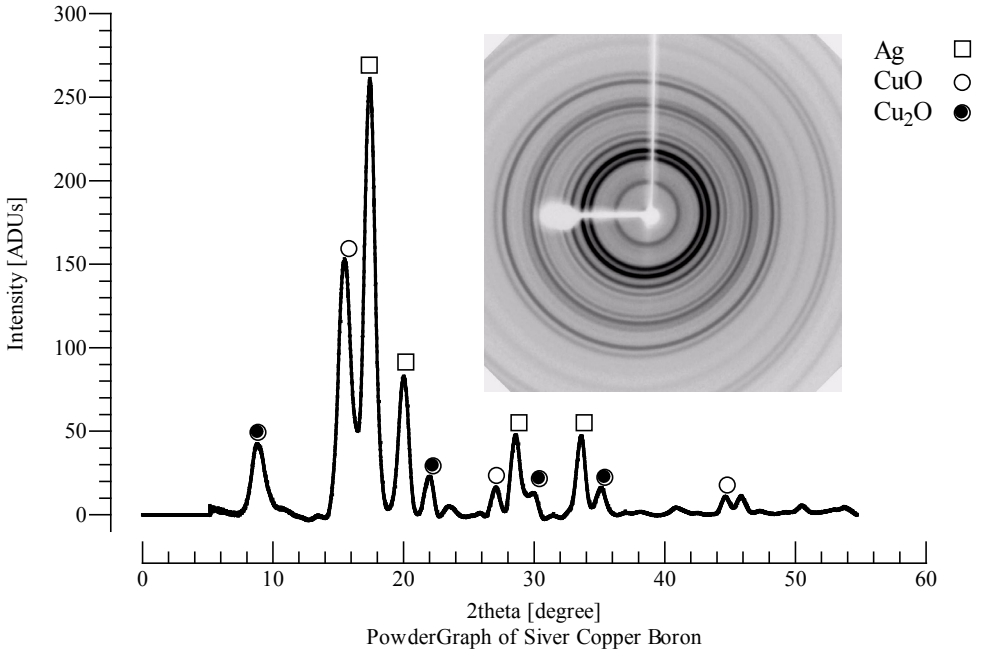

Figure 2.4. Powder graph of Silver-Copper-Boron.

Table 2.2. XRD diffraction peaks of Ag, CuO and Cu_2O.

	2theta [degree]			
Cu_2O	8.69	21.81	29.68	34.92
Cu0	15.41	26.86	44.42	
Ag	17.37	28.43	33.3	

2.3.3. Scanning Electron Microscopy

SEM characterization was followed as mentioned earlier. SEM Images of Ag-Cu-B nanoparticles showed nanoparticles are rectangular in shape with average size ranging between 80 to 140 nm. However, with lactic acid and sonication treatment was effective to reduce the size between 15 to 20 nm. Size measurements were performed by Quartz-8 imaging software as shown in Figure 2.5.

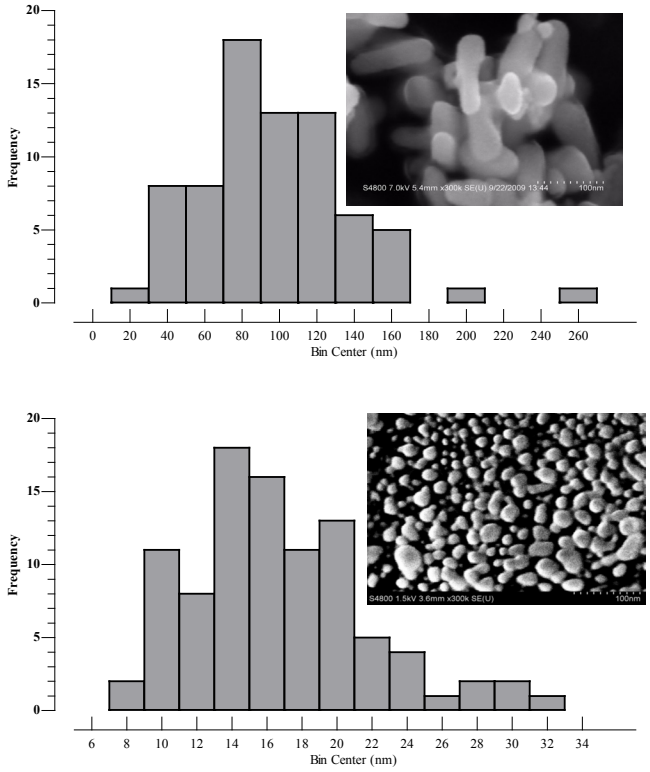

Figure 2.5. SEM images and Histogram of nanoparticles. Upper and lower histograms shows without or with Lactic Acid treatment respectively.

2.3.4. Energy dispersive X-ray spectroscopy (EDS)

Elemental identification and semi-quantitative analysis was provided by EDS Oxford spectroscopy by using INCA software, sample was analyzed by Point and ID protocol, which is bulletin option in INCA software for acquiring X-ray spectrum from point of interest. As shown in Figure 2.6, only two nanoparticles were selected to get the X –ray spectrum in order to minimize the interference from surrounding materials and shown the distribution of elements in each particle. The results are summarized in table

2.3 which are generated directly by INCA software for each spectrum and are exported into word file.

Table 2.3. EDS analysis of ACB nanoparticles.

Element	**App**	**Intensity**	**Weight%**	**Weight%**	**Atomic%**
	Conc.	Corrn.		Sigma	
O K	50.17	0.3280	12.41	1.21	45.64
Cu K	208.96	0.9770	17.36	0.39	16.07
Ag L	807.91	0.9337	70.23	1.02	38.29
Totals			100.00		

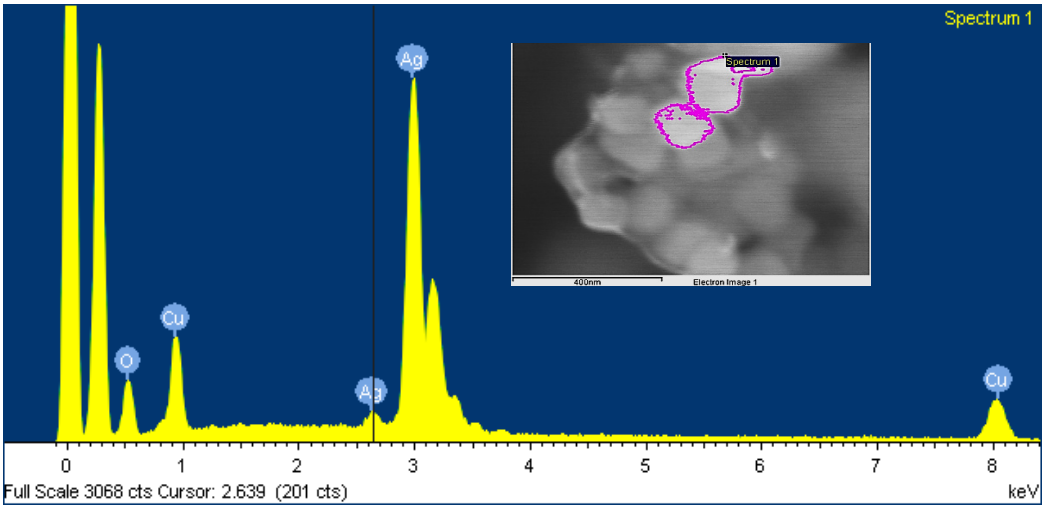

Figure 2.6. EDS spectrum silver –copper –boron nanoparticles. Electron image acquired by point selection.

Silver, copper and oxygen ratio was 70.23, 17.36 and 12.41 respectively as shown in figure 2.6; Copper is oxidized rapidly so the oxygen was expected to be associated on the surface of nanoparticles. Boron was difficult to identify by EDS because of lower atomic number.

2.3.5. ICP –OES 700

The procedure for ICP-OES by standard addition was same as described earlier for Silver–copper-lithium nanoparticles. All three elements were quantified by ICP-ES spectroscopy as shown in Figure 2.7; data provided the elemental ratio within nanoparticles such as 6.9 ppm, 2.06 ppm and 1.4 ppm of silver copper and boron respectively from a 10 ppm nanoparticles suspension. It is obvious from the data (figure 2.7) that 1 µg of ACB nanoparticles will have 690 ng, 200.6 ng and 140 ng of silver copper and boron respectively.

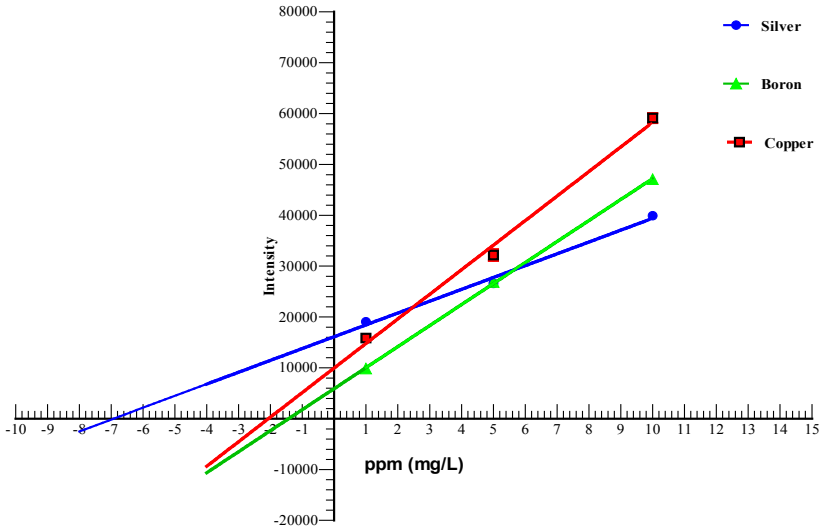

Figure 2.7. ICP-OES of silver –copper –boron nanoparticles.

2.3.6. Zeta potential

Zeta potential for silver –copper –boron was studied to measure the quality of dispersion of nanoparticles in aqueous solution and the surface charge on nanoparticles. The zeta-potential measured for silver –copper –boron nanoparticles was -30mV as shown in figure 2.8

The effect of glacial acetic acid, on ACB nanoparticles a shift in zeta-potential from -30 mV to +3 mV was observed (figure 2.9). The glacial acetic acid reacts of copper oxide and not with metal copper [59]. Copper oxide reaction with glacial acetic acid as follows:

(1) $CuO + 2CH_3COOH \longrightarrow Cu(CH3COO)2 + H_2O$

(2) $Cu_2O + 4CH_3COOH \longrightarrow 2Cu(CH3COO)2 + H_2O + H_2$

Copper has low reduction potential of (0.34 V) Cu^0/Cu^{2+} comparing to silver (0.8 V) [55], hence it is problematic that silver –copper nanoparticles can have copper oxide growth on their surfaces. Freeze drying in inert atmosphere reduces the oxidation of copper. ACB particles were functionalized with mercaptopropionic acid which has thiol group with high affinity towards metals. Mercaptopropinic acid was added to 1 mg/ml of ACB nanoparticles at a final concentration of 100 mM and incubated for 30 minutes with 3 seconds sonication after every 10 minutes. Latter particles were centrifuged at 13000 rpm for 10 minutes and pellet was resuspended in deionized water, this procedure was repeated 5 times to remove the unbound Mercaptopropionic acid. The zeta-potential was -30 mV (Figure 2.10) that may be due to carboxylic group available on the surface of nanoparticles. Further tuning was done by conjugating with polyethylineamine (PEI) by using EDC (1-Ethyl-3-carbodiimide hydrochloride) coupling (see figure 2.11) [80]. Zeta-potential after conjugating with PEI, flip from -30 mV to + 60 mV (Figure 2.10). Positive zeta-potential is believed to be due to amine terminal groups.

This study suggests that these nanoparticles can be functionalized by organic molecules and polymers to make them aqueous soluble nanoparticles and the risk of toxicity can be reduced.

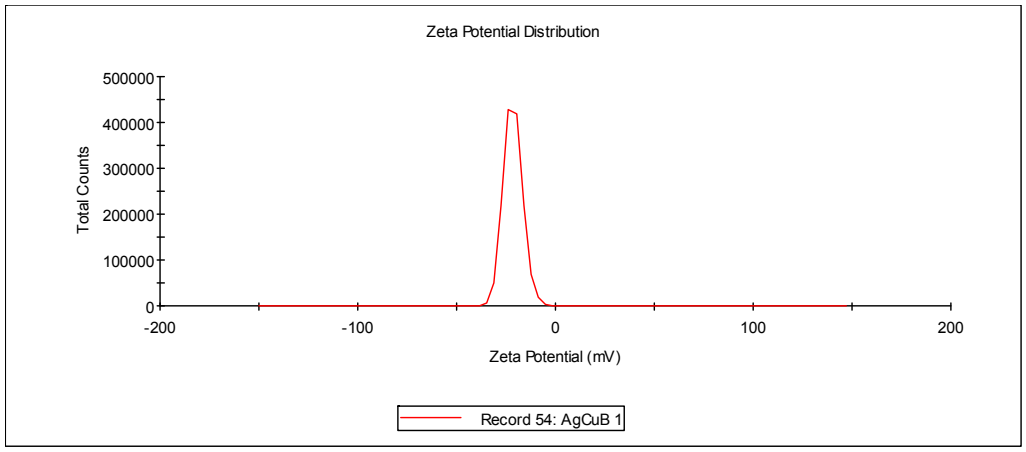

Figure 2.8. Zeta potential of ACB nanoparticles after sonication.

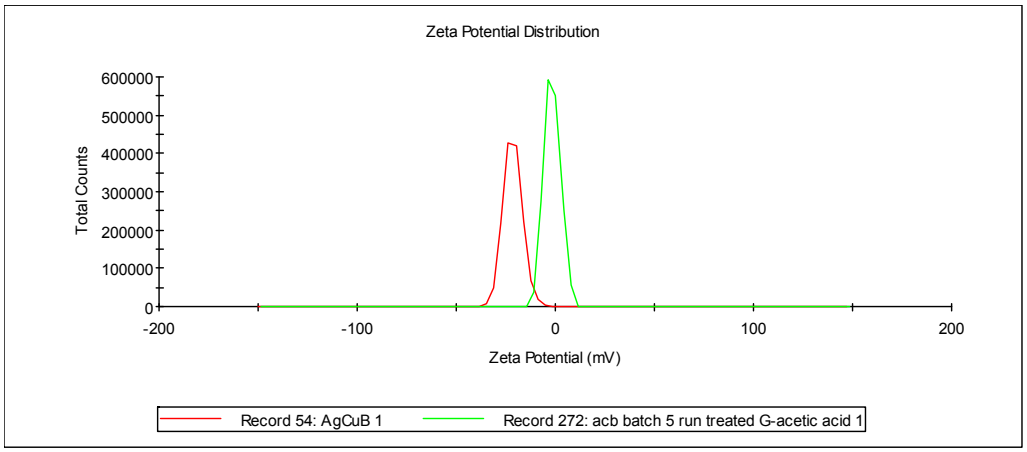

Figure 2.9. Zeta-potential after glacial acetic acid treatment.

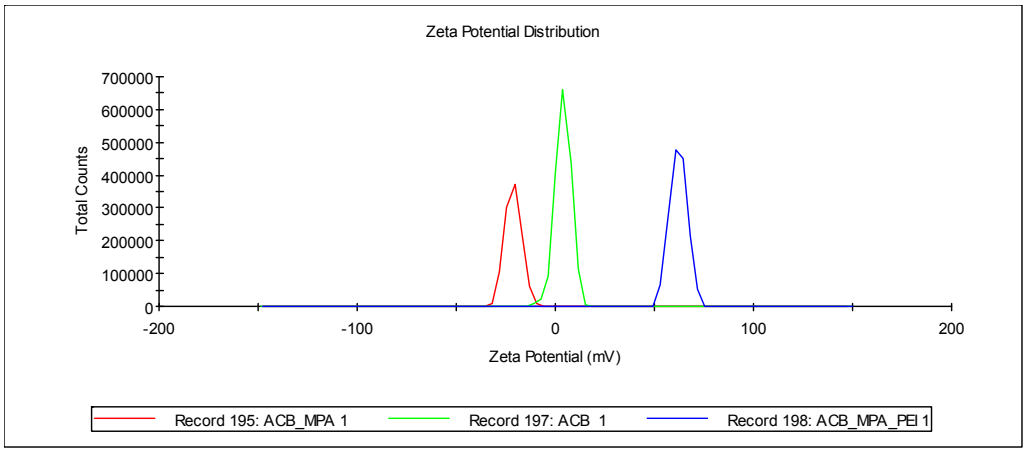

Figure 2.10. Zeta-potential of functionalized nanoparticles. Left red peak is after ACB nanoparticles are functionalized with 3-Mercaptopropionic acid, green peak in the middle after treatment with glacial acetic acid, blue peak on Right after conjugation of PEI with 3-Mercaptopropionic acid.

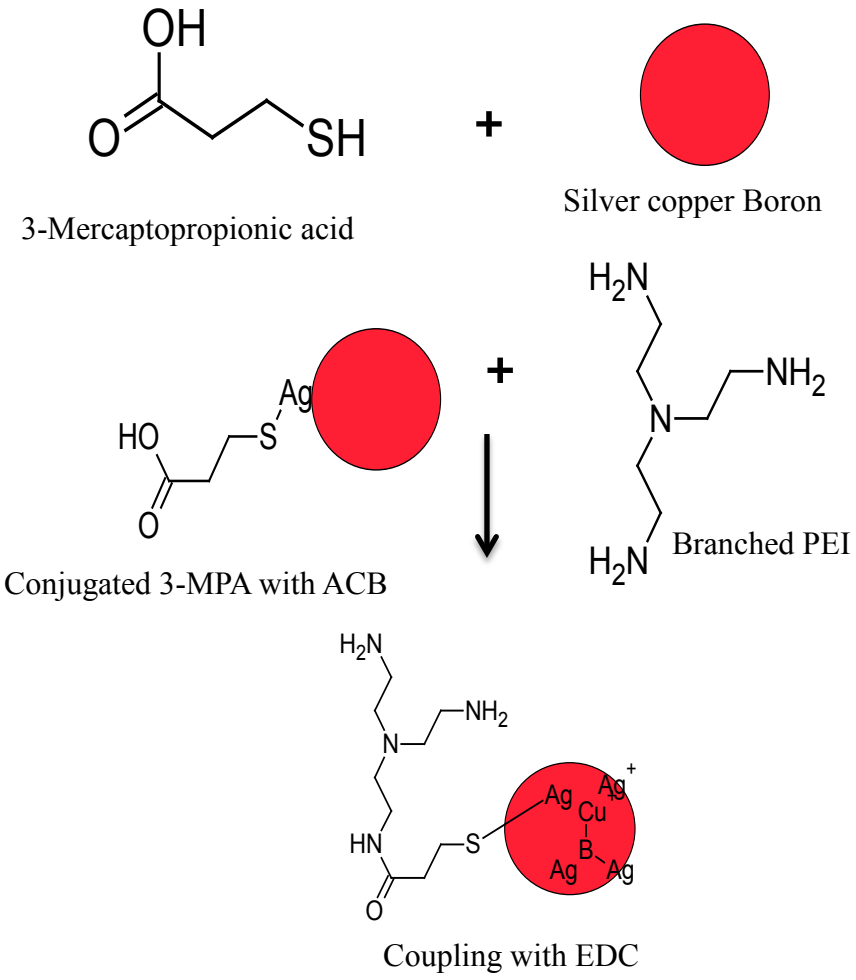

Figure 2.11. Schematic representation of nanoparticle tuning.

CHAPTER III

ANTIMICROBIAL ACTIVITY OF NANOPARTICLES

The antimicrobial nature of the silver and copper are well documented. In this chapter our aim was to evaluate the antimicrobial efficacy of the silver-copper-lithium and silver-copper-boron against *S. aureus*.

3.1. Antimicrobial Activity Of Silver-Copper-Lithium

3.1.1. Materials and methods

The *S. aureus* strain used in this study was obtained from ATCC (Cat# 700260). It was streaked on T. soy agar plates. Stock was stored in glycerol at -80°C. Bacterial colonies, grown on T. soy agar plates, were inoculated into a 5 ml of T-soy broth and cultured stationary overnight at 37°C with aeration. The overnight grown bacterial suspension was then sub-cultured at 1:5 ratio and grown to mid-log phase for another 2 hours with shaking at 200 rpm and was stopped when O.D. reached to 0.5 at 600 nm which were equivalent to 5×10^7 CFU/ml. Cells were harvested by centrifugation for 20 minutes at 4300g and pellet was washed with PBS. Serial dilutions were prepared in sterile T-soy broth and used at initial concentration of 5×10^5 CFUs per ml for each experimental sample.

3.1.2. Antimicrobial effect of ACL

The antimicrobial assay was performed in duplicates with different groups by incubating 5×10^5 CFUs/ml of *S. aureus* bacterial suspension. Each group with different concentrations of ACL nanoparticlexs at 10, 5, 1, 0.5 and 0.01 µg/ml and were grown at 37°C for 24 hours in an orbital shaker. Post 24 hours culturing, serial dilutions were then made in sterile PBS buffer for each group and 100 µl aliquots were plated on T-soy agar plates. Bacterial colony forming units (CFUs) were enumerated after overnight incubation of S. *aureus* with different concentrations of nanoparticles resulted in a substantial reduction in the number of viable *S. aureus* organisms (Figure 3.1). The degree of inhibition was dependent on the concentration of nanoparticles used, such as CFUs reduction by 4.8 logs, 3.6 logs, 3 logs for 5 µg/ml, 1 µg/ml and 0.5 µg/ml respectively. While as 0.01 µg/ml concentration of nanoparticles did not show inhibition of *S. aureus* growth.

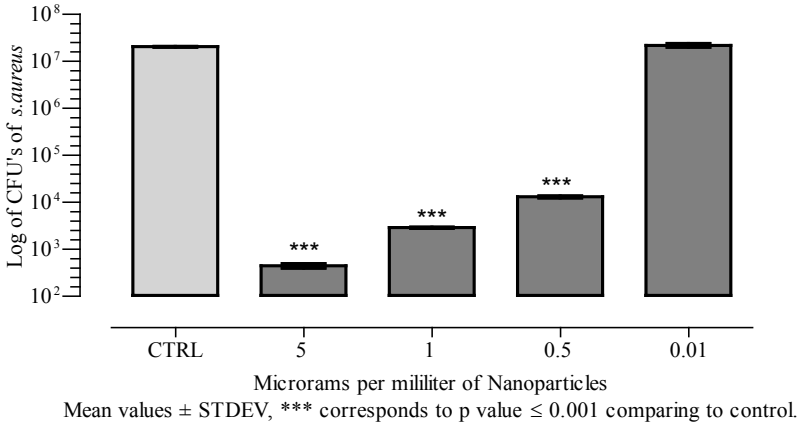

Figure 3.1. Antimicrobial activity of ACL Nanoparticles. *S. aureus* bacteria were incubated with different concentration of ACL nanoparticles for 24 hours, each bar represents the reduction in CFUs.

3.1.3. Effectiveness of ACL nanoparticles on S. *aureus*-infected osteoblasts

Human osteoblast cell culture and invasion assay

The hFOB 1.19 human osteoblast cell line was obtained from ATCC (*Cat# CRL-11372*). Cells were cultured as per ATCC recommendations in 10% FBS phenol free DMEM: F12 and G418 – 300 µg/ml. Osteoblast cells were cultured in a 6-well plate to 90% confluency. Cells were washed with antibiotic free media six times, and then infected with *S. aureus* at a ratio of 250:1 (MOI=250:1) for two hours. Cells were then washed three times with antibiotic free media and incubated in medium containing 200 µg/ml of gentamicin for 2 hours to eradicate non-internalized bacteria. After another cycle of three washes, nanoparticles were added at a final concentration of 1, 5, or 10 µg/ml to the osteoblast cell cultures in an antibiotic free media and incubated for further 24 hours. Control was grown under similar conditions except nanoparticles were not added to culture. Cells were then washed again three times and harvested after

trypsinization in 1 ml of 0.25 % of trypsin (Sigma Aldrich *Cat # T 4049*). Cell lysates were prepared in 0.5 ml of lyses buffer (PBS+0.1% Triton X-100) and serially diluted in 1 ml of PBS buffer. 100 µl from each dilution was plated on T-soy agar plate and incubated overnight for enumeration of intracellular bacterial CFUs. Similar assays were repeated using a fixed concentration of 1 µg/ml of nanoparticles and varying the incubation time with the infected osteoblasts from 17 to 80 hours.

Antimicrobial activity

To assess the potential antimicrobial activity of ACL nanoparticles on infected osteoblasts, experiments were carried out on *S. aureus*-infected osteoblasts using three different concentrations of nanoparticles (1, 5, and 10 µg/ml). The experimental set up was designed to specifically evaluate the effectiveness of the nanoparticles against bacterial organisms, which have invaded the osteoblasts, thereby mimicking the conditions of human osteomyelitis. As can be seen from figure 3.2, the effect of nanoparticles on osteoblast-internalized bacteria was very significant. At a nanoparticle concentration of 1 µg/ml, there was 43% reduction in bacterial CFU's; the degree of inhibition was increased to 97% at nanoparticle concentrations of 5 and 10 µg/ml as shown in figure 3.2. Similar assays were carried out by fixing the concentration of nanoparticles to 1 µg/ml and varying the incubation period of infected osteoblasts with the nanoparticles (17, 48, 60 and 80 hr). The results of these studies are depicted in figure 3.3, which shows effectiveness of antimicrobial activity increased with prolonged incubation time. Using the sub-optimal concentration of 1 µg/ml, while degree of inhibition was only 32% after 17 hour of incubation, whereas inhibitory effect to > 95%

by 45 hours (Figure 3.2). These experiments bring out that antimicrobial efficacy may be dependent on both incubation time and concentration of nanoparticles. This data demonstrated that the addition of nanoparticles at concentrations as low as 0.5 µg/ml resulted in a more than 50% inhibition *S. aureus* bacterial growth within 24 hrs and while as 1 µg/ml also showed more than 99% MBC, Based on our bactericidal findings, here similar dose and higher concentrations up to 15 µg/ml to find the cellular toxicity.

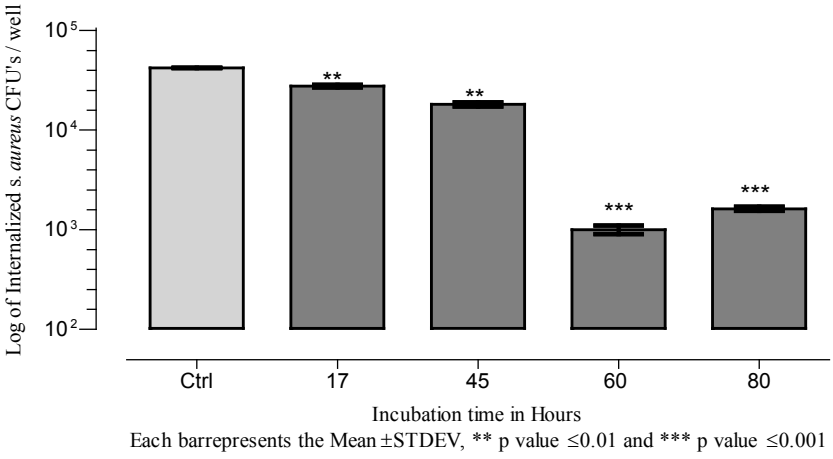

Figure 3.2. Effect of ACL on internalized bacteria.

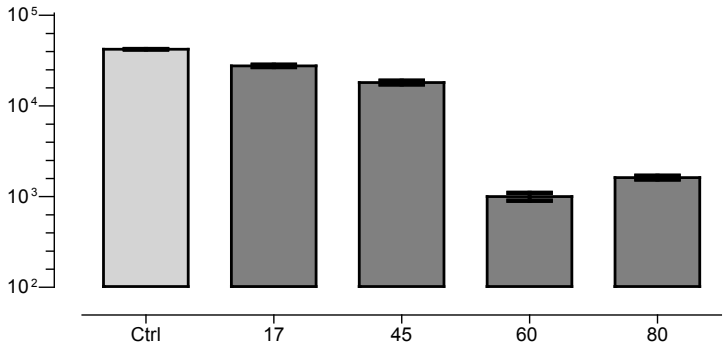

Figure 3.3. Time dependent Effect of ACL on internalized bacteria.

3.2. Antimicrobial Efficacy Of Silver-Copper-Boron Nanoparticles

Silver –copper –boron (ACB) nanoparticles, synthesis and characterization described in chapter 2. Antimicrobial activity evaluation of ACB were performed similar to ACL nanoparticles using the same strain of *S. aureus* and for invasion assay same cell line of osteoblast cells were used, however the antimicrobial activity was performed in Osteoblast cell culture media (DMEM:F12 with L-glutamine and 10%FCS) instead of Tryptic Soy Broth. In addition to *S. aureus*, another strain XEN 36 which was obtained from Caliper life science, Xen36 was derived from the parental strain *S. aureus* ATCC 49525 (Wright), a clinical isolate from bacteremia patient. *S. aureus.* Xen-36 possesses a stable copy of the modified *Photorhabdus luminescence lux ABCDE* operon at a single integration site on a native plasmid. Xen-36 should be stored at -80°C.

3.2.1. Bacterial strain and growth

The *S. aureus* strain used in this study was obtained from ATCC (Cat# 700260) and kept as frozen glycerol stocks at -80°c. Bacterial colonies, grown on trypticase soy

agar plates, were inoculated into a 5 ml T-soy broth and cultured stationary overnight at 37°C with aeration. The bacterial suspension was then sub-cultured at 1:5 ratios and grown to mid-log phase for another 2 hours with shaking. Cells were harvested by centrifugation for 20 minutes at 4300g and pellet was washed with PBS. Cell density was measured spectrophotometrically. Serial dilutions were prepared in sterile PBS buffer and used at 1×10^5 CFUs per experimental sample.

3.2.2. Antibacterial effect of ACB nanoparticles against *S. aureus*

The assay was performed in a 24 well corning cell culture plate in a final volume of 1 ml by incubating *S. aureus* with cell density of 1×10^5 CFUs / ml in a DMEM:F12 media with L-Glutamine (Cat. No 21041025) and 10% Fetal calf serum (FCS) with or without different concentrations of nanoparticles 1, 5, 10, 20 and 30 µg/ml the suspension was incubated in a dry incubator overnight and absorbance was measured at 600 nm using BioTek spectrophotometer. Furthermore similar assay were done in 96 well plate in 200 µl volume with or without nanoparticle concentrations 1, 2, 3, 4 and 5 µg/ml. After incubation time bacterial cells were harvested by centrifugation and resuspended in 1ml of warm PBS buffer pH 7.4 and were serially diluted and 100 µl was poured in TSB-agar culture plate and incubated at 37 degree C. overnight and following day CFU's were counted. Incubation of *S. aureus* with nanoparticles at different concentrations resulted in substantial reduction in number of viable *S. aureus* microorganism Figure 3.4. The degree of reduction was dependent on the concentration of nanoparticles and incubation time and was observed as O.D. value at 600 nm, where 1µg/ml concentration exhibited

28 % inhibition by while 5, 10, 20, 30 µg/ml concentration inhibited from a range of 90 to 99%.

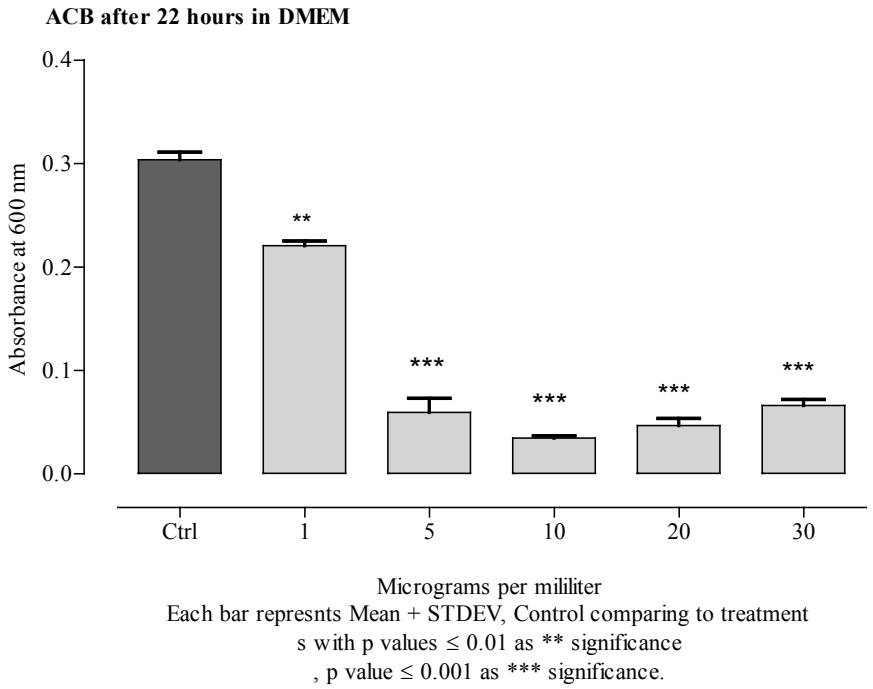

Figure 3.4. Antimicrobial activity of ACB nanoparticles.

3.2.3. Antimicrobial activity in XEN-36 and native *S. aureus* strain

Similar antimicrobial testing of ACB nanoparticles ranging from 1, 2, 3, 4, and 5 µg/ml against *S. aureus* in 1 ml cell culture media was performed as mentioned earlier. Moreover XEN-36 bacterial strain, which is bioluminescent, was also utilized. In addition to O.D. measurements, Biotek Luminometer was utilized to measure Bio-luminescence for treated and non-treated *XEN-36* bacterial strain. Bioluminescence methods have used to for analysis efficacy of antimicrobial compounds [81]. Vancomycin was also used as control to evaluate the antimicrobial activity of the

particles against a known antibiotic. Vancomycin remains the standard of care for treating serious methicillin-resistant *S. aureus* (MRSA) infections. However, vancomycin resistant *S. aureus* (VRSA) was reported first from a renal dialysis patient in 2002 in Michigan [82]. *XEN-36* and parental strain *S. aureus* both were susceptible to vancomycin. The MIC of vancomycin against *S.aureus* was determined as 0.5 µg/ml [80].

Antimicrobial activity of ACB nanoparticles using 1, 2, 3, 4 and 5 µg/ml concentration showed that *XEN-36* strain and native *S. aureus* have similar behavior. Antimicrobial activity in a narrow range from 1 µg/ml to 5 µg/ml concentration was observed, where 1 µg/ml has 0.5 log difference comparing to control which corresponds to 63.8 % reduction while 2 µg/ml has 5 log difference and 3, 4 and 5 µg/ml has more than 5 log difference compared to control which corresponds inhibition by greater than 99% as shown in figure 3.5.

Bioluminescence based assay results showed similar pattern of inhibition for vancomycin and ACB nanoparticles. Bioluminescence method as shown in figure 3.6 was used to evaluate the degree of inhibition.

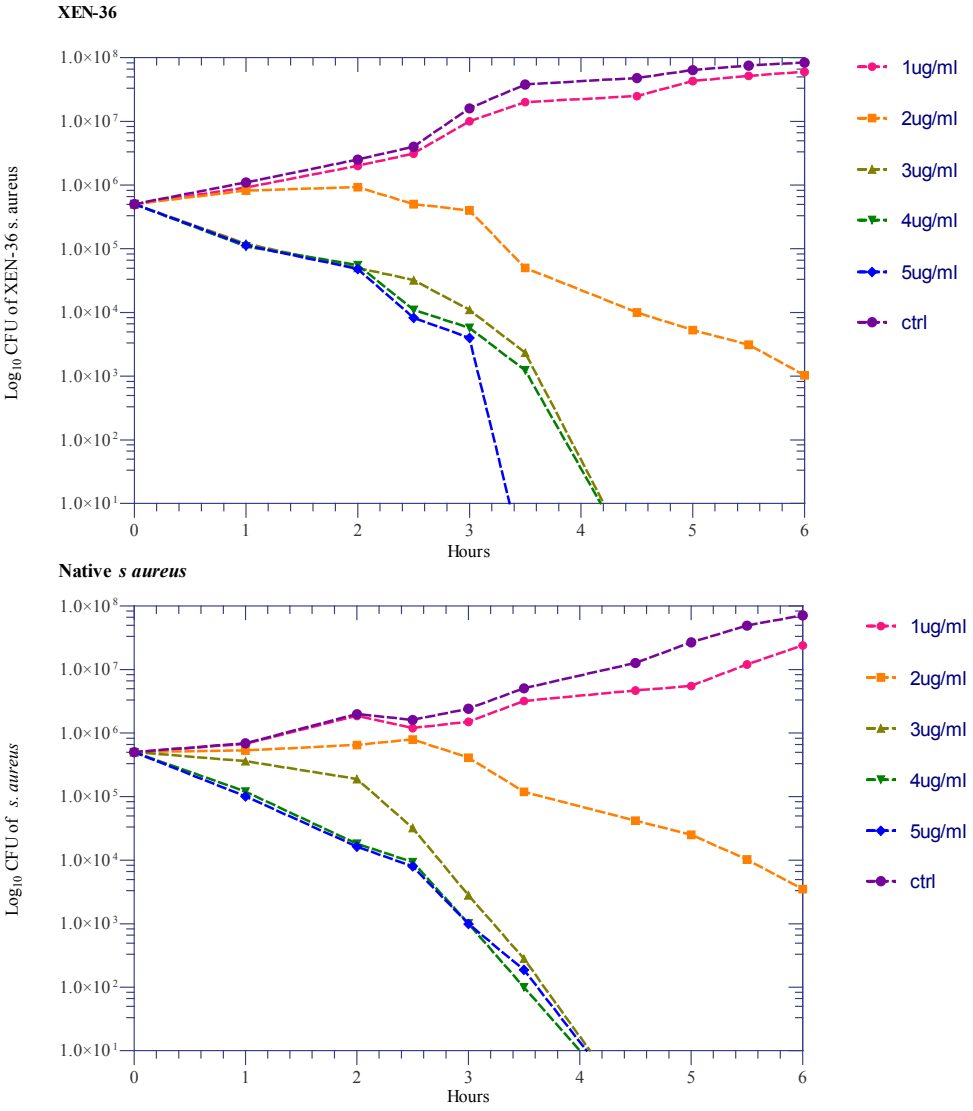

Figure 3.5. Antimicrobial activity in XEN-36 strain and native *s. aureus.* Upper graph represents the reduction in number of Log CFU XEN 36, and lower graph represents the reduction in number of Log of CFU *S. aureus*

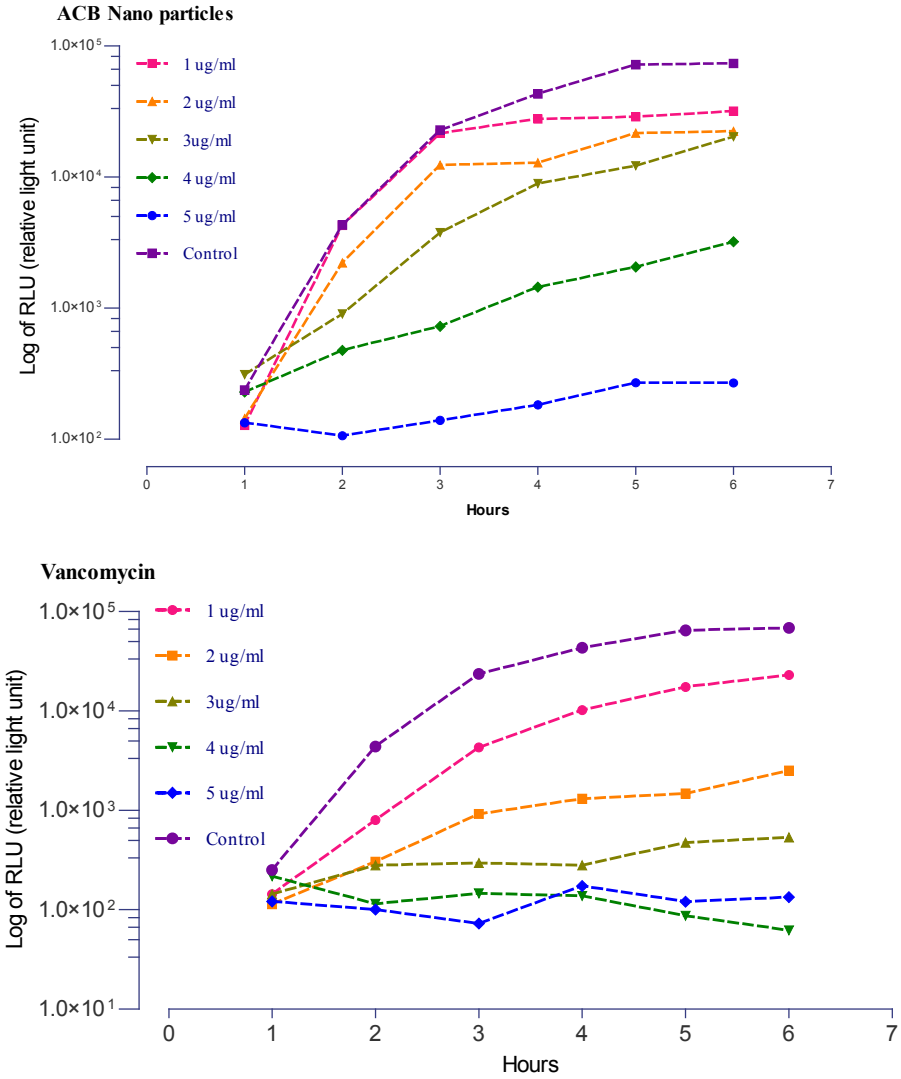

Figure 3.6. Bioluminescence measurements of XEN-36. Upper graph showed the antimicrobial activity by ACB nanoparticles whereas bottom graph represents the antimicrobial activity by antibiotic vancomycin.

3.2.4. Antimicrobial activity on osteoblast cells invaded by *S. aureus*

Osteoblast cell invasion assay was performed as discussed in section 3.1.4. Osteoblast cells infected with *S. aureus* with MOI of 250:1. To assess the antimicrobial activity of internalized bacteria, here in this study the dose was used as 1 µg/ml and 5

µg/ml concentration for 24 hours and 48 hours incubation time. In 24 hour incubation time with 1 µg/ml viable count of internalized bacteria was 1.5 logs less comparing to control as shown in Figure 3.7, while in 48 hours incubation time was seen 4.5 logs down. Similarly, 24 hour incubation time with 5 µg/ml of concentration showed inhibition of infection by 2.5 Logs and while in 48 hours incubation *S. aureus* infection was inhibited by 7.5 logs.

In this study the developed ACB nanoparticles are capable of eliminating the intracellular infection in osteoblast cells similar to ACL nanoparticles; however the antimicrobial activity of ACL was significantly higher than ACB nanoparticles. The importance of ACB nanoparticles over ACL is that, that cellular toxicity will be less comparing to ACL. As will be shown in chapter 4, it was found that ACL nanoparticles exhibited toxicity at 10 µg/ml so the target is to produce equally effective antimicrobial nanoparticles with less toxicity in eukaryotes. In this study it is shown that 1 µg/ml was effective antimicrobial activity in 48 hours it has shown reduction by 4.5 logs which is close to 99.9% inhibition of infection. The cellular toxicity assays associated with ACB nanoparticles will be explored.

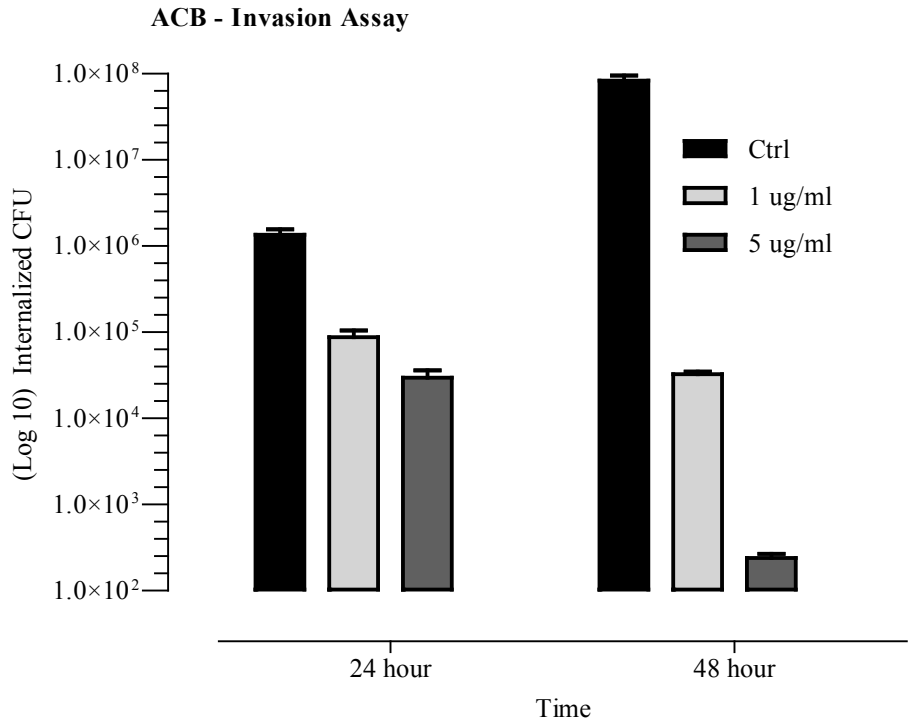

Figure 3.7. ACB – Invasion Assay. Antimicrobial activity of internalized bacteria in osteoblast cells.

CHAPTER IV

TOXICITY ASSAY FOR ACL NANOPARTICLES

Four different assays were used to determine the potential toxicity of nanoparticles on osteoblasts. These assays measure the degree of cell survival/proliferation (MTT assay), or degree of cellular oxidative stress (L-Glutathione depletion, catalase activity and protein carbonyl content).

4.1. MTT Proliferation/Survival Assay

This is simple method for determining cell viability or proliferation. MTT assay developed by Mossman is still among one of the most versatile and popular assays. The MTT assay involves the conversion of the water soluble MTT (3-(4,5-dimethylthiazol-2-yl)-2,5-diphenyltetrazolium bromide) to an insoluble formazan.2-4. The formazan is then solubilized, and the concentration determined by optical density at 570 nm.

Kit was purchased from Invitrogen (*Cat# M-6494*), standard protocol was followed as directed by company in a 96 well plate with 10,000 osteoblast cells / well and nanoparticles with concentrations 1, 5, 10 and 20 μg/ml were added to different wells and incubated for 24 hours, after incubation nanoparticles were washed and MTT assay was performed as directed by kit. By pipetting insoluble pellet was dispersed and absorbance was measured at 570/630 nm.

The co-culture of osteoblasts with nanoparticles for 24 hours at concentrations of 1 or 5 µg/ml had no effect on viability as shown in Figure 4.1. Cell viability was reduced by 25% and 70% when nanoparticle concentration was increased to 10 or 20 µg/ml, respectively; however, 10 µg/ml was statistically non-significant.

It is concluded from the MTT assay, that ACL nanoparticles may be toxic from 10 µg/ml concentration. Further oxidative stress markers will be used in this study to see if less than 10 µg/ml can be toxic to the cell.

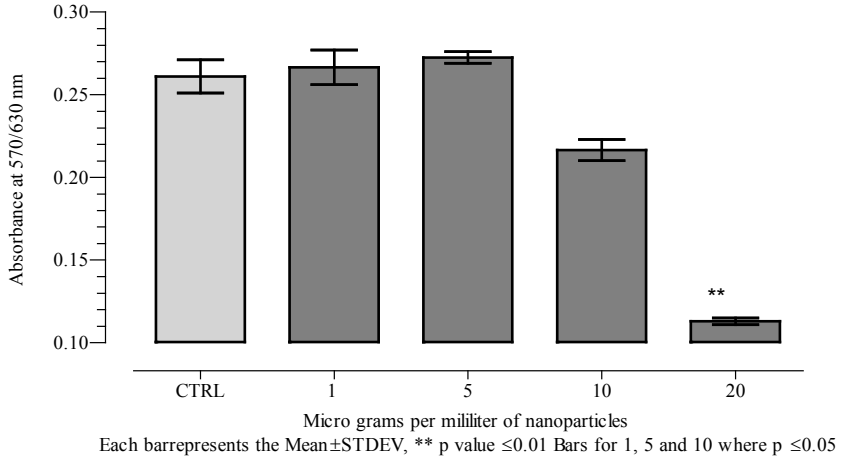

Figure 4.1. MTT assay. Osteoblast cells treated with ACL nanoparticles.

4.2. Oxidative Stress Assays

Osteoblast cells were grown in T-25 culture flasks. When cells were 90% confluent different concentration of nanoparticles as 1, 5, 10 and 15 µg/ml were added and incubated for 24 hours. After incubation cells were washed by PBS buffer pH 7.4 and lysed in a 1 ml of lysis buffer pH-8.8 (50mM of Tris and 1mM EDTA) by cell disruptor in cold conditions. Cells were centrifuged at 10,000g for 10 minutes in a cold centrifuge and supernatant was collected for glutathione assay, catalase activity and carbonyl content. Total protein obtained from supernatant was measured by BCA assay Cat: No. 23227

4.2.1. Glutathione assay

Glutathione is a tripeptide comprised of cysteine, glycine and glutamate. It is an antioxidant, preventing damage to cellular components caused by reactive oxygen species such as free radicals and peroxides. GSH reduces disulfide bonds formed within cytoplasmic proteins to cysteines by serving as an electron donor. In this process GSH is oxidized to glutathione disulfide (GSSG). Reduced glutathione (GSH) was measured by Coleman et al [83]. 2.5 mM of GSH (L-Glutathione) cat# G6013 from sigma, was made in Tris EDTA pH 8.8 buffer, and was serially diluted in Tris-EDTA buffer in a 96 well plate. Each well was added with 100 µl of 2.5 mM of 5,5′-Dithiobis (2-nitroobenzoic acid) DTNB Cat# D8130) from sigma, which was prepared in Tris-EDTA buffer. Plate was incubated for 10 minutes and absorbance was measured at 405 nm. A standard curve was generated from GSH in nanomoles verses Absorbance measured. 100 µl of supernatant of different samples were added to different wells of 96 well plate and

followed by addition of 100 µl of 2.5 mM DTNB reagent and incubated for 10 minutes, absorbance was measured at 405 nm and concentration of reduced glutathione was calculated from standard curve. Concentration of reduced glutathione for each sample was normalized with total protein of each sample and GSH concentration was expressed in nmoles/mg of total protein.

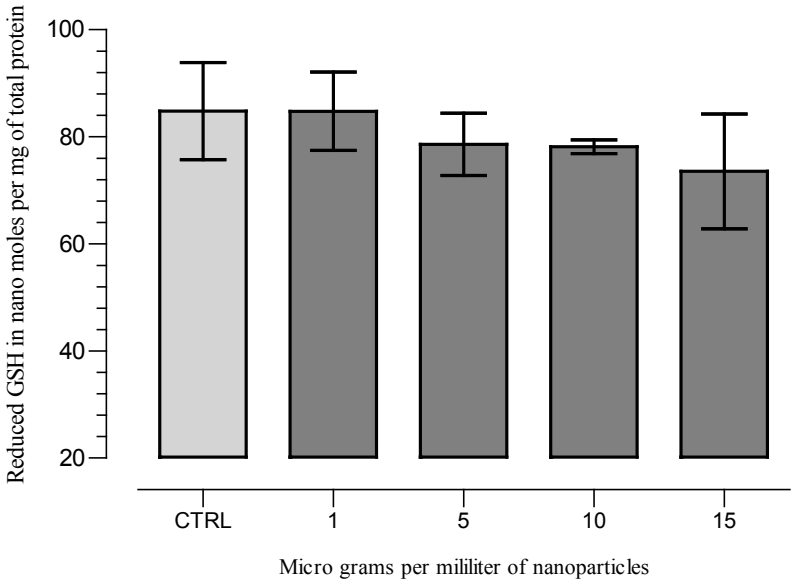

Figure 4.2. GSH assay. ACL nanoparticles were incubated with osteoblast cells for 24 hour, post incubation GSH concentration was measured from soluble proteins.

4.2.2. Catalase assay and protein carbonyl assay

Catalase activity and protein carbonyl content of samples from supernatant of cell lysate was measured by the help of catalase assay kit and protein carbonyl kit respectively and both the kits were used as directed by the manufacturer and were

purchased from Cayman, Catalase Assay kit *Cat. No.707002* and Protein carbonyl assay kit *Cat. No. 10005020*.

4.3. Results And Discussion

The antioxidant activity was measured by determining the levels of reduced glutathione in osteoblast cell cultures after treatment with nanoparticles at different concentrations for 60 hours. As shown in Figure 4.2, no significant decrease in reduced GSH levels was observed up to a concentration of 15 μg/ml of nanoparticles.

The protein carbonyl content was determined in the culture supernatants of osteoblasts after co-culture with nanoparticles. The results, shown in Figure 4.3, indicate that essentially no change in protein carbonyl content was observed when cells were treated with up to 5 μg/ml of nanoparticles. When nanoparticles concentration was increased to 10 μg/ml, a slight but insignificant increase was observed. However, at 15 μg/ml concentration, there was >2.5-fold increase in protein carbonyl content which was statistically significant, suggesting that there is an increase in protein oxidation at higher concentrations of nanoparticles. In a fourth assay, the level of catalase activity was measured, an antioxidant enzyme responsible for the detoxification of hydrogen peroxide, a reactive oxygen species (ROS) and a toxic product of both normal aerobic metabolism and a reactive oxygen intermediate produced in response to microbial pathogens by inflammatory cells. The results of this assay demonstrate that there was a gradual decrease in catalase activity with increasing concentration of nanoparticles Figure 4.3. However, significant reduction in catalase activity was only seen at nanoparticles concentrations 10 μg/ml and above. Taken together, the cellular toxicity data demonstrate

that nanoparticles induce significant toxicity in osteoblasts at concentrations of ≥ 10 μg/ml. Since our study have shown that nanoparticles are effective against intracellular *S. aureus* organisms at 1 μg/ml concentrations, our findings demonstrate that there may be no toxic side effects of nanoparticles on osteoblasts at 1 μg/ml concentration.

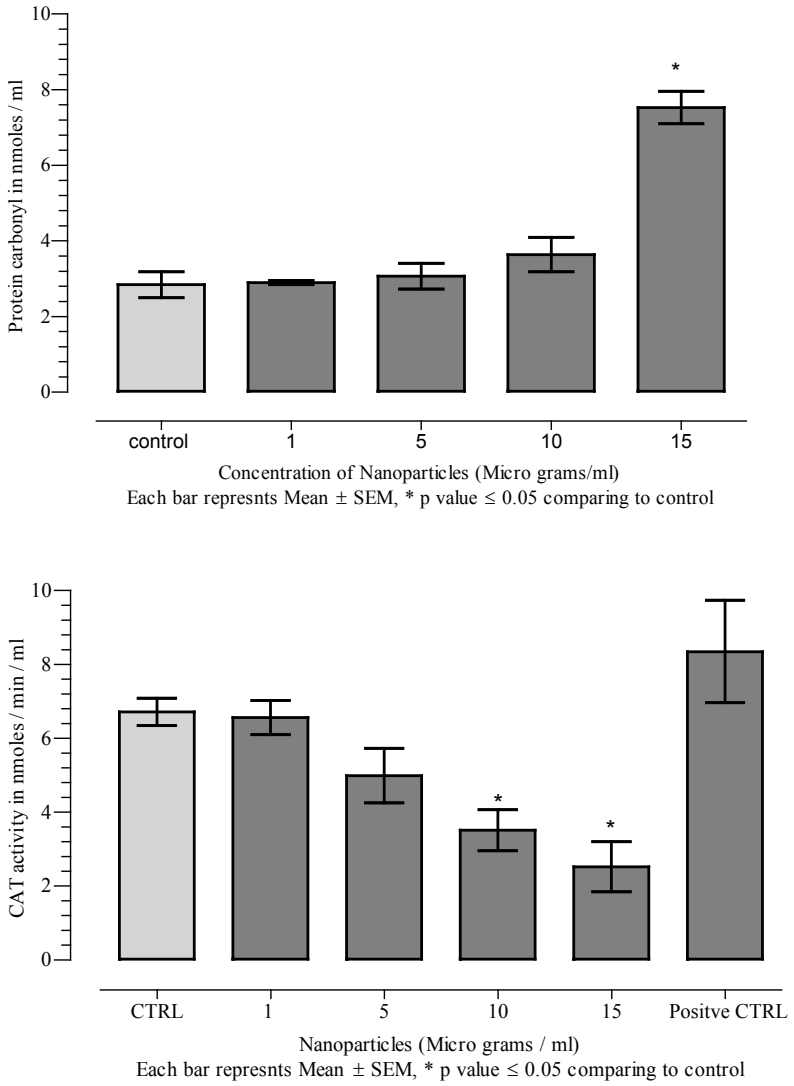

Figure 4.3. Protein carbonyl and Catalase measurement Assay. Upper figure protein carbonyl assay and lower figure catalase assay for ACL nanoparticles.

CHAPTER V

CELLULAR TOXICITY FOR ACB NANOPARTICLES

Toxicity of ACB nanoparticles was assessed similar to ACL nanoparticles, however in addition LDH (lactate dehydrogenase assay); SOD (super oxide dismutase assay) and membrane lipid oxidation assay using C11-BODIPY $^{581/591}$-experiments were performed. Cell proliferation assay WST-1 assay was used instead of MTT assay which forms soluble salt in aqueous so easier to perform; otherwise both have almost similar antimicrobial efficiency and sensitivity.

5.1. Toxicity Assays Of ACB Particles

5.1.1. LDH assay

LDH assay can be performed by assessing LDH (lactate dehydrogenase) release in to the media as a marker of dead cells or membrane damage. CytoTox-ONE assay kit was purchased from Promega Cat. No. G7890. It is a fluorescent measure of the release of lactate dehydrogenase (LDH) from cells with damaged membrane. In this assay conversion of resazurin into resorufin which is a fluorescent with excitation wavelength 560 nm and emission wavelength at 590 nm. Experiment was performed in a 96 well plate with osteoblast cells 10,000 per well. Nanoparticles were added to each well with different concentration from 1 μg/ml to 20 μg/ml concentration and were incubated for

24 hours. LDH assay was performed as directed by manufacturer; fluorescence was measure by using Biotek plate reader.

5.1.2. WST1 Proliferation / survival assay

WST1 Kit was purchased from Clontech (Cat. No. 630118) and was used as directed by company in a 96 well plate with average of 10,000 cells/well in a DMEM: F12 with L-glutamine and 10% Fetal Calf Serum (complete media) and nanoparticles with concentration 1, 5, 10, 15, 20, and 30 µg/ml were added and incubated for 24 hours, after incubation each well was washed with PBS buffer to remove nanoparticles and fresh media was added and WST1 assay was performed as directed by manufacturer. Absorbance was measured at 450 nm.

5.1.3. Oxidative stress measurement assays

Osteoblast cells were grown in a T-25 flask. Different concentrations (1, 5, 10, 15, 20 or 30 µg/ml) of ACB nanoparticles were added and incubated for 24 hours. After incubation cells were washed with PBS buffer pH 7.4 and lysed in a lysis buffer pH 8.8 (50 mM of Tris and 1 mM of EDTA) with protease inhibitor (Sigma Cat. No. P8340) by cell disruptor in cold conditions. Cell lysate was collected in eppendorf tube and centrifuged at 10,000g for 10 minutes in cold centrifuge and supernatant was collected for glutathione assay, catalase activity and carbonyl content. Total protein content in the supernatant was measured by BCA assay and kit which was purchased from Thermo Scientific Cat. No. 23227 and was used as directed by manufacturer, reagents A and B were mixed in 50:1 ratio and 180 µl of mixture of A and B was added to 20 µl of sample

or dilutions of standard curve in a 96 well flat bottom plate. Plate was covered and incubated for 30 minutes. Absorbance was measured at 562 nm by Biotek Plate Reader.

5.1.4. Glutathione (GSH) assay

Biochemical assay by Coleman *et al*.[83] was performed to detect the reduced glutathione from the supernatant of cell extract. 2.5 mM of reduced GSH was dissolved in 10 ml of Tris EDTA buffer and 2.5 mM of DTNB were dissolved in 10 ml of Tris-EDTA buffer pH 8.8, 100 µl of GSH with different molar concentrations were pipetted out in a 96-well plate and then 100 µl of DTNB was added to each 96-well. Absorbance was measured at 405 nm and standard curve was plotted. 100 µl of supernatant from treated or non-treated cells were added to 96-well plate and 100 µl of DTNB reagent was added. Absorbance was measured at 405 nm and concentration of reduced glutathione was calculated from standard curve.

5.1.5. Protein carbonyl and catalase assay

Protein carbonyl content nmoles/ml was measured from supernatant of treated cells with the help of protein Carbonyl kit which was purchased from Cayman, Cat. No. 10005020. Catalytic activity in nmoles/min/ml was measured from supernatant of treated or non -treated cells with the help of Catalase kit purchased from Cayman Cat. No. 707002.

5.1.6. Super oxide dismutase (SOD) assay

Cayman's superoxide dismutase assay kit utilizes a tetrazolium salt for detection superoxide radicals generated by xanthine oxidase and hypoxanthine. One unit of SOD is defined as the amount of enzyme needed to exhibit 50% dismutation of the superoxide

radical. The SOD assay measures all three types of SOD (Cu/Zn, Mn, and FeSOD). The assay was performed as described by manufacturer (Cayman Cat # 706002). Osteoblast cells were grown in T-25 flask cell and at 70% confluency, fresh media was fed to the cells and treated with different concentration of nanoparticles ranging from 1 μg/ml to 20 μg/ml and were incubated for 15 hour hours (overnight incubation) or 48 hours (two days). Post incubation cells were harvested by gently scrapping using rubber policeman and cells were homogenized in a recommended buffer by manufacturer as mentioned in the kit. Standard curve was generated under the instructions of manufacturer and cellular SOD was calculated.

5.1.7. Ration- fluorescence assay of C11-BODIPY $^{581/591}$

Lipid oxidation in cellular membranes has been monitored by undecylamine fluorescein and Hexadecanoyl BODYIP-FL, which monitors only non-oxidized form of these fluorophores, however BODYIP $^{581/591}$ is very suitable for ratio-fluorescence of oxidation process in membranes of living cells [84]. In another study, it was reported that C11-BODIPY is susceptible to oxidation and thereby losing its bright red fluorescence and shifting towards shorter wavelength of excitation and emission 500/510, both spectra are well separated and are used to quantify the fraction of oxidized and non-oxidized C11-BODIPY $^{581/591}$ simultaneously at any time point. These fluorophores are called as surrogate markers of lipid peroxidation [84, 85].

Here fluorophores were used to study the oxidation of membrane lipids in osteoblast cells grown in costar flat bottom 96 well plate. Initially cells were treated with different concentration of nanoparticles of 1, 5, 10, 15, and 20 μg/ml and were incubated

for 24 hours, post incubation cells were washed with PBS buffer pH7.4 Ca^{++} and Mg^{++} free and fed with 100 µl of warm fresh PBS buffer and 5 µM of C11-BODIPY $^{581/591}$ was added to each well. Positive control well 5 mM or 10 mM of hydrogen peroxide was used and incubated for 30 minutes at room temperature. Fluorescence was measured at both wavelengths at the following excitation and emission 575/595 and 505/515 for red and green respectively using Biotek Fluorometer. Data was normalized to percent by taking 10 mM of hydrogen peroxide as positive control 100 % emission for green fluorescence while as negative control was taken as 100% emission for red fluorescence.

5.2. Confocal Microscopy

Osteoblast cells were grown on 18 mm sterile cover slips in a 6 well plate and were cultured up to 60 % confluency. Internalization of bacteria was performed as discussed earlier followed with treatment with nanoparticles with 3 µg/ml, and incubated 24 hours. Cells were washed again with pre-warmed PBS buffer three times and were semi fixed for stability to keep internalized bacteria alive in a 0.5 % formalin for 10 minutes. Post fixation, cells were again washed thrice with PBS buffer and 0.05 % of saponin (Cat. No. 47036, *sigma*) in PBS was added and incubated for 20 minutes, which permeabilized osteoblast cell membrane for propidium iodide dye. Confocal microscopy was used to detect live and dead bacteria; the stain used was from Invitrogen Cat. No. L-7012 with two types of dyes SYTO 9 dye component A and propidium iodide component B. Both the components were mixed in 1:1 ratio final volume of 600 µL solution, out of it 3 µL was added to each well with 3 ml of PBS buffer containing permeabilized cultured cells. Plates were incubated in dark for 15 minutes. Cover slips with growing cultured

cells lying between cover slip and glass slide containing 50 µL of 10% glycerol. Slides were examined Carl Zeiss Axio Observer Z1, Microscope-Spinning Disc Confocal Scanning was done along XYZ plane z height was 15 µm and each section was scanned at 500 nm, to get the three dimensional picture.

5.3. Results

Premixed WST1 assay

Viability in response to cytotoxic effect of nanoparticles on *osteoblast cells measured by premixed WST1 assay.* Cell survival can be assed in response to cytotoxic effect of nanoparticle and was first screened as a measure of mitochondrial dehydrogenase activity; cells treated with 1, 5, 10 15, 20 or 30 µg/ml concentration of ACB nanoparticles did not show any difference comparing to control cells as shown in Figure 5.1. However 20 and 30 µg/ml was significantly different comparing to control.

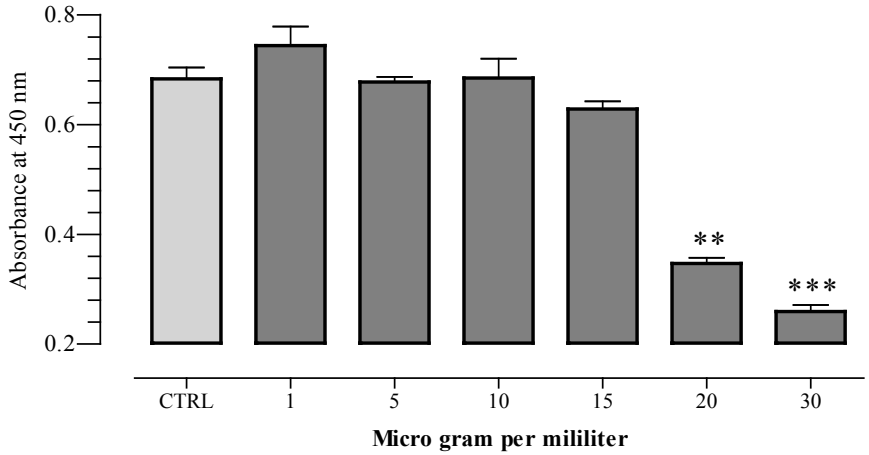

Each Bar represent Mean + SEM, P value ≤ 0.01 as ** and p value ≤ as *** siginificance

Figure 5.1. WST-1 Assay. ACB nanoparticles incubated with osteoblast cells for 24 hours.

LDH assay

This assay is used to analyze the effects on cell growth inhibition and cell death; damaged cell membrane can cause the LDH to leak from the cells and is measured from supernatant. Positive control where maximum LDH is released in supernatant by lysing the cells, here in our study, Triton X-100 was used to lyse the cells as mentioned in protocol, a significant amount of LDH was released at 20 µg/ml concentration of ACB nanoparticles as shown in figure 5.2. These results also confer the results of WST1 assay where 20 µg/ml was also toxic. From 1 to 15 µg/ml concentration of ACB nanoparticles did not show any difference comparing to control group.

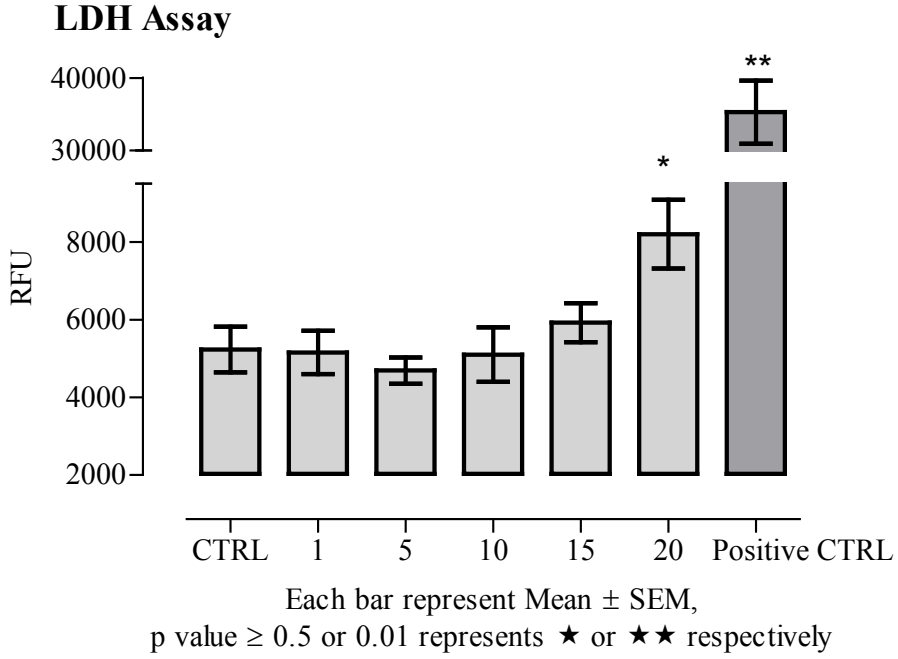

Figure 5.2. Cell Viability and toxicity assay. LDH assay by measuring LDH release from osteoblast cells in cell culture media of osteoblast cells treated with ACB nanoparticles.

Oxidative stress

Oxidative stress was a measure of reduced glutathione, protein carbonyl content and catalase activity. Oxidative stress could be measured by elevated or decreased levels of reduced GSH, If the concentration of free radicals generated exceed to reduced GSH molecules that will result in overall reduction in reduced glutathione and is considered as oxidative stress generated by ROS species, however an elevated level of reduced GSH in treated cells could be mild stress where ROS species are lesser than reduced GSH molecules, that elicits feedback cellular response and generates more reduced glutathione to protect cellular compartment from oxidative stress damage.

Reduced glutathione was measured from non-treated and treated cells as described in methods. ACB nanoparticles with concentrations of 1, 5, 10, and 15 µg/ml did not show any difference comparing to non-treated cells as shown in figure 5.3. However 20 and 30 µg/ml concentration was discontinued in the experiment because of toxicity observed in proliferation assay. Reduced glutathione concentration was normalized with total protein extract obtained from osteoblast cells.

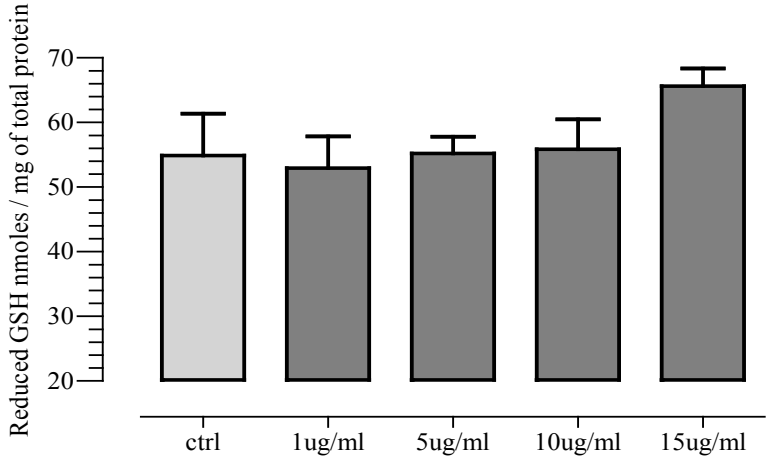

Each Bar represent Mean + SEM, P value > 0.05 as non-siginificance

Figure 5.3. GSH assay. Measured reduced GSH concentration in ACB nanoparticles treated Osteoblast cells for 24 hour.

Protein carbonyl content is a measure of oxidation of proteins and in this experiment following concentrations 1, 5, 10 and 15 µg/ml concentration of nanoparticles did not show any difference comparing to non-treated cells but 15 µg/ml was considered as toxic dose and was statistically significant comparing to control as shown in figure 5.4 upper panel. Catalase activity was also measured for the same protein extract which was used for glutathione and protein carbonyl content. Catalase enzyme is ubiquitous enzyme

that is present in most aerobic cells. Catalase (CAT) is involved in detoxification of hydrogen peroxide, a reactive oxygen species (ROS), which is toxic product of both normal aerobic metabolism and pathogenic ROS production. This enzyme catalyzes the conversion of two molecules of hydrogen peroxide to molecular oxygen and two molecules of oxygen (catalytic activity). CAT also demonstrates peroxidatic activity, in which low molecular weight alcohols can serve as electron donors. The nanoparticles concentrations 1, 5, 10 and 15 µg/ml was non-significant using student t-test comparing to control group as shown in figure 5.4 lower panel, although catalytic activity of 10 and 15 µg/ml was suspected might have toxicity because the catalase activity difference was by 3 nmoles comparing to control group but statistically was non-significant with p value = 0.162 and 0.152 for 10 and 15 µg/ml concentration respectively.

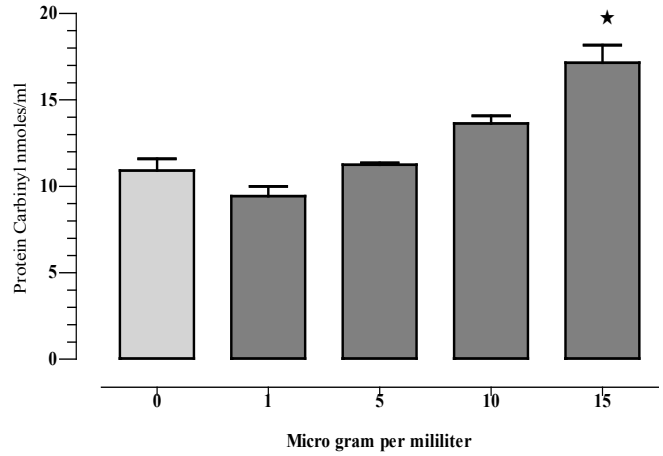

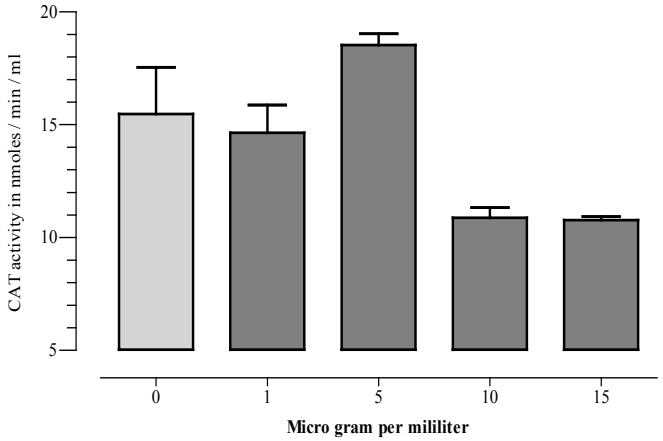

Figure 5.4. Protein carbonyl and Catalase assay. Upper figure shows Protein carbonyl content of ACB nanoparticles treated osteoblast cells for 24 hour and lower figure shows catalase activity of ACB nanoparticles treated osteoblast cells for 24 hour.

Superoxide dismutases (SODs) are metalloenzymes that catalyze the dismutation of the superoxide anion to molecular oxygen and hydrogen peroxide and form a crucial part of cellular antioxidant defense mechanism. In human three forms of SOD: cytosolic Cu/Zn-SOD, Mitochondrial Mn-SOD, and extracellular SOD, in this assay all three SODs are measured as total SOD activity.

SOD activity was measured after treating osteoblast cells with nanoparticles for 15 hours or 48 hours with different concentrations of nanoparticles as shown in Figure 5.5. Standard curve was generated from the designed experiment to obtain final results. In 24 hr. incubation of osteoblast cells with nanoparticles at different concentrations such as 1, 5, 10, 15 and 20 μg/ml, there was no significant change observed in SOD activity comparing to control group up to 15 μg/ml of ACB nanoparticle concentration, however at 20 μg/ml the SOD activity was slightly higher comparing to control and student T test was performed where p value was ≤ 0.05 and showed statistically significant difference for 20 μg/ml. which indicated the higher activity of superoxide dismutase within the intracellular environment possibly because of Superoxide radicals generated by nanoparticles, and keeps the superoxide radicals low to prevent cells from oxidative stress. This protective mechanism of SOD may also be responsible for lowering the toxicity of metallic nanoparticles from further damage.

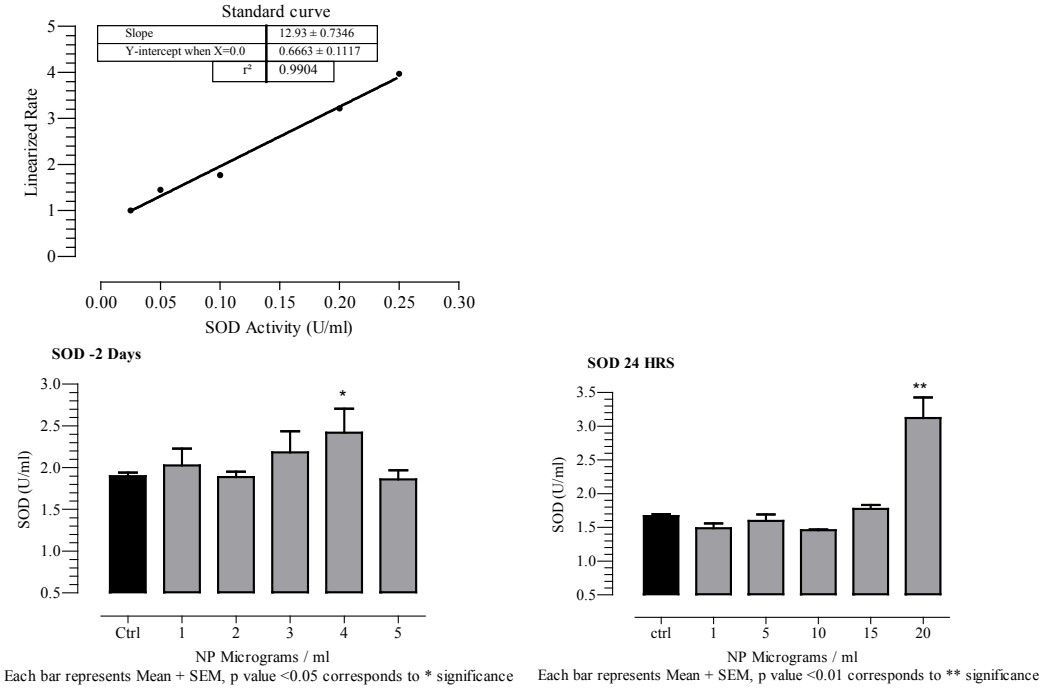

Figure 5.5. SOD Assay. SOD activity of osteoblast cells treated with ACB nanoparticles for 24 hours in middle panel of the graph and Lower panel of graph shows the SOD activity for 48 hours treatment of ACB nanoparticles. Upper panel of graph represents standard curve.

BODIPY® $^{581/591}$ undecanoic acid can be used to detect reactive oxygen species (ROS) in cells and membranes. Oxidation of the polyunsaturated butadienyl portion of the dye results in a shift of the fluorescence emission peak from ~590 nm to ~ 510 nm. Ratio-fluorescence of C11-BODIPY $^{581/591}$ data was obtained and normalized to percent of emission of fluorescence as mentioned earlier in protocol. We did not observe any significant changes in emission spectra of groups treated with ACB nanoparticles comparing to non-treated group control, however at concentration 20 µg/ml there was 10% loss of emission of red fluorescence which indicates oxidation of lipids in

membrane and same time there was gain of 13.5% of green fluorescence as shown in figure 5.6. This emission loss and gain corresponds to oxidation of lipids in the membrane. However it cannot be specified which group of lipids is oxidized; this assay can quantify whole lipids within the cell membrane.

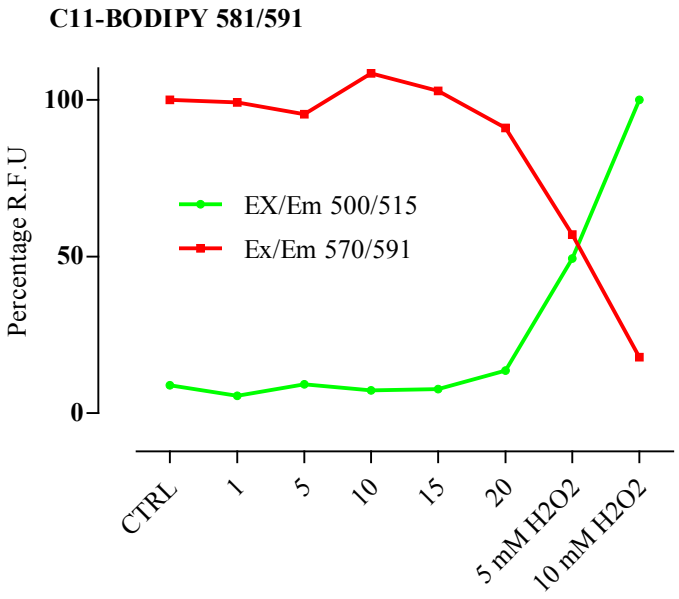

Figure 5.6. Lipid oxidation Assay. Cell membranes of osteoblasts stained by C11-BODIPY $^{581/591}$ after treating with ACB nanoparticles for 24 hours.

Confocal results

The fate of internalized bacteria was enumerated as live or dead for green or red color respectively by confocal microscopy as shown in figure 5.7. **Control Group 1** was neither infected nor treated with antibiotic or nanoparticles and did not show any sign of infection in terms of dense green or red sports. **Group 2 *S. aureus* infected**, was observed as *S. aureus* infected as green spots and was not treated with gentamicin or ACB nanoparticles hence no dead bacteria were expected and the population of internalized bacteria was high comparing to treated groups. **Group 3, *S. aureus* infected and treated with 200 µg/ml of gentamicin**, live *S. aureus* were seen as green spots and few dead bacteria 2-3 in number per each cell were dead because in 48 hour incubation gentamicin may get permeabilized at very low concentration can cause death of bacteria, moreover dead bacteria can also be internalized as efficiently as live bacteria. Overall the bacterial population was reduced in gentamicin treated group, gentamicin in media keeps continuously killing bacteria coming out of cells, bacterial cells transport in and out spontaneously as a result also leads to reduction in infection. **Group 4 infected with *S. aureus* and treated with Ag-Cu-B** (ACB) nanoparticles, red spots seen were dead *S. aureus* and few green which were considered alive, also the total number of bacteria (live and dead) were very few comparing to gentamicin treated group. This experiment also confirmed the antimicrobial activity of ACB nanoparticles at intracellular level and also supports the experiment of invasion assay for antimicrobial activity in internalized *S. aureus*.

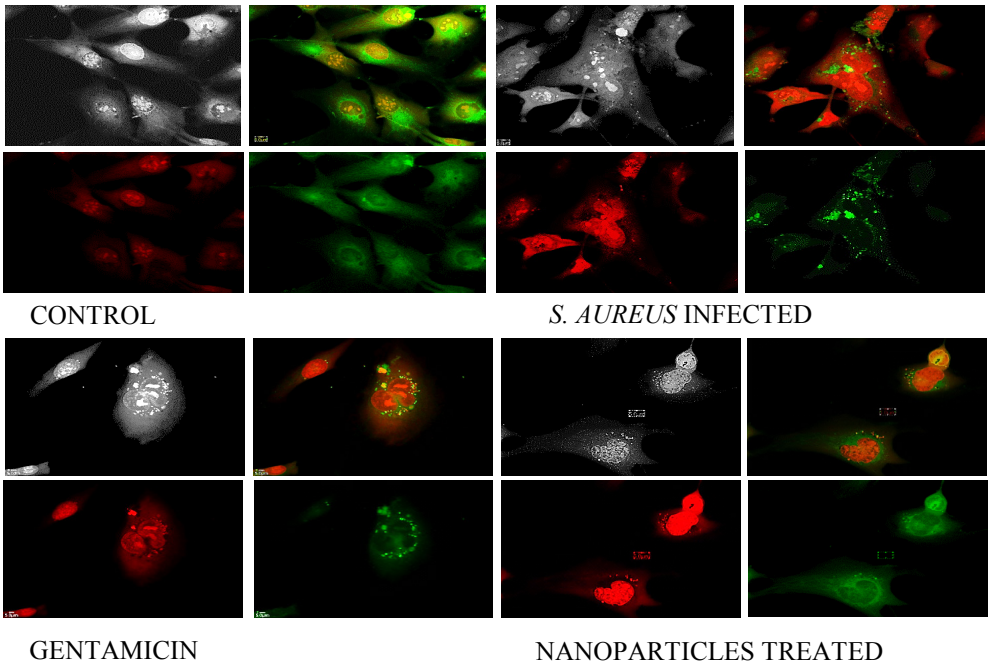

Figure 5.7. Confocal studies. Osteoblast cells invaded by *S. aureus* and treated with Gentamicin or ACB nanoparticles. Upper left panel shows control group and upper right panel shows osteoblast cells infected with *S. aureus* without treatment, Lower left panel shows infected osteoblast cells treated with Gentamicin and Lower left panel shows infected Osteoblast cells treated with 1 µg/ml ACB nanoparticles.

5.4 Conclusion

The antimicrobial efficacy and cellular toxicity associated with ACL and ACB nanoparticles is presented. It was found that ACL particles were more efficient antimicrobial nanoparticles comparing to ACB, however the toxicity associated with ACL particles was close to or 10 µg/ml which was shown by catalase activity. In comparison, the significant toxicity for ACB nanoparticles was observed at 20µg/ml by WST1 and LDH assay, only protein carbonyl content for ACB nanoparticles was significant at 15 µg/ml which was analyzed as very low stress comparing to ACL

nanoparticles. Efficacy of ACB nanoparticles were also shown my confocal studies where 1 µg/ml concentration showed significant reduction in internalized CFU.

Based on the antimicrobial efficiency and minimum toxicity of ACB nanoparticles, this study suggested use of animal study to explore the toxicity in *in-vivo* in which similar dose 1 mg/kg of b. wt. was parallel to 1 µg/ml used in *in-vitro* studies. However 2 mg/kg of b. wt. was also studied as higher dose.

This study has shown the efficacy of ACB particles to clear internalized infection and encouraged the development of osteomyelitis model in mouse to evaluate the efficiency of antimicrobial activity in *in-vivo*.

CHAPTER VI

TOXICITY IN ANIMAL STUDIES

Based on the antimicrobial potential of ACB nanoparticles to fight against internalized infection at in-vitro study, animal toxicity experiments were conducted to predict the safe dose that can be used in *in-vivo* study. Silver nanoparticles distribution in vital organs have been reported among rats, mouse, and rabbit [86]. It was shown that the silver nanoparticles are excreted from the body. The silver nanoparticles dose varied from 9 mg/kg of body weight to 90 mg/kg of body weight for 28 days. Silver clearance was studied from post 28 days for 1 week or 8 weeks, it was found with time silver was cleared from tissues except the concentration of silver in brain and testis was high [86]. However the silver ions released from nanoparticles caused biological activity [87, 88]. ACB nanoparticles are different than early suggested nanoparticle by composition which are composed of three elements as discussed, besides silver-copper antimicrobial activity, it is believed that boron helps in slowing the release of ions which may also help in reducing the toxicity and long term antimicrobial effect. Hence, it is suspected that ACB nanoparticles might have less toxicity compared to silver alone nanoparticles where release of silver ions is very random and fast.

6.1. Animal Use

All experiments were conducted at the Animal Care Facilities of Faculty of Medicine and Health Sciences at the University of United Arab Emirates at Al Ain UAE. The animal facility provides for, and is in charge of care of, the laboratory animals in accordance with all policies of United Arab Emirates that are similar to USDA and US Public Health Service. A Surgeon, professor of Anatomy (Dr. Eric Brown), and certified animal care support personnel were available and were able to provide professional veterinary, surgical and animal care services in support of investigators' animal use studies. Animal welfare is closely monitored by a committee appointed by the University Chancellor.

6.2. Methods And Materials

All Animals studies were performed under university committee for animal resources approved protocols. After i.p. injections of nanoparticles, animals were returned to standard isolator cages. B-6 mice (20 g) mice with 7 mice in each group, one group were injected i.p. with ½ ml of 40 μg/ml (1 mg/kg of body weight) of ACB nanoparticles (equivalent of 1 ml of 20 μg/ml localized injection) and the second group was injected i.p with ½ ml of 80 μg/ml (2 mg/kg of body weight) with ACB nanoparticles (equivalent of 1 ml of 40 μg/ml localized injection). Following the nanoparticles injection by 4 hours and 24 hours blood was collected for platelets, white blood cells and red blood cells count and hemoglobin, enzyme analysis (AST, ALT, LDH, BUN, Creatinine). Group of mice with 4 hour and 24 hour post subcutaneous injection of nanoparticles were sacrificed and vital organs including; brain, heart, lungs,

kidney and liver were dissected out and fixed in 4% formalin, post fixation portion of each vital organ was lyophilized and 500 mg of each organ weighed out and digested in 5% nitric acid overnight and homogenized. Aliquot of homogenate was diluted in 5% nitric acid serial dilutions were made for use of ICP-ES-700 spectrophotometer for estimation of silver, copper and boron elements.

6.3. Results

In-vivo toxicity was primarily screened from blood profile as shown in figure 6.1; to check the immunotoxicity. Platelet count (PLTS), red blood cells (RBC), white blood cell count (WBC), hematocrit (HCT) and hemoglobin (Hgb) value. Treated groups of mice were non-significant compared to control as shown in figure 6.1. All the values were observed in the normal range as control with no significant change.

Blood biochemical analysis was carried out for 4 hour and 24 hour post nanoparticle injection on the groups with low dose (1 mg/kg of body weight) as shown in figure 6.2. There was no change in any enzyme tested compared to control. AST and ALT is indicative of liver injury. Theses enzymes in all groups of treated or non-treated in the normal range, signifying there was no indication of acute hepatotoxicity. LDH and BUN which are markers for tissue damage and renal function respectively and both were also in the normal range for treated and non-treated group. Another group of mice for 4 hour post nanoparticle injection with high dose (2 mg/kg of body weight) as shown in figure 6.3 for blood profile, there was no change observed compared to control group. However, the group with high dose 2 mg/kg of body weight, post 4 hour injection; liver enzymes (AST and ALT) were significantly different than control group, whereas LDH, BUN and

creatinine was normal as shown in figure 6.4. Group with 1 mg/kg of body weight injection via i.p. post 4 hour and 24 hour injection the distribution of silver, copper and boron is as shown in Figure 6.5. In 4 hour treatment the amount of nanoparticles in vital organs was increased in 24 hour incubation which was indication that the ACB nanoparticles takes longer than 4 hour to be distributed in organs and tissues, while as boron was very less in 24 hr compared to 4 hr and was believed may be due to its low concentration compared to silver or copper. With 2 mg/kg of body weight the nanoparticles was slightly higher in liver comparing to other organs as shown in figure 6.6. and measured for 4 hr only.

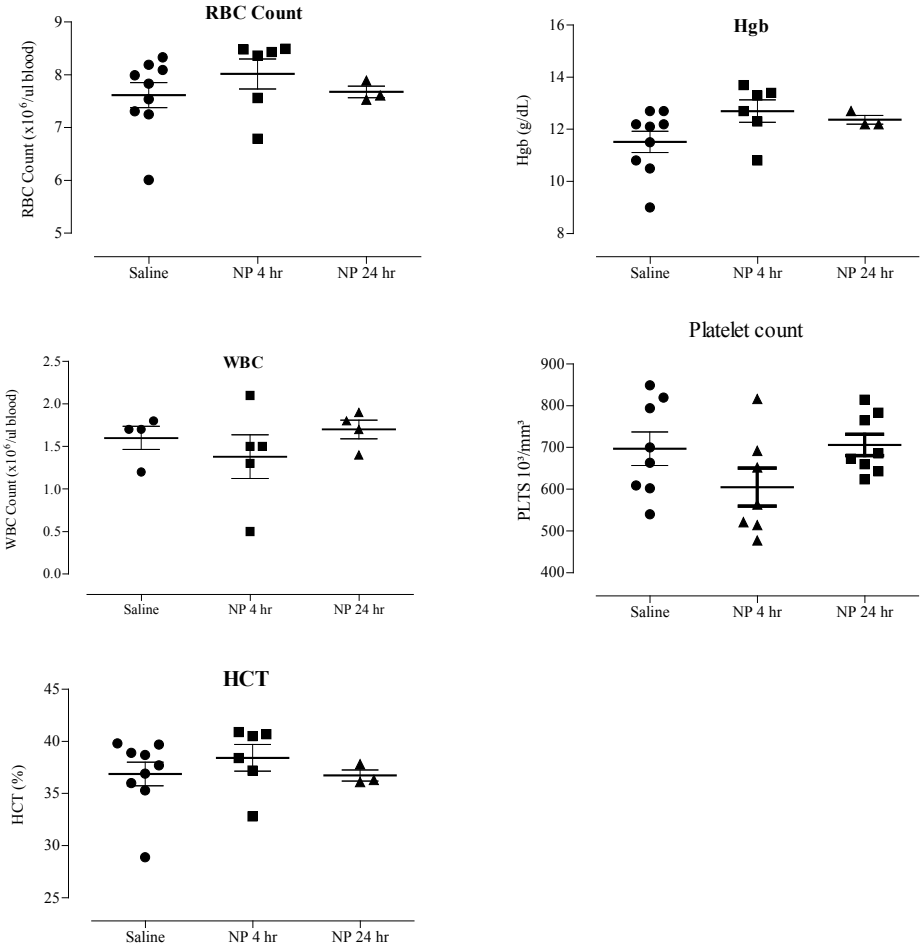

Figure 6.1. Blood analysis of B-6 mice. Groups treated post 4 hour or 24 hour with nanoparticle injection or saline.

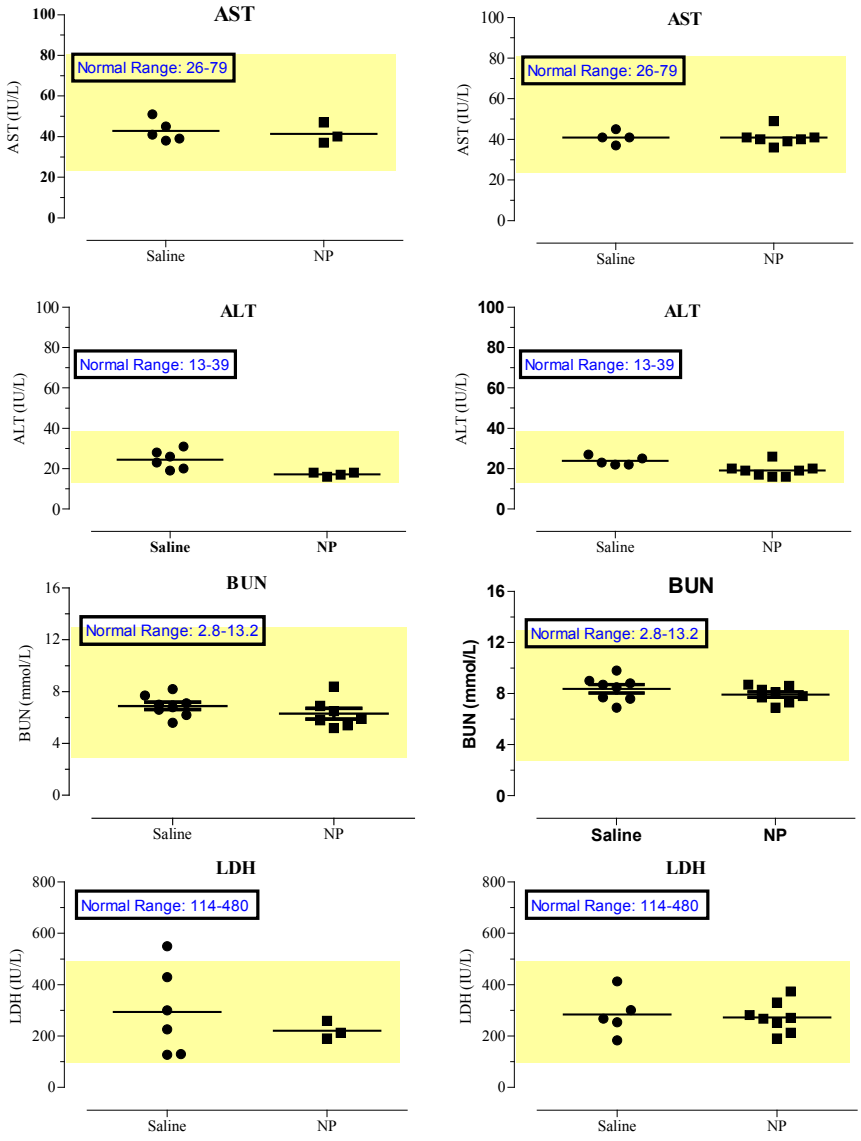

Figure 6.2. Enzyme analysis of B-6 mice. Groups treated with ACB nanoparticle 1 mg/Kg body weight or saline via i.p. Left panel shows post 4 hour treatment analysis and right panel shows post 24 hour treatment analysis.

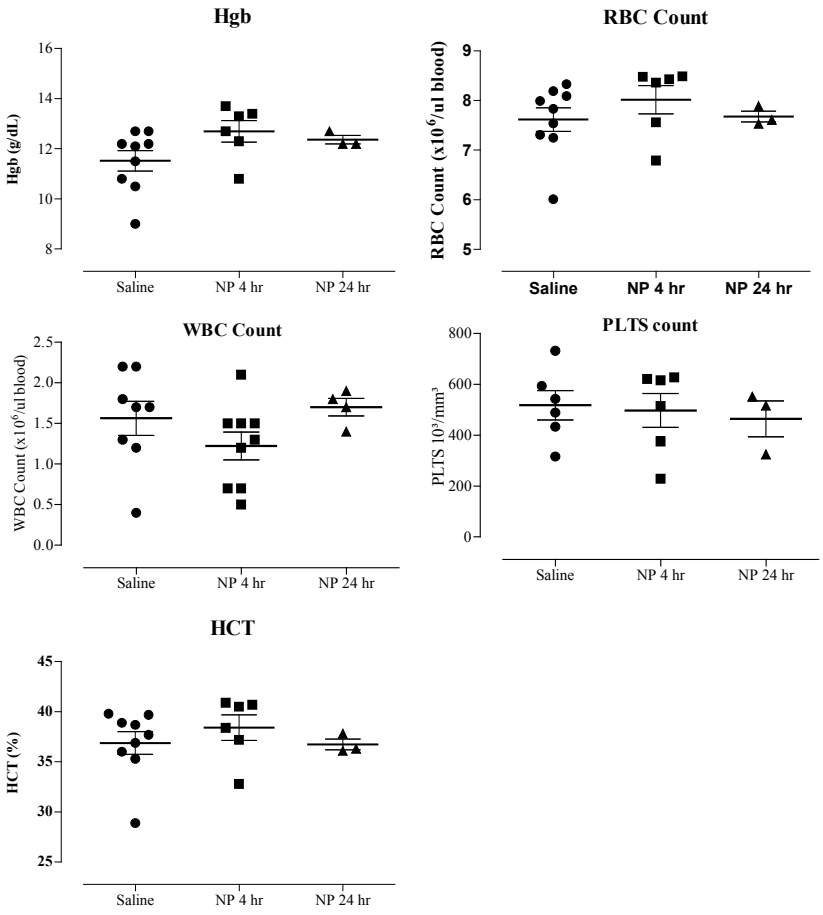

Figure 6.3. Blood profile of B-6 mice. Analysis done post 4 hour treatment with 2 mg/kg of body or saline via i.p.

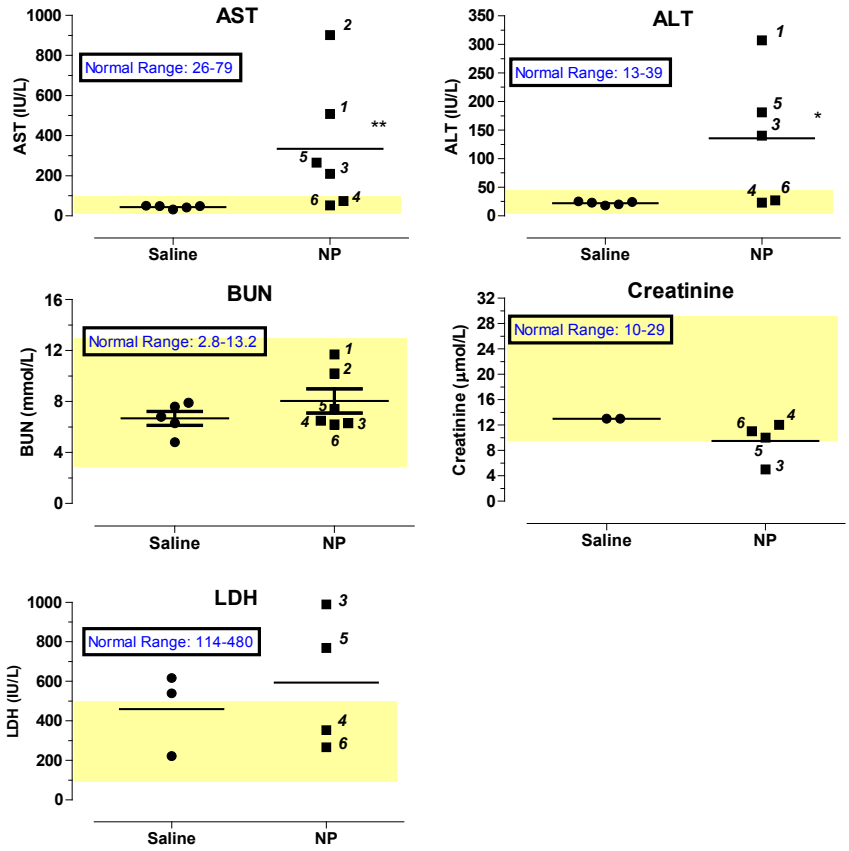

Figure 6.4. Enzyme analyses for 2 mg/kg of body weight. Treated and non-treated groups were analyzed post 4 hour of nanoparticle injection or saline via i.p.

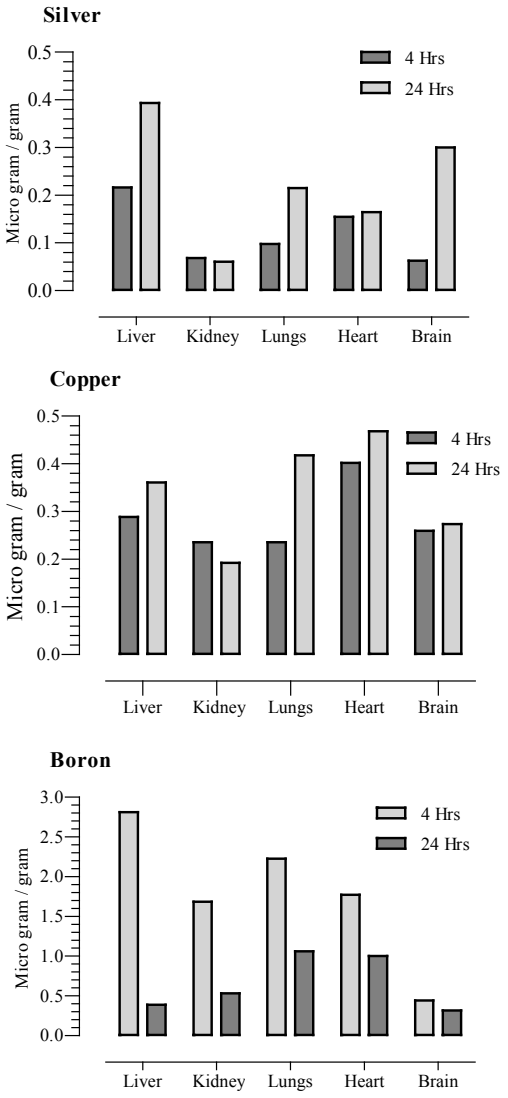

Figure 6.5. Elemental distribution for 1 mg/kg b.wt. of nanocidals. Groups injected with ACB nanocidals via i.p. were analyzed post 4 hour or 24 hour treatment.

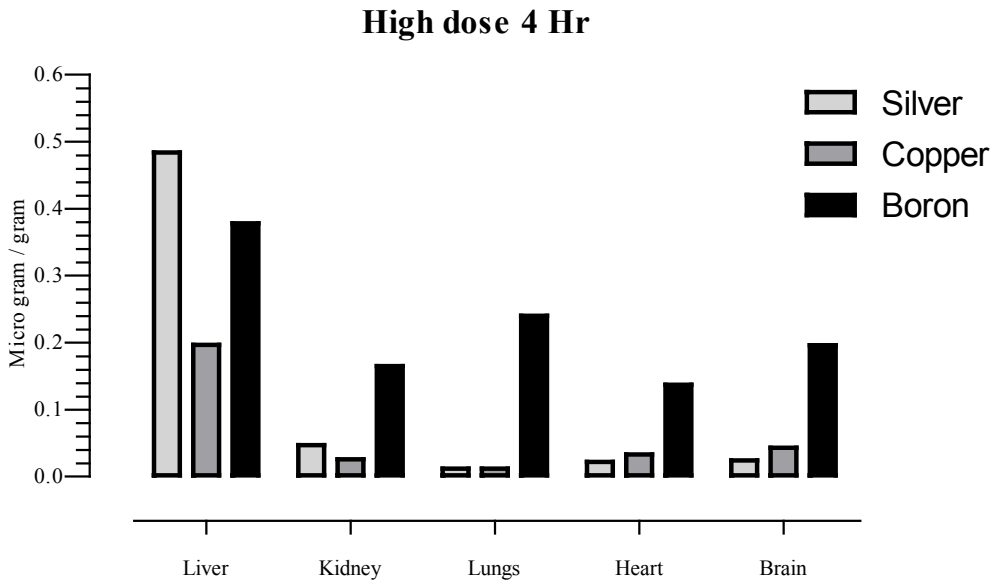

Figure 6.6. Elemental distribution for 2 mg/kg of b. wt. of nanocidals. B6 mice groups injected with nanocidals were analyzed post 4 hour treatment.

6.4 Discussion

In-vivo experiments were carried in this study to detect the toxic dose among animals. It was found that nanoparticles administered via i.p 1 or 2 mg/kg of body weight did not show any response in blood profile comparing to non-treated post 4 or 24 hrs. of i.p. administration which signifies that there was no non-specific immune response. The liver enzymes aspartate aminotransferase (AST) and Alanine aminotransferase (ALT) which are biomarkers for liver damage were studied. Lactate dehydrogenase (LDH) enzyme in glycolysis used as biomarker for tissue damage. Blood Urea nitrogen (BUN) as a measure of renal function. For groups treated with 1 mg/kg of body weight there was no significant change was seen in AST, ALT, LDH, and BUN compared to non-treated groups of mice, which is signifying that there may be no acute hepatotoxicity or renal

toxicity associated and neither any tissue damage within the body. However in groups treated with 2 mg/kg of body weight, there was significant changes observed in liver enzyme ALT and LDH, this sign may be considered as toxic dose and was speculated that ACB nanoparticles or ions released may accumulate in liver at certain concentration. In previous study, it was reported that mice were exposed to silver for 28 days by oral administration, with 0.25, 0.5 and 1 mg/kg of body weight only, 1 mg/kg showed significant changes in liver enzymes [89]. In another study, rats were exposed to 90 or 9 mg/kg of body weight with nano-silver or sliver salts for 28 days and did not observe any significant changes in liver enzymes, and 8 weeks post dosing silver was cleared from most of organs except from brain tissues where concentration was higher compared to other organs [86]. In these studies, it is not understood the reason for 1 or 90 mg/kg of body weight being nontoxic or toxic respectively, It is concluded that animals has tolerance for silver and it varies for other types of animals.

However, 2 mg/kg of body weight did show elevation in liver enzymes but such changes in liver enzyme concentration could be reversible. More studies are required to explain the toxicity from the silver nanoparticles or ionic silver. The fate of nanoparticles after injection in mouse is not studied well but the assumption is that once they reach to tissues, nanoparticles can be digested into ions because of lactic acid present in tissue, as mentioned elsewhere in paper lactic acid was used to reduce the size of nanoparticles, in humans most of lactic acid is produced from red blood cells and muscles [90]. Moreover, the distribution of released ions of silver, copper and boron in mice was examined by ICP-ES spectrophotometer and our data suggested these ions are excreted from the body

with time and it takes more than 4 hours to be absorbed from i.p. for its distribution via blood to rest of the body tissues or organs. Mice with toxic dose, nanoparticle accumulation was higher in liver that could be another reason for significant changes in liver enzymes and it was studied only for two experimental groups 4 hours and 24 hours. The experiment was designed to evaluate the rapid distribution of nanoparticles or ions released from nanoparticles so the data cannot be assumed as total retention of nanoparticles by organs or tissues. It is observed that in 4 hours all vital organs has lesser silver or copper concentration comparing to 24 hr, from this data it is concluded that 4 hr may be less time to be absorbed 100% of the loaded particles and may require more than 4 hours. Although the boron behavior was opposite to that of silver and copper, higher concentration at 4 hr and less in 24 hr, this may be due to the fact that boron is present in trace amounts compared to silver or copper. Further investigation is required with groups more than 2 days to 7 days of post i.p. Injection for elemental analysis and equally if any immunogenic response is elicited also need to investigated.

CHAPTER VII

OSTEOMYELITIS ANIMAL MODEL

Osteomyelitis animal model was first attempted by Rodet 1885, followed by Lexer 1894 where they simply injected attenuated *S. aureus* into rabbits and determined that it is impossible to develop medullary infection by intravenous injection of *S. aureus* alone [91]. Only few works were followed in first half of 19th century by Starr in 1922 and Haldeman in 1934 and Thompson and Dudos in 1938 where they inject *S. aureus* directly or indirectly into the bone, osteomyelitis lesions were observed and did not mimic human infection conditions [92]. Several years latter chronic osteomyelitis model was reported by Scheman et al in 1941 [93] by using rabbits, *S. aureus* and sodium morhuate was directly injected into the tibia metaphysis. This rabbit model was further studied and nurtured by Nordon in 1970 [94] and Andriole et al in 1973 [95]. From 1960 up to 1997 several animal models were developed including rats, dogs, chicken, guinea pigs and very few models of mice.

7.1. Mouse Tibial Models

First mouse tibial model was demonstrated by Ueno in 1974 and followed by numerous scientists. A 3 –mm long briaded silk suture with size 3-0 was soaked in *S. aureus* and *P. aeruginosa* suspensions and this piece of infected thread was inserted in needle-created hole at tibial metaphysis of mice. This model was reported as successful model of osteo-myelitis and resembles as human osteomyelitis.

In 1979 an excellent mouse hematogenous model was reported by Kobayakawa and investigated the effect of foreign body (3mm long silk thread size 5-0) introduction in to the proximal tibial metaphysis. They observed that almost all bones were infected first and latter significant proliferation was in femur and tibia. They believe thread has significant effect in retention of bacteria in bone and two weeks post inoculation they also reported that thread exerts no effect in on distribution and proliferation except the retention of bacteria in bone. Chadha et al and Yoon et al reported another model of osteomyelitis by involving upper epiphyseal injuries and intravenous injection of bacteria. They observed swelling and warmth of limb and abscess formation was evident in proximal tibia. They also showed histological studies for the evidence of osteomyelitis and evidence of recovery of *S. aureus* from infection site.

Common routes of inoculation

Three routes have been reported:

1. Local inoculation to the bone cavity.
2. Local inoculation through nutrient arteries and systemic infection through i.v.
3. Local inoculation of bacterial suspension by whole drilled in bone.

An alternative method is by implanting foreign material with infection that was recently developed. *S. aureus* strain was incubated with stainless steel and mouse tibia bone was drilled by 18g needle and infected pin was inserted and sides were bent. *S aureu*s strain they used was XEN-36 a bioluminescent bacteria where the progression of infection was monitored by Xenogen IVIS camera system. Table 3.1 summarizes the different routs to induce osteomyelitis in animals [92]

Table 7.1. Animal and bacterial species for inducing experimental Osteomyelitis.

Animal	Bacteria	Site	Implant
Chicken	***S. aureus / E. coli***	**i.v.**	
Guinea pig	***S. aureus***	**Femur**	**IM pin**
Rabbit	***S. aureus***	**Tibia**	
Dog	***S. aureus***	**Tibia**	
Sheep	***S. aureus***	**Tibia**	
Goat	***S. aureus***	**Tibia**	**Bone wax**
Rat	***S. aureus***	**Tibia**	**IM K-wire**
Mouse	***S. aureus***	**Tibia**	**Silk thread**
Mouse	***S. aureus***	**Tibia**	**Transcortical pin**

7.2. Methods And Material In Osteomyelitis Mouse Model (BALB/C)

In this study BALB/c mouse was used to generate osteomyelitis in left tibia bone infected with *S. aureus* with the aid of braided silk suture. The formation of osteomyelitis was followed by injection of ACB particles. Osteotomy of tibia was performed under aid of anesthetics Xylazine 100mg/kg of body weight and Ketamine 10 mg/kg of body weight.

S.aureus XEN-36 strain which was derived from the parental strain *S. aureus* ATCC 49525, stock was stored in glycerol at -80°C. This kanamycin resistant XEN 36 was streaked on tryptic soy agar plate and recommended dose of kanamycin was 200 µg/ml. Bacterial colonies grown on T-soy agar plate were inoculated into 5 ml of T-soy broth and cultured stationary overnight with aeration. The overnight grown bacterial

culture was then sub-cultured at 1:5 ratio and grown to mid-log phase for another 2 hours with shaking at 200 rpm and was stopped when O.D. reached to 0.5 at 600 nm.

7.2.1. Confirmation of CFU's with O.D 0.5 at 600 nm

With 0.5 O.D. at 600 nm, bacterial cells in 5 ml of T-soy broth were harvested by centrifugation at 4000 rpm for 20 minutes and the pellet was re-suspended in 5 ml of PBS pH 7.4. Serial dilutions were performed in sterile PBS and 100 µl aliquots were plated on T-soy agar plates with 200 µg/ml kanamycin. With bacterial colony forming units (CFU's) were enumerated after overnight incubation at 37°C. Moreover selected colonies were dissolved in PBS buffer with pH 7.4 and bioluminescence was measured using Perkin Elmer Illuminometer to confirm the XEN-36 strain besides kanamycin selection.

7.2.2. XEN-36- *S. aureus* growth on braided silk suture

Braided silk suture 0-3 size reverse cutting edge was purchased from SMI, REF.NO. 8151516, LOT NO. 110623 was immersed in a culture of XEN-36 in T-soy broth with 200 µg/ml of kanamycin with 0.5 O.D. at 600 nm which corresponds to 7×10^7 CFU' per ml. Silk suture was incubated in bacterial broth for 45 minutes or 150 minutes. After incubation silk suture was gently washed in PBS and a piece of 2 cm was cut with the help of sterile scissor and 2 cm length was further chopped into small pieces by sterile scissor in 1 ml of PBS and followed by homogenization by tissue homogenizer. Serial dilutions of silk homogenate were performed in sterile PBS and 100 µl was plated in T-soy agar plates with kanamycin. Number of CFU's were enumerated after overnight grown at 37 °C in incubator.

7.3. Methods And Material Of Osteotomy

8-12 week old BALB/c female mice were anesthetized with a combination of Xylazine 10 mg/kg of body Wt.) and ketamine **(**100 mg/kg of body wt). Xylazine and Ketamine ratio were made in a final volume of 10 ml PBS. 0.1 ml of combined Xylazine and Ketamine was administered as single intra-peritoneal injection (i.p.) After thorough cleaning the whole of the lower limb with 70% ethanol the shin was sectioned with a scalpel blade to expose the whole tibia. The muscles posterior to the tibia were retracted to expose the posterior aspect of the bone, care being taken not to fracture the fibula. By means of a drilling machine (Cole palmer), sterile steel drill bit of tip diameter 0.25 mm (size) was designed in Mechanical Engineering Department at the United Arab Emirates University, a hole of size 0.5-1.0 mm was made immediately below the tibial tubercle of mouse. The bone was drilled from posterior to the anterior aspects of the bone. Sterile braided silk suture or braided silk suture with XEN-36-*S. aureus* was passed through the hole of tibia bone and silk suture was stabilized by putting double knot, and sides were cut close to knot, approximately 1.5 cm of thread was used for each bone. Stabilizing the knot is important; mouse usually bites his stiches and displaces the tissue that could remove the silk suture from the hole. Prior to stitching of skin, exposed area of bone and surrounding tissue was wiped with 70% ethanol that prevented the systemic or myositis infection. Mice recovery from anesthesia was observed after 2 hours and were returned to fresh cages. After surgery mice were fed normally for 6 days, on the sixth day mice were euthanized via inhalation carbon dioxide and were used for analysis. The steps of surgery are as shown in figure 7.1.

Mouse processing and homogenization of tibia bone

Post 5th day of surgery, mice were sacrificed, immediately lower abdomen was operated by one horizontal incision and two vertical incisions from either side of abdomen, intestines were pushed on side and inferior vena-cava was used for blood collection. A piece of liver and whole spleen was collected and weighed. From the left leg tibia bone was isolated from the tissue, care was taken not to break the bone and tissues attached to the bone were separated in order to get clean tibia free from tissues as shown in figure 7.2. Site of surgery was identified and tibia bone was weighed. After weighing, bone was added in 1 ml of sterile PBS buffer pH 7.4 and placed in a 35 mm petri-dish and was chopped with the help of sterile scissor. 1ml of bone soup was transferred in 2 ml Pyrex tube for homogenization including the chopped bone pieces with the help of forceps and followed by homogenization. Liver and spleen tissues after weighing were directly placed in 1ml of PBS buffer pH 7.4 for homogenization in 2 ml Pyrex tubes. After homogenization of tissues, samples were serially diluted by 10 fold in sterile PBS and 100 µl aliquot was placed on T-soy agar plate containing 200 µg/ml of kanamycin. Remaining of the homogenized tissue was utilized for other biochemical analysis and were stored in -80ºC.

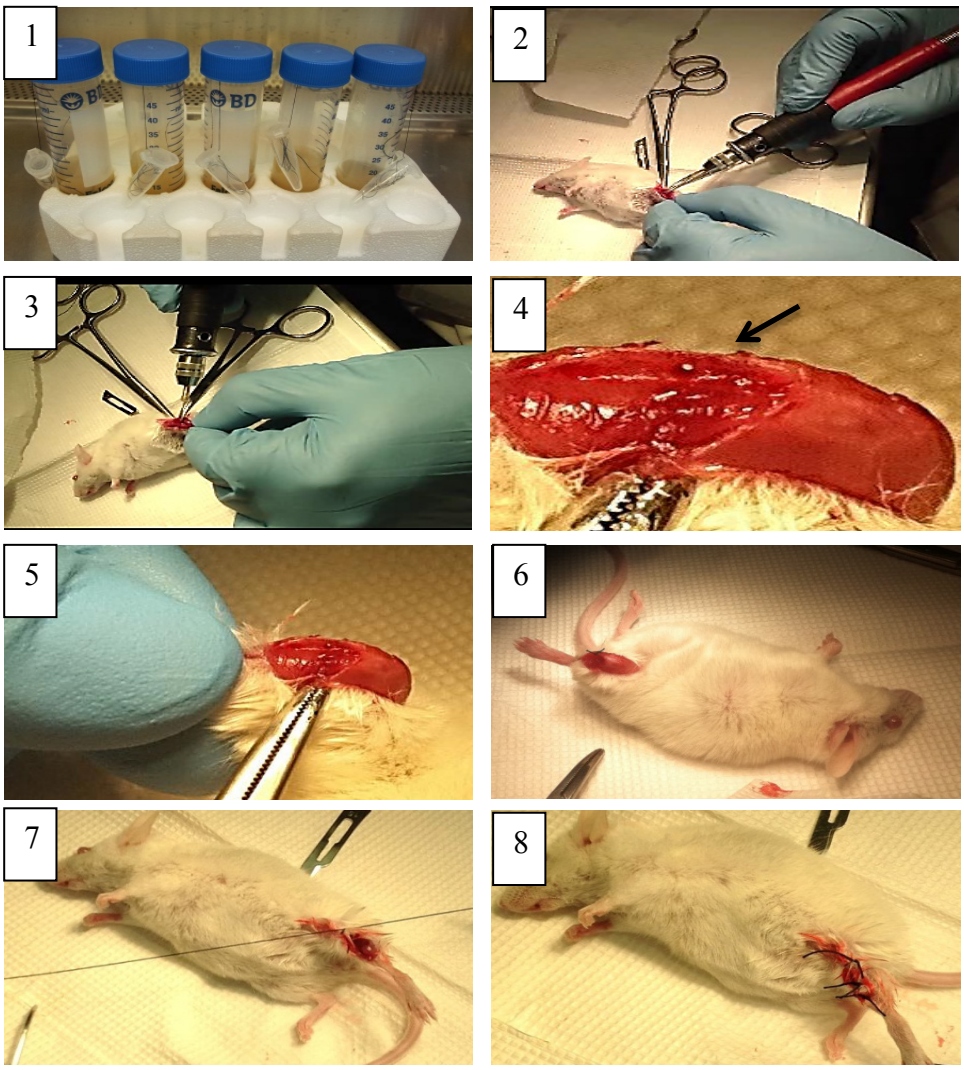

Figure 7.1. Representation of surgical procedures. 1 shows the incubation of silk suture with *s. aureus* bacteria in TSB broth, 2 and 3 shows drilling tibia bone with 0.25 mm drill bit, 4 and 5 shows the drilled hole in tibia without damaging surrounding tissues, 6 shows the infected silk suture in bone , 7 and 8 shows suture of skin of leg.

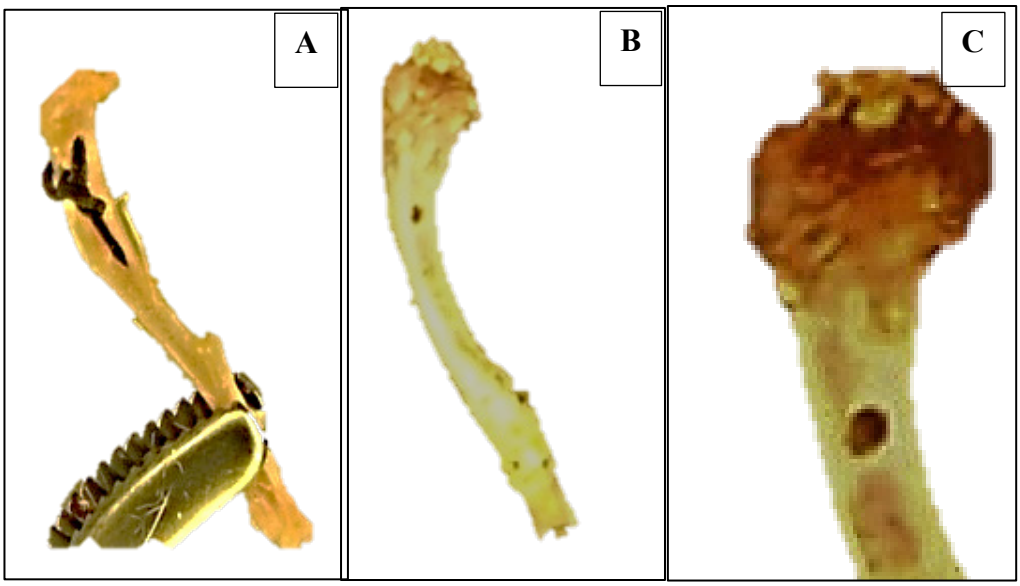

Figure 7.2 Bone Processing. Tibia bone with silk suture thread attached (A), Tibia bone cleaned (B), Focused drilled hole in tibia

7.4. Experiments

7.4.1. 1 mg/kg b. wt. of ACB nanocidals via i.v injection for treatment of osteomyelitis induced by XEN-36-*S. aureus*

Post 5th day of surgery, two groups were selected as, Control group with n = 6 mice and treated group of n = 10 mice. The treated group received ACB dose of 1 mg/kg b.wt via intravenous (I.V.) through dorsal vein of tail. Control group was given saline of equal volume like control group via i.v. through dorsal vein of tail. Prior to i.v. injection mouse was kept under IR-light to warm up the tail for dilation of veins. After receiving i.v. injection either ACB or saline mice were transferred to fresh cages. After 24 hours of treatment mice were sacrificed and tissues of bone, live and spleen were weighed and homogenized in 1 ml of PBS. Blood was collected from inferior vena cava. Serial

dilutions of tissues were performed in sterile PBS buffer and 100 µl aliquots were pipetted in T-soy agar plates with 200 µg/ml. CFU's were enumerated after overnight incubation at 37°C.

7.4.2. 0.1 mg/kg b. wt. of ACB nanocidals via i.v injection for treatment of osteomyelitis induced by XEN-36-*S. aureus*

Two groups each with 5 mice. Post 5th day of infection, treated group received ACB nanocidals treatment with 0.1 mg/kg b. wt and control group received saline alone. After 24 hours of treatment mice were sacrificed, blood, liver, bone and spleen was collected. Tissues were homogenized in 1ml of PBS buffer pH 7.4 and aliquots from each sample were spread on kanamycin treated T. soy agar plate. CFU's were enumerated after overnight incubation at 37 degree C.

7.4.3. 0.5 mg/kg b. wt. of ACB nanocidals via i.v injection for treatment of osteomyelitis induced by XEN-36-*S. aureus*

This experiment was similar to experiment 2 except the dose was 0.5 mg/kg b.wt. and processing was same as above experiment. CFU's were enumerated from each tissue.

7.4.4. 1 mg/kg b. wt. of ACB nanocidals via i.m. near injection site for treatment of osteomyelitis induced by XEN-36-*S. aureus*

Osteomyelitis infection was developed in each group as discussed as earlier. Post 5th day of surgery two groups were selected, with 5 mice in each group, one control group was treated with saline alone and other group was treated with ACB 1 mg/kg b.wt. After 24 hours of treatment mice were sacrificed, blood, liver, spleen and tibia bone was obtained from each mouse and were processed. Aliquot of each tissue homogenate was

serially diluted and 100 µl was spread on T. soy agar plate with 200 µg/ml of kanamycin. After overnight incubation of culture plates, CFU's were enumerated and normalized per gram of tissue.

7.4.5. Antibiotic Co-trimoxazole and negative control of ACB nanocidals for treatment of osteomyelitis induced by XEN-36-*S. aureus*

In this study three groups each with five mice and all surgeries were performed same day to induce infection in tibia. Post 5th day of surgery, control group received saline alone via i.v. and antibiotic treated group received trimethoprim/sulfamethoxazole via drinking water for 24 hours and negative nanoparticles group received iron oxide nanoparticles 1 mg/kg of b. wt. via i.v. The average size of iron oxide nanoparticles was 20 nm and were synthesized in lab. After 24 hour of treatment mice were sacrificed and tissues were collected. Sample processing was done similar to as explained for other experiments. CFU's were enumerated from each tissue.

7.4.6. Survival – post ACB nanocidals treatment of osteomyelitis induced by XEN-36-*S. aureus*

In this study 15 mice were grouped into three groups, 1st group – control group received saline every once a week, 2nd group – treated with ACB 1 mg/kg b. wt. as single dose and 3rd group – treated with ACB 1 mg /kg b. wt. as multiple doses, each dose once in a week for three months. Every day cages were inspected to evaluate the morbidity or death of mouse.

7.5. Results And Discussion

A prophylactic model was developed to treat osteomyelitis using nanocidals. However, in reported models have associated systemic infection and did not study antimicrobial activity by silver or silver alloy nanoparticles. The model developed in this study, was highly localized and without any sign of hematogenous infection nor any colonies from liver or spleen were found. The model is similar to Ueno *et al* 1974 model which was the first tibial mouse model reported except the modifications that machine to drill hole and drill bit size at the tip was 0.25 mm, that made surgery very easy and reproducible. The upper wider part of tibia just below the tubercle is just few millimeters wide then bone tappers until distal end. The outer layer of the calcified bone makes it stiff and fragile that was the reason rabbit and rat tibial osteomyelitis model are developed well in comparison to mouse model. Attempt to induce a hole in tibia with help of 25g or 18g needle as reported in literature was associated with multiples difficulties like high risk of fractures, while holding distal end of tibia there was chance to damage fibula, also induced damage to muscles and surrounding tissues. It needs manually more pressure on needle that caused fractures. In an experiment, a group of 5 mice was used in which 2 mice had fractures in tibia bone and other 3 developed necrosis of foot post ten days of surgery. Leg is highly vascularized if vessels are cut during surgery that will lead to necrosis of bone or associated tissue, especially posterior tibial artery that supplies posterior compartments of leg and plantar surface of foot. In this study, the tibia bone was exposed and retracted gently gastrocnemius muscles and soleus muscles to expose posterior tibia. The tibia bone was drilled from posterior to anterior side to prevent

damage of posterior tibial artery; this technique has major advantage of reducing damage to surrounding parts and drilling bone at a desired place with precision. The number of bacteria XEN-36 corresponding to OD value was estimated. It was found that with 0.5 O.D. at 600 nm is approximately equal to 6.45×10^7 CFU's per ml as shown in figure 7.3 panel A, and the O.D. value was fixed for all experiments to incubate the silk suture for 45 minutes, furthermore the number of XEN-36 bacteria per cm of silk suture was enumerated. It was found that 1×10^4 CFU's/ml in 45 minutes incubation and 150 minutes as 5.1×10^6 CFU's per cm as shown in figure 7.3 panel B.

In the surgical procedure the infected silk suture utilized was 1.5 cm in length including the knot which corresponds to approximately $1.5.\times 10^6$ CFU's, however a part of thread as tiny knot was outside the drilled hole, so the number of CFU's was average between 1×10^5 to 1×10^6 CFU that were utilized for development of infection.

Experiment 1, in this study, post 5^{th} day of surgery 1mg/kg of body wt. of nanocidals were given through intravenous (i.v.) as shown in figure 7.4. The aim for i.v. injection was to ensure it reaches to all parts of the body in short time in order to observe antimicrobial activity in 24 hr, however in this method nanocidals can be excreted at faster rate.

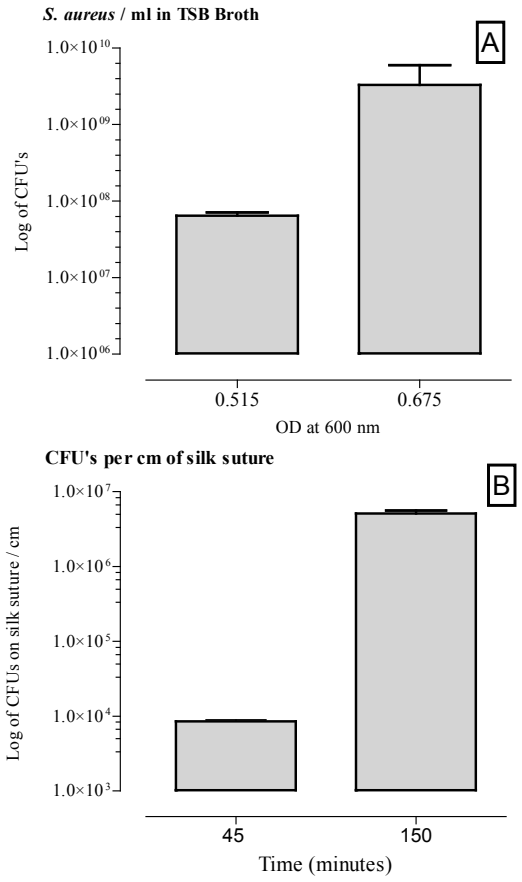

Figure 7.3. Growth of XEN-36 strain. Growth in TSB media (A), number of XEN-36 bacteria on silk suture (B).

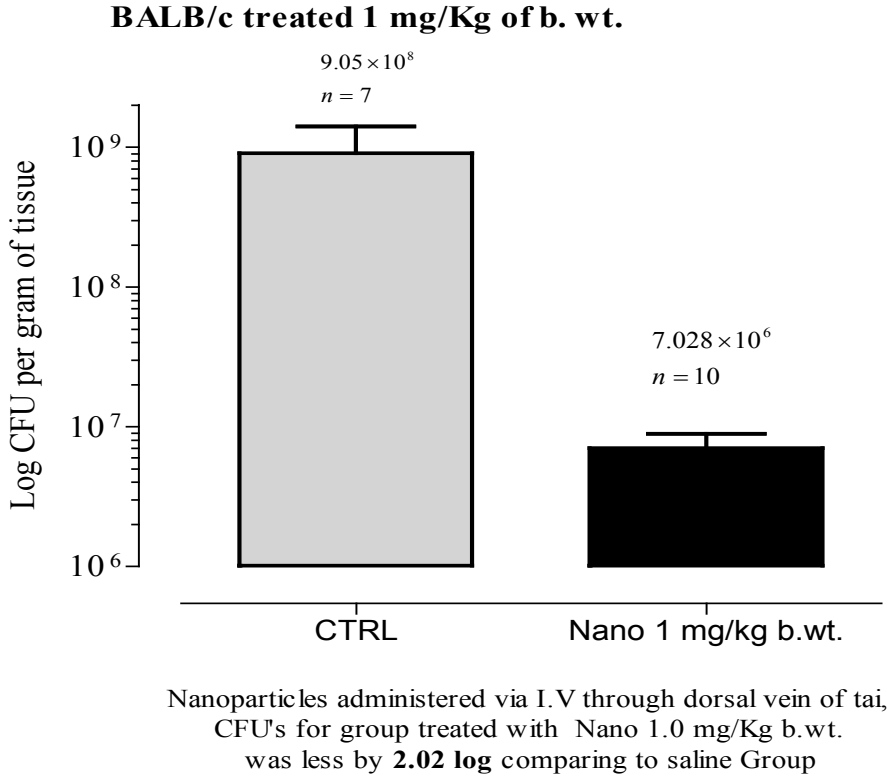

Figure 7.4. Osteomyelitic mice treated with nanocidals. CFU's present in tibia bone were enumerated post 24 hour treatment.

Data shown in Figure 7.4, represent the growth of XEN 36 in tibia bone and with the treatment of nanocidals for 24 hours a significant reduction in CFU's was observed comparing to sham group by 2 logs down, p-value < 0.0012 and no growth was positive for blood, spleen, and liver. p-value was obtained by Mann whitney test. This data supported our following clims: (1) this method of inducing osteomyelitis will be a localized infection and does not show systemic infection. (2) nanocidals were effective antimicrobial agent in *in-vivo*.

Two more experiments were carried out in which low doses were used as shown in figure 7.5. ACB nanocidals with 0.1 and 0.5 mg/kg of b. wt. was injected i.v. and It was found that CFU reduction by 0.69 logs down by using 0.5 mg/kg of b. wt. comparing to control group and statistically was non-significant with p-value 0.2, in figure 7.5- panel A and while in ACB nanocidals with 0.1 mg/kg of b. wt. there was 0.355 logs down and statistically non-significant with p-value 1 in figure 7.5- panel B. These findings suggest that ACB with 1 mg/kg b. wt has potential to reduce infection by more than 50% with single dose, and data for 0.5 and 0.1 mg/kg of b. wt. showed a pattern in reduction like 0.69 logs and 0.355 logs respectively, which also showed that antimicrobial activity was proportional to the concentration of dose, by increasing the concentration of ACB nanocidals the antimicrobial activity was increased proportionally.

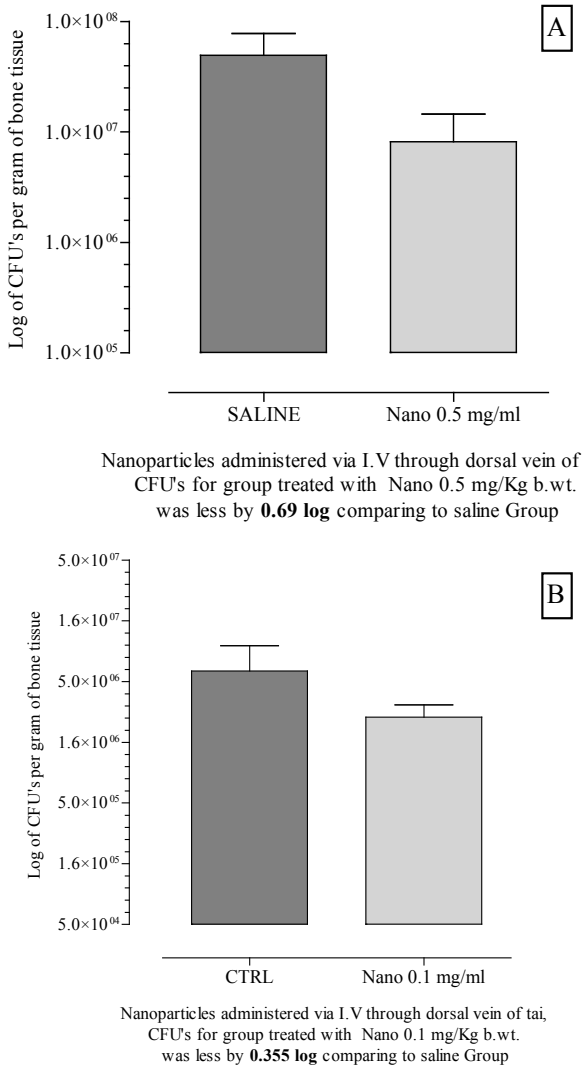

Figure 7.5. Low dose of ACB Nanocidals. Treatment with 0.5 mg/Kg of b. wt. (A) and 0.1 mg/Kg of b. wt. (B).

In this study the effect of localized delivery of ACB nanocidals was evaluated. ACB particles were injected locally near the infection site as a model for local delivery as shown in figure 7.6. panel-A. The aim of this experiment was to find the efficacy of ACB if given near infection site via intra-muscular (i.m.). It was found that in 24 hours post injection of ACB there was 1.8 logs reduction with p-value = 0.0121, however it was

clear from the data that i.v. delivery or local delivery were equally effective. This data provides additional insight that these ACB nanocidals can be delivered into the body either intravenous or intramuscular similar to antibiotics. Moreover infection was obviously in tibia bone so i.m. delivery near the infection site was not so accurate method of local delivery it may work better if injected directly in bone, which is as good to another surgery. While injecting ACB in i.m. the mice was anethetesized with xylazine and ketamine, believing that i.m. injection in gastrocnemius or soleus muscles is painful. Finally concluded that ACB nanocidals delivery via i.m. is also another route of delivery

In the next round of surgery to induce osteomyelitis on 15 mice those were distributed in 3 groups with 5 mice in each group , One group was used for negative control for nanoparticles, considering they are not antimicrobial but are metallic nanoparticles (iron oxide), 2nd group was used for commercially available antibiotics which was provided by Prof. Basel K Ramadi, a faculty at United Arab Emirates University, as Co-trimoxazole with salt of trimethoprim/sulfamethoxazole which broad spectrum antibiotics. As shown in figure 7.6 panel-B, negative control of ACB nanocidals did not show any difference comparing to control group given saline alone, however antibiotics did not show any significant data statistically p-value = 0.1, but results obtained cannot be ignored if statistically non-significant it was found 0.8 logs down which is close to 25% reduction, dose of Co-trimoxazole antibiotic was 200 μg/ml.

Animal survival studies were also conducted, another set of 15 mice ready post 5th day of surgery Group 1 control injected via i.v. saline only, Group 2 single dose of ACB nanocidals with 1 mg/kg of b. wt via i.v. Group 3 multiple dose of 1 mg/kg of body

weight once in every week via i.v. as shown in figure 7.7, here experiment was carried out for 16 weeks and no death of any mouse from any group occurred. Moreover no signs of morbidity or suppressed physical activities were observed, both the groups either single dose or multiple dose act similar to control group. This was encouraging data that these nanoparticles with multiple doses did not kill the animal; it is believed that the reason for successful 100% survival could be ACB are excreted from tissues with time at higher rate. Initially these particles are distributed everywhere in the body and shows short-term retention of nanoparticles. One of the studies has shown that for 28 days silver nanoparticles were given and up to 90 days almost all silver is excreted from the body except from testis and brain where retention was slightly higher.

7.6. Reduced Glutathione Assay

Glutathione a tripeptide is a most potent free radical scavenger found in our body and is almost found in all cells or tissues present in our body, it constitutes nearly 90% of all radical scavengers present in human body, as a result is widely used a known marker for oxidative stress.

7.6.1. Methods and materials

This assay was done similar to *in vitro* studies as Coleman et al.[83] homogenized tissue in Tris-EDTA buffer pH 8.8 was further diluted 50 folds in same buffer. Homogenized sample was centrifuged at 4000 rpm for 20 minutes at 4 degree C. supernatant was collected for GSH assay and total protein assay. Procedure for GSH was followed as discussed in chapter 2. Total protein estimation was done by BCA assay assay as mentioned elsewhere and its standard curve was generated by using bovine

serum albumin. Similarly for GSH assay Standard curve was generated from standard reduced L-glutathione.

7.7. Results

Groups of mice used in osteotomy experiments were used to measure the GSH levels.Group of mice treated with 1 mg/kg of b. wt. via i.m. and its control group treated with saline only were used for GSH assay as shown in figure 7.8, it was found that there was no significant difference in bone, liver and spleen, however in bone there was 30% increase in GSH level although test was non-significant but showed tendency to increase the GSH level, increasing or decreasing GSH level after treatment notifies the presence of oxidants in the tissue. Increase in GSH level is due to feedback mechanism where cellular GSH levels are consumed and expression of GSH increases to counter attack the presence of radicals. However, when the concentration of ACB accedes to GSH level, net intracellular GSH level drops down causing oxidative stress but that was not observed in this study. GSH plays an important role in scavenging free radicals and protects cells from dying or aging. Here the results showed no significant difference by 1 mg/kg b. wt. exposure of ACB nanocidals comparing to control group. Similarly using ACB with 0.5 mg/kg of b. wt, antibiotic trimol via drinking water, and negative control 1 mg/kg of b. wt of nanoparticles of iron oxide did not show any significant changes in GSH levels

It is concluded from data that ACB up to 1 mg/kg of b. wt may be safe to use in animal studies for antimicrobial treatment.

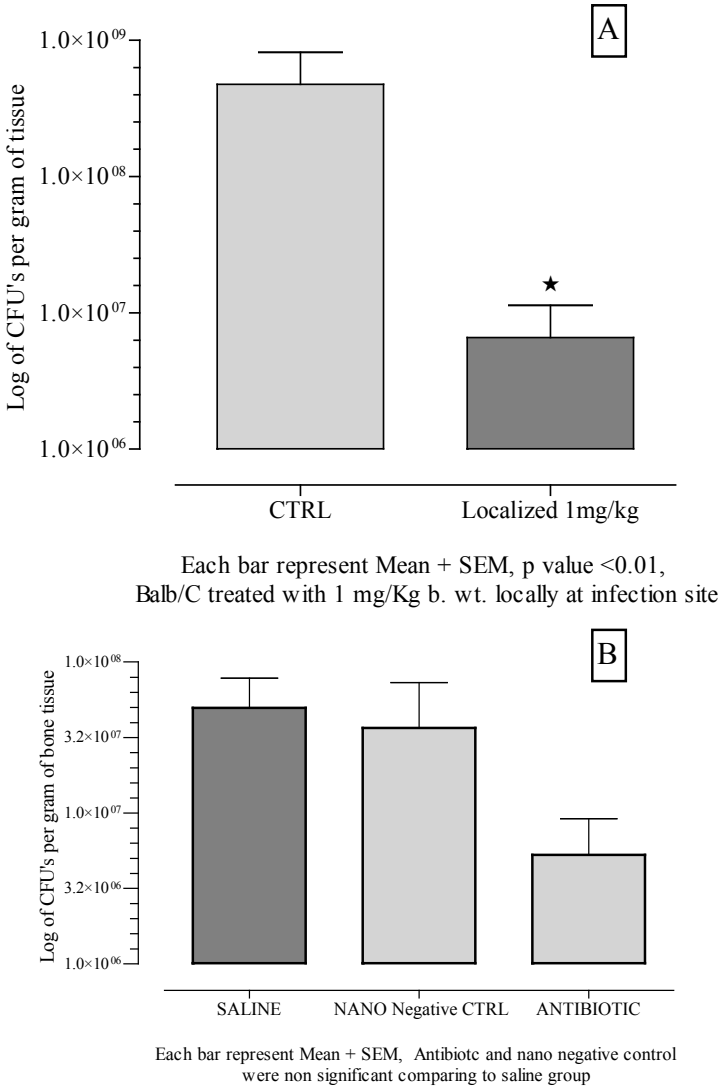

Figure 7.6. Localized delivery. ACB nanocidals treated with 1mg/kg of b. wt via i.m. (A), negative control of ACB nanocidals via i.v. and antibiotic via drinking water.(B).

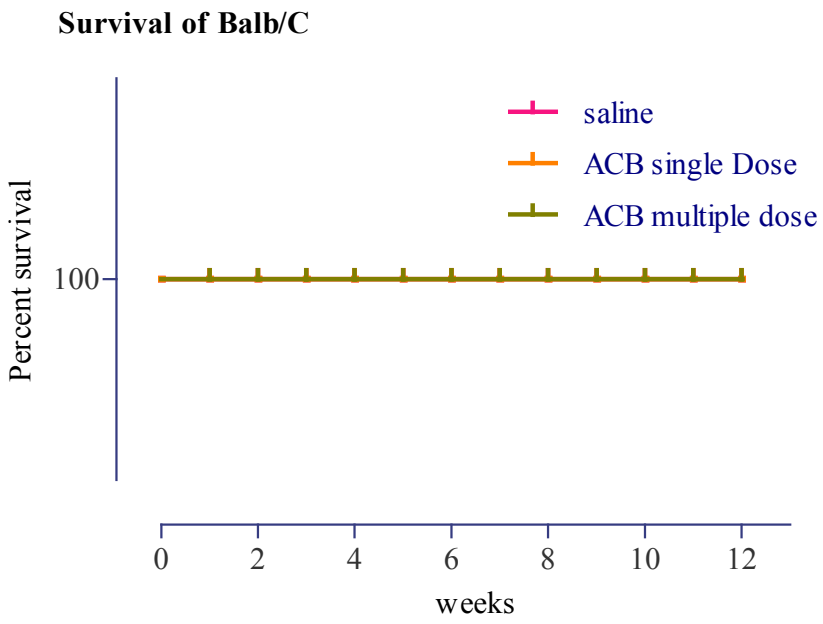

Figure 7.7. Mice survival. Groups of mice treated with ACB nanoparticles where orange color for single dose, green for multiple doses and red as control group treated with saline.

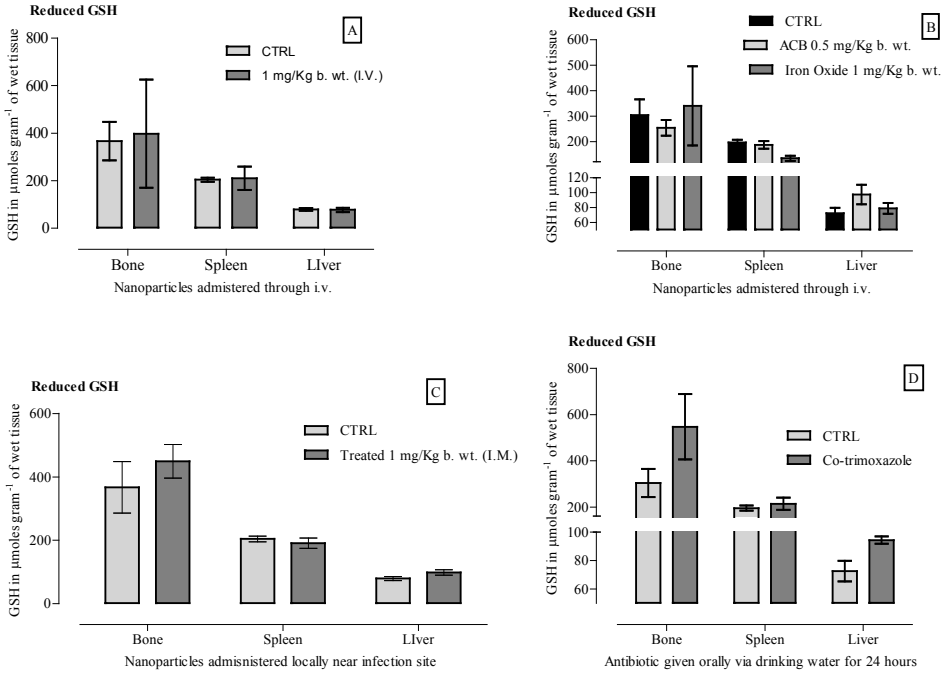

Figure 7.8. GSH Assay *in-vivo* study. Effect of nanocidals 1 mg/kg b. wt via i.v. (A). Effect of negative control Iron oxide 1 mg/Kg of b. wt and ACB nanoparticles 0.5 mg/Kg of b. wt.(B) Effect of ACB nanoparticles administered locally (C). Effect of antibiotic Co-trimoxazole (D).

7.8. Histology Materials And Methods

Groups of BALB/c mice treated with ACB nanoparticles, dose 1 mg/kg of b. wt. and control groups treated with saline only were euthanized after 24 hours of treatment. Liver, spleen and tibia bone were collected as mentioned earlier and were fixed in formalin 10% for overnight, bone was decalcified by treating tibia bone with 0.5 M EDTA in a PBS buffer and were kept overnight at room temperature. After decalcification, decalcified bone, Liver, and spleen were processed an embedded in parafilm. 4 µm thickness sections were cut and then were stained with hematoxylin and eosin stain.

7.9. Results And Discussion

To determine the proliferation of blood cells or inflammatory infiltrate and morphology of cells within the organs, BALB/c mice with *S. aureus* infected tibia bone by surgical procedure using braided silk suture as explained earlier in surgical procedure were treated with 1 mg/kg b.wt. or saline via intravenous injection though dorsal vein of tail. Histological slides were harvested from liver, spleen and tibia bone post 24 hour treatment. Liver and spleen slides did not show any difference in cell morphology comparing to control groups neither was any significant infiltration of neutrophils seen in treated groups as shown in figures 7.9 and 7.10. Tibia bone showed higher number of neutrophils in for both in treated and control group as shown in figure 7.11 which was expected to be a normal post surgery inflammatory response in bone, however there was not any additional significant change in tibia bone treated with nanoparticles.

As toxicity is the major issue related to nanoparticles, higher doses of silver or silver based nanoparticles shown that they reside in liver [86, 89] and may cause toxicity. To confirm the ACB nanoparticles at 1mg/kg b. wt may cause the changes in morphology or cause immune response against nanoparticles and could be observed by histological studies but the findings did not show any significant changes among groups treated or non-treat for liver, spleen or tibia bone. In liver, morphology of hepatocytes was seen as normal along with bile ducts and blood vessels and no significant change was observed. Similarly for spleen white and red pulp was clearly distinguished without any sign of pathogenicity in treated or non-treated groups. Sections of bone were observed for treated and non-treated groups and both the groups intercellular bone matrix with osteocytes

were observed and no significant difference was seen among the groups. Our findings from liver enzymes for treated or non-treated group also suggest there was no significant change observed. Moreover, our histological analysis supports the biochemical tests and oxidative stress markers which were non-significant comparing to control groups when treated with 1 mg/kg b. wt. of ACB nanoparticles.

LIVER

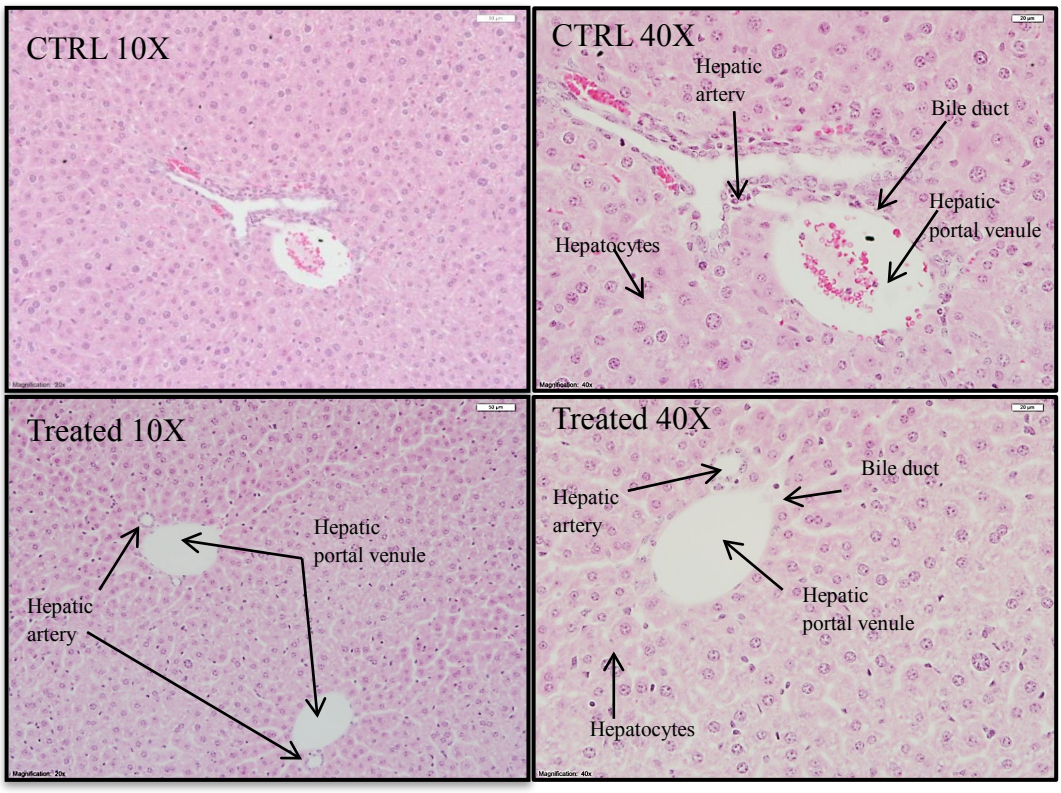

Figure 7.9. Histology of Liver by H&E stain. Upper panel shows Control group treated with saline and lower panel Treated group with 1 mg/kg b. wt. of ACB Nanocidals.

SPLEEN

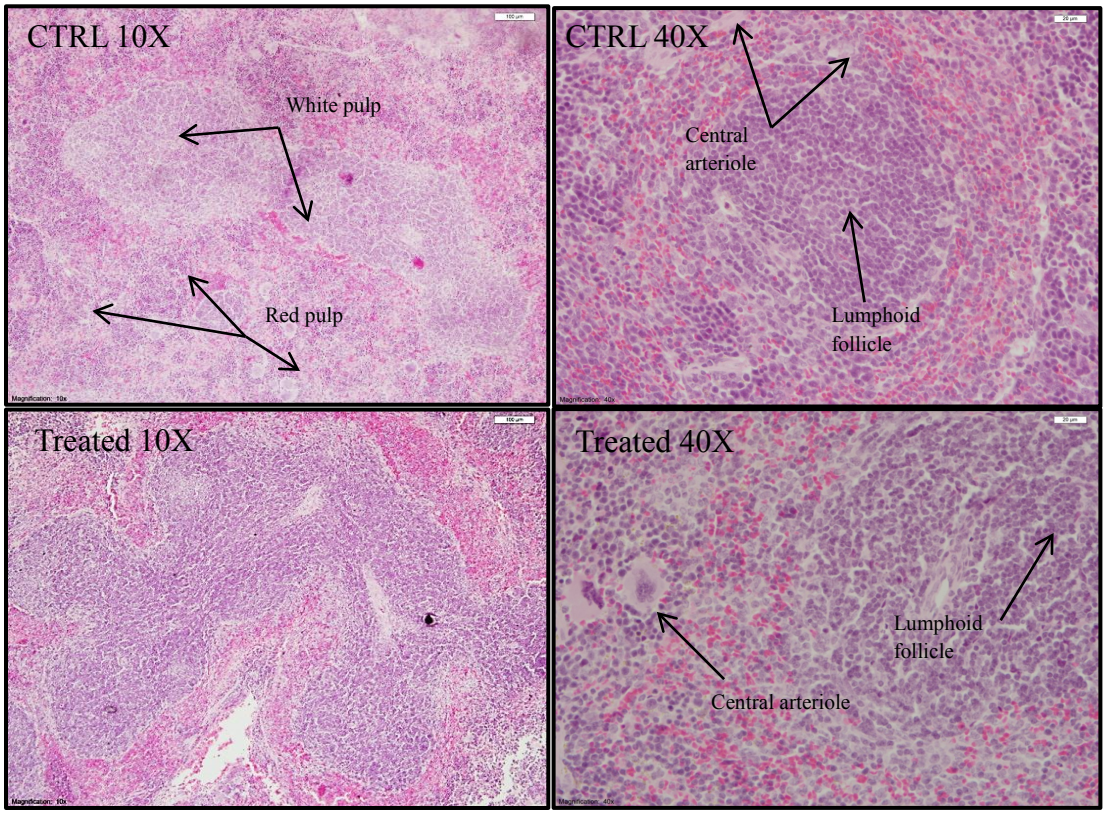

Figure 7.10. Histology of Spleen by H&E stain. Upper panel shows s, Control group treated with saline and lower panel shows Treated group with 1 mg/kg b. wt. of ACB Nanocidals.

BONE

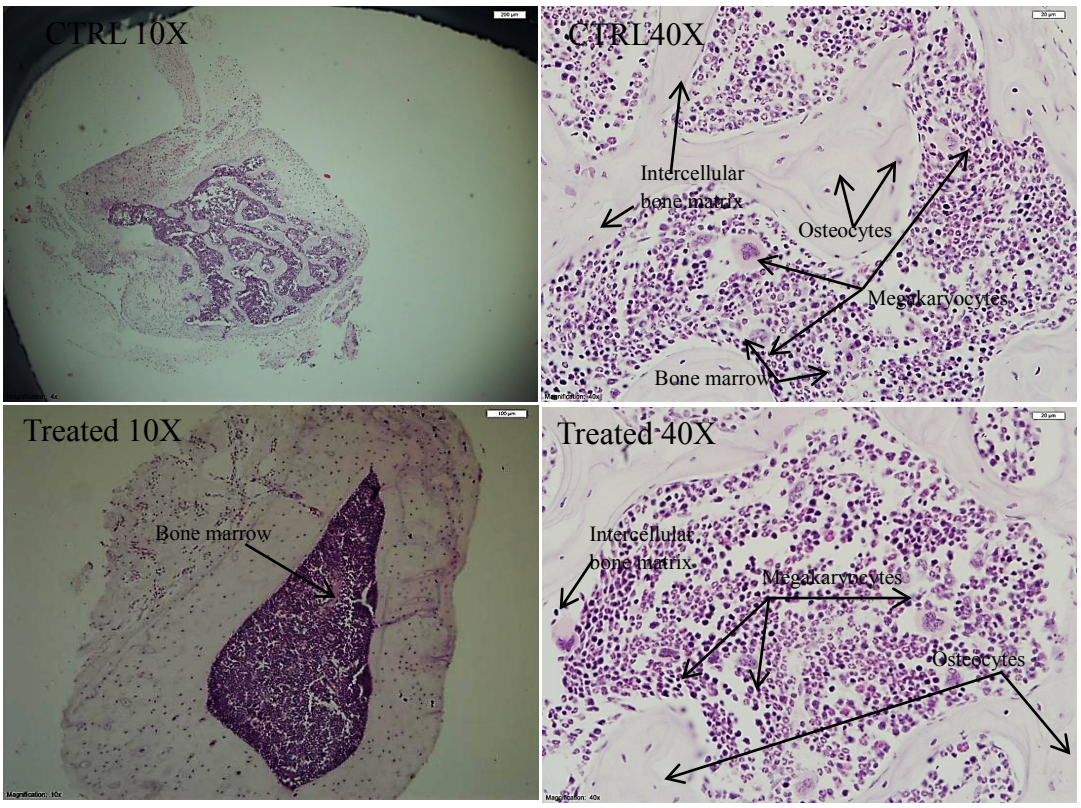

Figure 7.11. Histology of Tibia bone by H&E stain. Upper panel shows Control group with saline and lower panel shows Treated group with 1 mg/kg of b. wt. of ACB nanocidals.

CHAPTER VIII

ONGOING STUDIES AND CONCLUSIONS

Silver-copper nanoparticles which are caped with glycine or embedded in glycine were synthesized. The aim was to produce nanoparticles which are safe for human. The newly synthesized nanoparticles need to be characterized for future use in treatment of osteomyelitis. It is hypothesized that the efficiency of the newly synthesized nanoparticles may be stronger because in this method copper element is protected from further oxidation, it has been shown metal copper is more strong antimicrobial than copper oxide [55]

8.1. Synthesis Of Silver-Copper Luminescent Nanoparticles

2 moles of glycine, 61.6 mmoles of silver nitrate and 26.4 mmoles of copper acetate were added to 50 ml conical flask. Dissolved in 10 ml of double distilled deionized water and heated till water evaporated. The solid phase reaction mixture was heated at 170^0C for 20 minutes by Zheng *at al* [96]. The reduction of silver-copper was monitored by change in color from black to brown with and a silver shine was observed to the sides of reaction glass vessel. The dried mixture pellet was re-suspended in 10 ml of distilled water and sonicated for two hours using micro-tip probe of 450S-Branson Sonicator, 50% power output was kept at maximum limit for micro-tip sonicator probe.To remove large aggregates and insoluble nanoparticles, the solution was centrifuged at 4000 rpm for 20 minutes, although no aggregates were observed. To

remove free glycine, solution was dialysed in water for 24 hours and after every 6 hours, replaced with fresh deionized water. The Slide-A-Lyzer Dialysis Cassettes with MWCO 2K was used for dialysis from thermo scientific Solution was collected from dialysis cassette and stored in 10 ml screw cap glass vial.

8.1.1. Characterization of Silver Copper polycrystalline nanoparticles

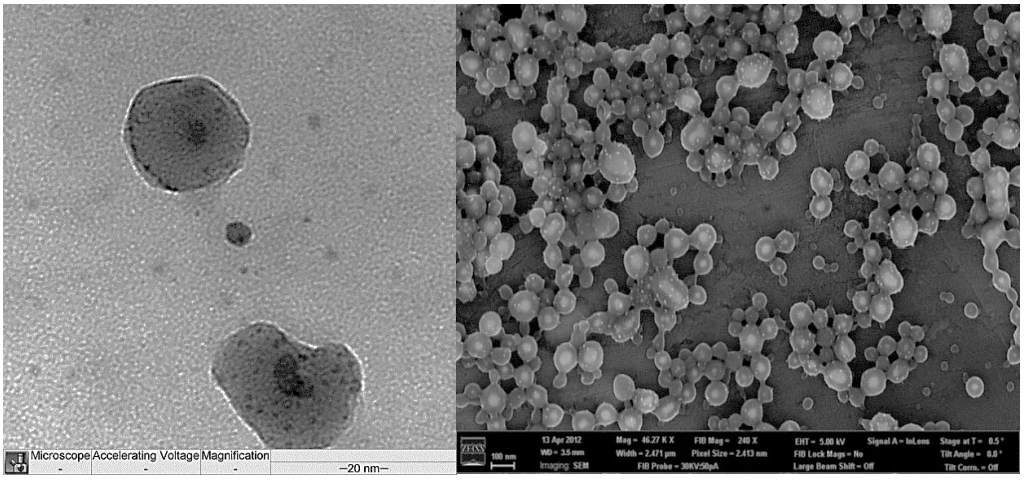

Figure 8.1. TEM and SEM images. TEM Characterization of nanoparticles on left and SEM image on right side.

Nanoparticles observed has a core shell and matrix which is formulation of glycine by solid phase synthesis, besides central core there are sub cure size grains seen in the matrix, suggesting a polycrystalline nature of nanoparticles. SEM imaging was performed at 5KV to observe the core shell, sub-core size grains and matrix as shown in figure 8.1 and figure 8.2, while as above or below 5KV energy, matrix was not differentiated from core shell as shown in figure 8.2-(A,B). At 1.92 KV and 3KV voltage nanoparticles appeared as spherical without any details of core or matrix, however it was

found the optimal voltage of 5 KV where matrix was differentiated from core along with the sub core size grains in matrix.

The data suggests that silver copper nanoparticles are capped with glycine matrix and matrix is embedded with 8 to 10 nm size silver-copper nanoparticles, particles in matrix were not in agglomerated form but distributed all over the matrix with a minimum gap of 10 nm or more, as a result these nanoparticles exhibit as polycrystalline in nature. Frequency distribution of size of nanoparticles, core shell and sub core particles in matrix are shown in Figure 8.3.

Stability of these nanoparticles has proven another add on advantage besides its optical properties, they are in same shape and size in aqueous suspension since 6 months. Earlier studies has shown the disadvantage of copper nanoparticles or Copper alloy for agglomeration because copper is readily oxidized as CuO and keeps growing as Copper oxide agglomerate, but our findings did not found any evidence of agglomeration since 6 months and the reason could be the glycine matrix which prevents nanoparticles from oxidation.

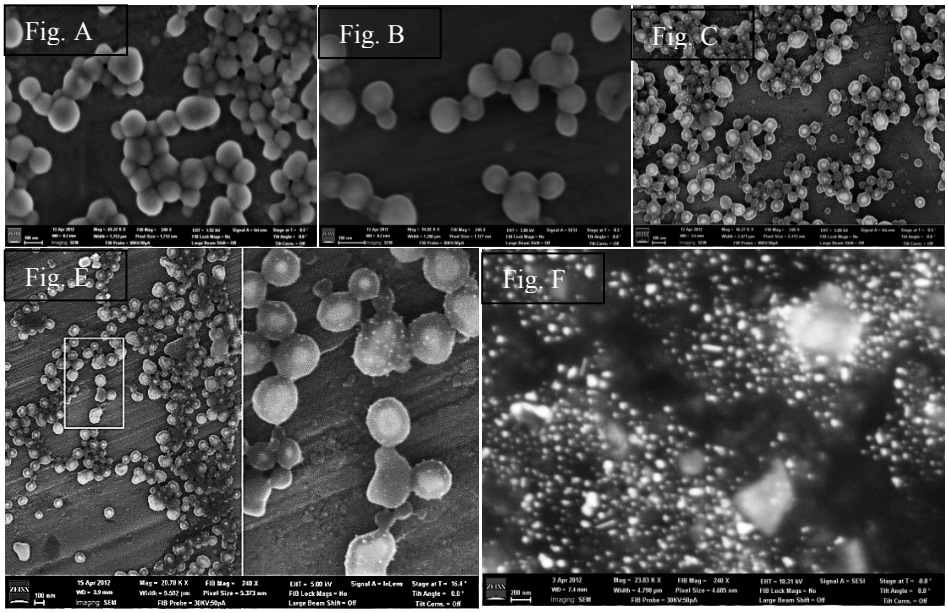

Figure 8.2. SEM image at different Kv. A and B panels at 1.9 and 3 kv respectively, SEM images at 5 kv in panel 2C and 2E. Above 5kv panel 2F.

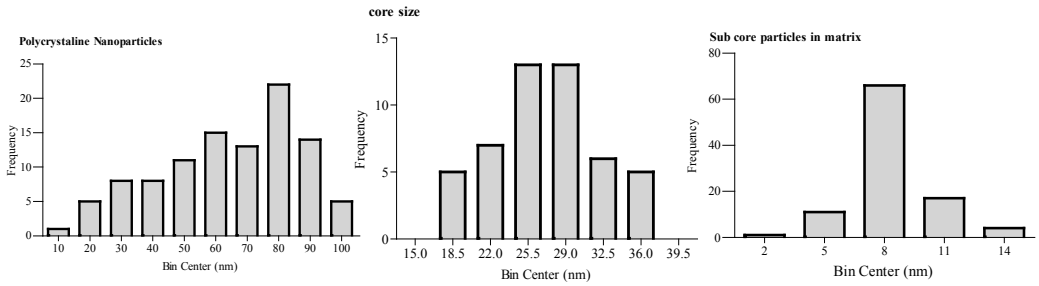

Figure 8.3. Histogram of nanoparticles. These histograms are corresponding to SEM images shown in figure 8.2. In this figure Histogram of polycrystalline nanoparticles on left, the middle histogram of core size in polycrystalline nanoparticles and on right the sub core particles in matrix of poly crystalline nanoparticles.

8.1.2. Spectroscopy techniques

We also studied the Absorption, excitation and emission spectra of nanoparticles. UV-Vis absorption scan showed maximum Absorption spectrum at 410 nm by using DU-800 COULTER spectrophotometer as shown in figure 8.4 which was close to silver Plasmon resonance of silver but with a wide shoulder which further depicts the optical properties of nanoparticles as earlier discussed for silver polycrystalline nanoparticles. These nanoparticles may have silver-copper distribution in a ration 80:20 because of concentration of moles of Silver and copper ions added during synthesis, Silver-Copper hybrid nanoparticles might have dominant silver properties because of higher concentration of silver comparing to copper. Fluorometric data analysis showed that there was maximum emission at 460 nm with Excitation at 400 nm, however there was shift in emission spectrum by changing the excitation wavelength from 400 nm to 450 nm at interval of 10nm. For each 10 nm increase in excitation there was shift by 10 nm in emission, however it was obvious from the data that the intensity of Emission spectrum

decreased significantly by changing the Excitation wavelength. Cary eclipse instrument was used to study Fluorescence with Ex. Slit (5 nm), Em. Slit (5 nm) and scan rate (300 nm/min).

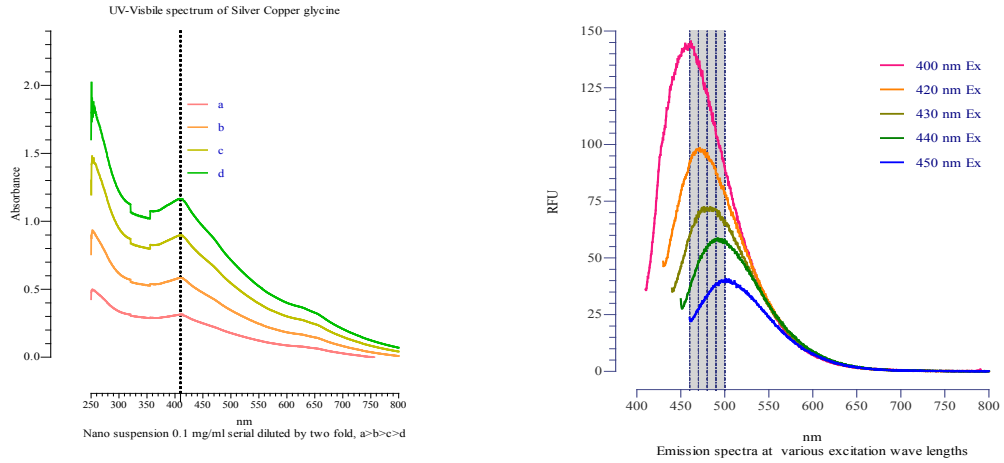

Figure 8.4. Fluorometric and spectrophotometric results. On the left side shown the visible spectrum of nanoparticles and on the right side Emission at different excitation wavelengths.

These luminescent silver-copper nanoparticles needs to evaluated for antimicrobial activity and however equally toxicity data must be explored, it is hypothesized that these nanoparticles will be the more suitable particles for antimicrobial testing with least toxicity associated because they are surface coated with glycine molecules. Moreover they can be used for live imaging using IVIS imaging device or good source of fluorophore for confocal microscopy.

8.2. Conclusions

In this study, results proved the efficiency of nanocidals against *s. aureus* infection in *in vitro* and *in vivo* with minimum toxicity associated which was revealed from chapters as discussed in this study.

Overview of ACL and ACB results: Both ACL and ACB exhibited antimicrobial activity, however ACL showed effective antimicrobial activity at 0.5 µg/ml, while as ACB nanoparticle showed antimicrobial activity at 1 µg/ml, which was 2 fold difference among ACL and ACB, moreover it can be seen that the antimicrobial activity varies with incubation time, but the choice of selection was determined by toxicity. The primary aim of this study was to find the optimal dose and in this study our optimal dose will be minimum concentration which is nontoxic. From the results it was found that ACL nanoparticles showed toxicity at 10 µg/ml which was determined by catalase activity however for ACB nanoparticles significant toxicity was shown at 20 µg/ml, except there was mild stress observed by protein carbonyl content which was indication oxidation of proteins at 15 µg/ml, herby our assumption that ACB nanoparticles may exhibit toxicity at this level. So based on the findings of this study, ACB nanoparticles were chosen to be used further for animal model toxicity and in osteomyelitis model.

In the animal model of toxicity, the distribution of elements among vital organs in just 4 hours and 24 hours post treatment was observed which was the first sign that these nanoparticles can go across all tissues in the body, however it is undesirable at some point which could not be controlled. The pattern of clearance from organs in 24 hours post injection was observed but most likely they were abundant in liver. However

the permanent retention of nanoparticle in organs cannot be determined in this study, which will need analysis of elements for several weeks to months and is one of planned future studies.

Development of murine model of osteomyelitis with localized infection was successfully achieved; primary role of this murine model was to check the efficacy of antimicrobial activity which was hypothesized from *in vitro* studies, the results of antimicrobial activity in murine model with induced osteomyelitis was promising. Decreasing the concentration of nanoparticles the efficiency of nanoparticles was decreased proportionally. Ideally an effective treatment would not have developed histopathology or immunogenic response, in this study addition to antimicrobial activity biochemical analysis for reduced glutathione to measure the oxidative stress if associated, using ACB Nanocidals with 1, 0.5 and 0.1 mg/kg b. wt. were conducted and it was found that no significant change was observed. Histological study for bone, liver, and spleen tissues were performed and there was no sign of change in morphology of cells nor any infiltration of neutrophils alone or blood cells.

It is concluded that ACB nanoparticles are a suitable potential for antimicrobial therapy for osteomyelitis disease. Further study is required to explore the clearance of nanoparticles from organs or tissues with respect to time.

In planned future studies silver-copper-glycine polycrystalline nanoparticles will also be investigated. The advantage of these nanoparticles could be less toxic because silver and copper is embedded in glycine core which may reduce the toxicity of nanoparticles. Another important characteristic of these nanoparticles is they are

luminescent they can be tracked in in-vitro studies or can be used in *in vivo* studies for imaging using IVIS imaging device for medical application including osteomyelitis.

REFERENCES

1. Houghton, T.J., et al., *Linking bisphosphonates to the free amino groups in fluoroquinolones: preparation of osteotropic prodrugs for the prevention of osteomyelitis.* J Med Chem, 2008. **51**(21): p. 6955-69.
2. El-Kamel, A.H. and M.M. Baddour, *Gatifloxacin biodegradable implant for treatment of experimental osteomyelitis: in vitro and in vivo evaluation.* Drug Deliv, 2007. **14**(6): p. 349-56.
3. Mendel, V., et al., *Therapy with gentamicin-PMMA beads, gentamicin-collagen sponge, and cefazolin for experimental osteomyelitis due to Staphylococcus aureus in rats.* Arch Orthop Trauma Surg, 2005. **125**(6): p. 363-8.
4. Webb, L.X., et al., *Osteomyelitis and intraosteoblastic Staphylococcus aureus.* J Surg Orthop Adv, 2007. **16**(2): p. 73-8.
5. Brady, R.A., et al., *Resolution of Staphylococcus aureus biofilm infection using vaccination and antibiotic treatment.* Infect Immun, 2011. **79**(4): p. 1797-803.
6. Brin, Y.S., et al., *Treatment of osteomyelitis in rats by injection of degradable polymer releasing gentamicin.* J Control Release, 2008. **131**(2): p. 121-7.
7. Ozturk, A.M., et al., *Alendronate enhances antibiotic-impregnated bone grafts in the treatment of osteomyelitis.* Int Orthop, 2008. **32**(6): p. 821-7.

8. Enwemeka, C.S., et al., *Blue 470-nm light kills methicillin-resistant Staphylococcus aureus (MRSA) in vitro.* Photomed Laser Surg, 2009. **27**(2): p. 221-6.

9. Enwemeka, C.S., et al., *Visible 405 nm SLD light photo-destroys methicillin-resistant Staphylococcus aureus (MRSA) in vitro.* Lasers Surg Med, 2008. **40**(10): p. 734-7.

10. Taubes, G., *The bacteria fight back.* Science, 2008. **321**(5887): p. 356-61.

11. Fowler, T., et al., *Cellular invasion by Staphylococcus aureus involves a fibronectin bridge between the bacterial fibronectin-binding MSCRAMMs and host cell beta1 integrins.* Eur J Cell Biol, 2000. **79**(10): p. 672-9.

12. Jevon, M., et al., *Mechanisms of internalization of Staphylococcus aureus by cultured human osteoblasts.* Infect Immun, 1999. **67**(5): p. 2677-81.

13. Hudson, M.C., et al., *Internalization of Staphylococcus aureus by cultured osteoblasts.* Microb Pathog, 1995. **19**(6): p. 409-19.

14. Finlay, B.B. and P. Cossart, *Exploitation of mammalian host cell functions by bacterial pathogens.* Science, 1997. **276**(5313): p. 718-25.

15. Ellington, J.K., et al., *Involvement of mitogen-activated protein kinase pathways in Staphylococcus aureus invasion of normal osteoblasts.* Infect Immun, 2001. **69**(9): p. 5235-42.

16. Pulverer, B.J., et al., *Phosphorylation of c-jun mediated by MAP kinases.* Nature, 1991. **353**(6345): p. 670-4.

17. Pace, J., M.J. Hayman, and J.E. Galán, *Signal transduction and invasion of epithelial cells by S. typhimurium.* Cell, 1993. **72**(4): p. 505-14.

18. Marriott, I., *Osteoblast responses to bacterial pathogens: a previously unappreciated role for bone-forming cells in host defense and disease progression.* Immunol Res, 2004. **30**(3): p. 291-308.

19. Bost, K., et al., *Monocyte chemoattractant protein-1 expression by osteoblasts following infection with Staphylococcus aureus or Salmonella.* J Interferon Cytokine Res, 2001. **21**(5): p. 297-304.

20. Bost, K., et al., *Induction of colony-stimulating factor expression following Staphylococcus or Salmonella interaction with mouse or human osteoblasts.* Infect Immun, 2000. **68**(9): p. 5075-83.

21. Bodén, M. and J. Flock, *Cloning and characterization of a gene for a 19 kDa fibrinogen-binding protein from Staphylococcus aureus.* Mol Microbiol, 1994. **12**(4): p. 599-606.

22. Jönsson, K., et al., *Two different genes encode fibronectin binding proteins in Staphylococcus aureus. The complete nucleotide sequence and characterization of the second gene.* Eur J Biochem, 1991. **202**(3): p. 1041-8.

23. McGavin, M., et al., *Identification of a Staphylococcus aureus extracellular matrix-binding protein with broad specificity.* Infect Immun, 1993. **61**(6): p. 2479-85.

24. Cheung, A., et al., *Cloning, expression, and nucleotide sequence of a Staphylococcus aureus gene (fbpA) encoding a fibrinogen-binding protein.* Infect Immun, 1995. **63**(5): p. 1914-20.

25. Nair, S., et al., *Surface-associated proteins from Staphylococcus aureus demonstrate potent bone resorbing activity.* J Bone Miner Res, 1995. **10**(5): p. 726-34.

26. Yasuda, H., et al., *Osteoclast differentiation factor is a ligand for osteoprotegerin/osteoclastogenesis-inhibitory factor and is identical to TRANCE/RANKL.* Proc Natl Acad Sci U S A, 1998. **95**(7): p. 3597-602.

27. Wada, T., et al., *RANKL-RANK signaling in osteoclastogenesis and bone disease.* Trends Mol Med, 2006. **12**(1): p. 17-25.

28. Somayaji, S.N., et al., *Staphylococcus aureus induces expression of receptor activator of NF-kappaB ligand and prostaglandin E2 in infected murine osteoblasts.* Infect Immun, 2008. **76**(11): p. 5120-6.

29. Trembleau, S., et al., *The role of IL-12 in the induction of organ-specific autoimmune diseases.* Immunol Today, 1995. **16**(8): p. 383-6.

30. Bost, K., et al., *Staphylococcus aureus infection of mouse or human osteoblasts induces high levels of interleukin-6 and interleukin-12 production.* J Infect Dis, 1999. **180**(6): p. 1912-20.

31. Gasper, N.A., et al., *Bacterium-induced CXCL10 secretion by osteoblasts can be mediated in part through toll-like receptor 4.* Infect Immun, 2002. **70**(8): p. 4075-82.

32. McCall, S.H., et al., *Osteoblasts express NLRP3, a nucleotide-binding domain and leucine-rich repeat region containing receptor implicated in bacterially induced cell death.* J Bone Miner Res, 2008. **23**(1): p. 30-40.

33. Jin, C. and R.A. Flavell, *Molecular mechanism of NLRP3 inflammasome activation.* J Clin Immunol, 2010. **30**(5): p. 628-31.

34. Marriott, I., et al., *Induction of Nod1 and Nod2 intracellular pattern recognition receptors in murine osteoblasts following bacterial challenge.* Infect Immun, 2005. **73**(5): p. 2967-73.

35. Le Bourhis, L., S. Benko, and S.E. Girardin, *Nod1 and Nod2 in innate immunity and human inflammatory disorders.* Biochem Soc Trans, 2007. **35**(Pt 6): p. 1479-84.

36. Ellington, J., et al., *Mechanisms of Staphylococcus aureus invasion of cultured osteoblasts.* Microb Pathog, 1999. **26**(6): p. 317-23.

37. Alexander, E., et al., *Staphylococcus aureus and Salmonella enterica serovar Dublin induce tumor necrosis factor-related apoptosis-inducing ligand expression by normal mouse and human osteoblasts.* Infect Immun, 2001. **69**(3): p. 1581-6.

38. Jevon, M., et al., *Mechanisms of internalization of Staphylococcus aureus by cultured human osteoblasts.* Infect Immun, 1999. **67**(5): p. 2677-81.

39. Tucker, K.A., et al., *Intracellular Staphylococcus aureus induces apoptosis in mouse osteoblasts.* FEMS Microbiol Lett, 2000. **186**(2): p. 151-6.

40. Alexander, E.H., et al., *Staphylococcus aureus - induced tumor necrosis factor - related apoptosis - inducing ligand expression mediates apoptosis and caspase-8 activation in infected osteoblasts.* BMC Microbiol, 2003. **3**: p. 5.

41. Marriott, I., et al., *Osteoblasts produce monocyte chemoattractant protein-1 in a murine model of Staphylococcus aureus osteomyelitis and infected human bone tissue.* Bone, 2005. **37**(4): p. 504-12.

42. Rossi, D. and A. Zlotnik, *The biology of chemokines and their receptors.* Annu Rev Immunol, 2000. **18**: p. 217-42.

43. Hofbauer, L.C. and A.E. Heufelder, *Intercellular chatter: osteoblasts, osteoclasts and interleukin 6.* Eur J Endocrinol, 1996. **134**(4): p. 425-6.

44. Labbé, J.L., et al., *Acute osteomyelitis in children: The pathogenesis revisited?* Orthopaedics & Traumatology: Surgery & Research, 2010. **96**(3): p. 268-275.

45. Classen, D.C., et al., *The timing of prophylactic administration of antibiotics and the risk of surgical-wound infection.* N Engl J Med, 1992. **326**(5): p. 281-6.

46. Jørgensen, P.H., K. Gromov, and K. Søballe, *[Prevention of prosthesis infections]*. Ugeskr Laeger, 2007. **169**(48): p. 4159-63.

47. Lew, D.P. and F.A. Waldvogel, *Osteomyelitis.* Lancet, 2004. **364**(9431): p. 369-79.

48. Eckardt, J.J., P.Z. Wirganowicz, and T. Mar, *An aggressive surgical approach to the management of chronic osteomyelitis.* Clin Orthop Relat Res, 1994(298): p. 229-39.

49. Hui, T., et al., *Treatment of osteomyelitis by liposomal gentamicin-impregnated calcium sulfate.* Arch Orthop Trauma Surg, 2009. **129**(10): p. 1301-8.

50. Wiley, B., Y. Sun, and Y. Xia, *Synthesis of Silver Nanostructures with Controlled Shapes and Properties.* Accounts of Chemical Research, 2007. **40**(10): p. 1067-1076.

51. Lu, L., et al., *Silver Nanoplates with Special Shapes: Controlled Synthesis and Their Surface Plasmon Resonance and Surface-Enhanced Raman Scattering Properties.* Chemistry of Materials, 2006. **18**(20): p. 4894-4901.

52. Shon, Y.-S. and E. Cutler, *Aqueous Synthesis of Alkanethiolate-Protected Ag Nanoparticles Using Bunte Salts.* Langmuir, 2004. **20**(16): p. 6626-6630.

53. Cao, R. Jin, and C.A. Mirkin, *DNA-Modified Core−Shell Ag/Au Nanoparticles.* Journal of the American Chemical Society, 2001. **123**(32): p. 7961-7962.

54. Cui, Y., et al., *Synthesis of AgcoreAushell Bimetallic Nanoparticles for Immunoassay Based on Surface-Enhanced Raman Spectroscopy.* The Journal of Physical Chemistry B, 2006. **110**(9): p. 4002-4006.

55. Taner, M., et al., *Synthesis, characterization and antibacterial investigation of silver-copper nanoalloys.* Journal of Materials Chemistry, 2011. **21**(35): p. 13150-13154.

56. Morones, J.R., et al., *The bactericidal effect of silver nanoparticles.* Nanotechnology, 2005. **16**(10): p. 2346-53.

57. Ji, J.H., et al., *Twenty-eight-day inhalation toxicity study of silver nanoparticles in Sprague-Dawley rats.* Inhal Toxicol, 2007. **19**(10): p. 857-71.

58. Azam, A., et al., *Size-dependent antimicrobial properties of CuO nanoparticles against Gram-positive and -negative bacterial strains.* Int J Nanomedicine, 2012. **7**: p. 3527-35.

59. Chan, G.H., et al., *Plasmonic Properties of Copper Nanoparticles Fabricated by Nanosphere Lithography.* Nano Letters, 2007. **7**(7): p. 1947-1952.

60. Zalavras, C.G., et al., *Treatment of persistent infection after anterior cruciate ligament surgery.* Clin Orthop Relat Res. , 2005. **439**: p. 52-57.

61. Rao, N., B.H. Ziran, and B.A. Lipsky, *Treating osteomyelitis: antibiotics and surgery.* Plast Reconstr Surg. , 2011. **Suppl 1**: p. 177-187.

62. Tanaka, K.S., et al., *Bisphosphonated fluoroquinolone esters as osteotropic prodrugs for the prevention of osteomyelitis.* Bioorg Med Chem, 2008. **16**(20): p. 9217-29.

63. Haik, Y. and S. Qadri. *Nanocidals for osteomylities managmenet*. in *ASME Global Congress on Nanoengineering for Medicine and Biology*. 2010. Houston, TX: ASME.

64. Sawafta, R., et al., *Nanocomposites with Residual Biocidal and Biostatic Properties*, in *US Patent Office*2008: USA.

65. Qadri, S., B. Ramadi, and Y. Haik, *Effective eradication of Staphylococcus aureus - infected human osteoblasts by silver-copper based composite nanoparticles.* Nanomedicine, 2011. **Submitted**

66. Sawafta, R. and Y. Haik, *Water Treatment and Method of Use*, in *US Patent Office*2009: USA.

67. Lok, C., et al., *Silver nanoparticles: partial oxidation and antibacterial activities.* J Biol Inorg Chem, 2007. **12**(4): p. 527-34.

68. Negm, N.A., M.F. Zaki, and M.A. Salem, *Cationic schiff base amphiphiles and their metal complexes: Surface and biocidal activities against bacteria and fungi.* Colloids Surf B Biointerfaces, 2010. **77**(1): p. 96-103.

69. Rawashdeh, R. and Y. Haik, *Antibacterial Mechanisms of Metallic Nanoparticles: A review.* Dynamic Biochemistry, Process Biotechnology and Molecular Biology, 2009. **3**(2): p. 12-20.

70. Sun, Y.-P., P. Atorngitjawat, and M.J. Meziani, *Preparation of Silver Nanoparticles via Rapid Expansion of Water in Carbon Dioxide Microemulsion into Reductant Solution.* Langmuir, 2001. **17**(19): p. 5707-5710.

71. Taleb, A., et al., *Local photon emission of self-assembled metal nanoparticles.* Applied Surface Science, 2000. **162–163**(0): p. 553-558.

72. Liu, Y.-C. and L.-H. Lin, *New pathway for the synthesis of ultrafine silver nanoparticles from bulk silver substrates in aqueous solutions by sonoelectrochemical methods.* Electrochemistry Communications, 2004. **6**(11): p. 1163-1168.

73. Wang, D., et al., *Synthesis of silver nanoparticles with flake-like shapes.* Materials Letters, 2005. **59**(14–15): p. 1760-1763.

74. Cai, M., J. Chen, and J. Zhou, *Reduction and morphology of silver nanoparticles via liquid–liquid method.* Applied Surface Science, 2004. **226**(4): p. 422-426.

75. He, S., et al., *Formation of Silver Nanoparticles and Self-Assembled Two-Dimensional Ordered Superlattice.* Langmuir, 2001. **17**(5): p. 1571-1575.

76. Sun, X. and Y. Luo, *Preparation and size control of silver nanoparticles by a thermal method.* Materials Letters, 2005. **59**(29–30): p. 3847-3850.

77. Lin, X.Z., X. Teng, and H. Yang, *Direct Synthesis of Narrowly Dispersed Silver Nanoparticles Using a Single-Source Precursor.* Langmuir, 2003. **19**(24): p. 10081-10085.

78. Mott, D., et al., *Aqueous synthesis and characterization of Ag and Ag-Au nanoparticles: addressing challenges in size, monodispersity and structure.* Philos Transact A Math Phys Eng Sci, 2010. **368**(1927): p. 4275-92.

79. Nishimura, S., et al., *Role of base in the formation of silver nanoparticles synthesized using sodium acrylate as a dual reducing and encapsulating agent.* Phys Chem Chem Phys, 2011. **13**(20): p. 9335-43.

80. Wang, G., et al., *Increased vancomycin MICs for Staphylococcus aureus clinical isolates from a university hospital during a 5-year period.* J Clin Microbiol, 2006. **44**(11): p. 3883-6.

81. Loimaranta, V., et al., *Generation of bioluminescent Streptococcus mutans and its usage in rapid analysis of the efficacy of antimicrobial compounds.* Antimicrob Agents Chemother, 1998. **42**(8): p. 1906-10.

82. Chang, S., et al., *Infection with vancomycin-resistant Staphylococcus aureus containing the vanA resistance gene.* N Engl J Med, 2003. **348**(14): p. 1342-7.

83. Coleman, C.A., et al., *The effect of m-xylene on cytotoxicity and cellular antioxidant status in rat dermal equivalents.* Toxicol Lett, 2003. **142**(1-2): p. 133-42.

84. Pap, E.H., et al., *Ratio-fluorescence microscopy of lipid oxidation in living cells using C11-BODIPY(581/591).* FEBS Lett, 1999. **453**(3): p. 278-82.

85. Shi, J., et al., *Microsomal Glutathione Transferase 1 Protects Against Toxicity Induced by Silica Nanoparticles but Not by Zinc Oxide Nanoparticles.* ACS Nano, 2012. **6**(3): p. 1925-1938.

86. van der Zande, M., et al., *Distribution, elimination, and toxicity of silver nanoparticles and silver ions in rats after 28-day oral exposure.* ACS Nano, 2012. **6**(8): p. 7427-42.

87. Loeschner, K., et al., *Distribution of silver in rats following 28 days of repeated oral exposure to silver nanoparticles or silver acetate.* Part Fibre Toxicol, 2011. **8**: p. 18.

88. Bouwmeester, H., et al., *Characterization of Translocation of Silver Nanoparticles and Effects on Whole-Genome Gene Expression Using an In Vitro Intestinal Epithelium Coculture Model.* ACS Nano, 2011. **5**(5): p. 4091-4103.

89. Park, E.J., et al., *Repeated-dose toxicity and inflammatory responses in mice by oral administration of silver nanoparticles.* Environ Toxicol Pharmacol, 2010. **30**(2): p. 162-8.

90. Poole, R.C. and A.P. Halestrap, *Transport of lactate and other monocarboxylates across mammalian plasma membranes.* Am J Physiol, 1993. **264**(4 Pt 1): p. C761-82.

91. Patel, M., et al., *Animal models for the study of osteomyelitis.* Semin Plast Surg, 2009. **23**(2): p. 148-54.

92. An, Y.H., Q.K. Kang, and C.R. Arciola, *Animal models of osteomyelitis.* Int J Artif Organs, 2006. **29**(4): p. 407-20.

93. Scheman L, Janota M, and L. P, *The production of experimental osteomyelitis: preliminary report.* JAMA, 1941. **177**: p. 5.

94. Norden, C.W., *Experimental osteomyelitis. I. A description of the model.* J Infect Dis, 1970. **122**(5): p. 410-8.

95. Andriole, V.T., D.A. Nagel, and W.O. Southwick, *A paradigm for human chronic osteomyelitis.* J Bone Joint Surg Am, 1973. **55**(7): p. 1511-5.

96. Zheng, J., et al., *Luminescent and Raman Active Silver Nanoparticles with Polycrystalline Structure.* Journal of the American Chemical Society, 2008. **130**(32): p. 10472-10473.